Consistent Scale-Up of the Freeze-Drying Process

Carvalho, Teresa de Melo

Publication date:
2018

Document Version
Publisher's PDF, also known as Version of record

CONSISTENT SCALE-UP OF THE FREEZE-DRYING PROCESS

PhD Thesis

Teresa Melo de Carvalho

Department of Chemical and Biochemical Engineering

Technical University of Denmark

October 2018

Supervisors

Krist V. Gernaey

Ulrich Krühne

Michelle Madsen

Anders Clausen

DTU Chemical Engineering
Department of Chemical and Biochemical Engineering

Preface

This thesis describes the work carried out at the Process and Systems Engineering Center (PROSYS), Department of Chemical and Biochemical Engineering, Technical University of Denmark. The thesis was written in partial fulfilment of the requirements for a Ph.D. degree in Engineering. The work conducted and presented in this thesis was performed in the period between August 2015 and October 2018, under the supervision of Professor Krist Gernaey and Associate Professor Ulrich Krühne from the Technical University of Denmark and by Department Manager Anders Clausen and Senior Principal Scientist Michelle Madsen from Chr.Hansen. This project is part of the BioRapid project which has received funding from the People Programme 8Marie Curie Actions, Multi-ITN) of the European Union's Seventh Framework Programme and Horizon 2020 fro research, tehcnologicla development and demonstration under grand agreements number 643056.

I would like to thank my supervisors Kris Gernaey, Ulrich Krühne, Anders Clausen and Michelle Madsen for the constant support and feedback. It has been a true pleasure working with them. A special thank goes to Christian Fridberg for the guidance and constructive discussions throughout the project. I would also like to thank Tina Iversen and Esben Ulrich Vulff for all the support performing experiments at laboratory/pilot scale. Additionally, I would like to thank Per Poulsen for his insight on industrial scale and invaluable process knowledge. And, I would like to thank Petra Foerst for the academic discussions and the opportunity of collaborating with the Technical University of Munich.

Thank you to all my colleagues at Chr.Hansen. It has been a great pleasure to work at Process during the past three years. Special thanks to Catarina, Christophe, Karen, Neda, Karen, Kim, Jimi, Hans and Susanne for all the support during the last three years.

I would also like to thank my friends and colleagues at PROSYS (Mafalda, Ricardo, Tannaz, Christian, Frederico, Robert, Leander, Mark) for all the collaborations and fun.

A special thank you goes for all the 14 ESRs involved in the BioRapid project (Ana, Andre, Angel, Emmanuel, Klaus, Viktor, Arathi, Patricia; Judite, Johannes, Tannaz, Robert, Micael and Lorenz). Thank you for all the collaborations and dinners during the last three years. Thank you also to all the SICs for the nice discussions throughout the project.

Finally, I would like to thank my family and Morten for all the support and encouragement.

Kgs.Lyngby, October 10th, 2018

Teresa Melo de Carvalho

Abstract

Lactic acid bacteria, are one of the most common examples of starter cultures due to their broad application for the production of fermented food products. After the fermentation and the concentration steps, starter cultures can be supplied in the frozen or in the dried state. Nowadays, dried products are preferred since they allow easier handling, transport, storage and application.

Freeze-drying or lyophilization is a drying process in which water is removed through a sublimation and a desorption step. It results in products with increased shelf stability, without losing its structural and shape characteristics. However, it is an expensive and time-consuming process frequently not operated in a robust and efficient way. Overly conservative freeze-drying cycles and scale-up based on empirical knowledge result in drawbacks not just from an economic standpoint but also from a product point of view. Thus, process development in this area has been focused on minimizing drying times while maintaining product quality.

This process is both dependent on the physical form of the material being dried and on the physical parameters and characteristics of the freeze-drying apparatus. The majority of the studies found in the scientific literature are applied to the pharmaceutical industry, therefore the available information for the freeze-drying of particulate material in open trays, mainly used in the food industry, is limited.

Freeze-drying of frozen particulate matter is characterized by a bimodal pore size distribution based on the intra-particle and inter-particle void space. Pore size distribution of the particle bed is determined by the particle size and how the particles are packed, while pore size distribution inside particles is dependent on the initial solid concentration and on the freezing rate. The ratio between the two pore size distributions plays has an important role for the dynamics of the freeze-drying process.

Local temperature and moisture content in the product are essential for the design of efficient freeze-drying cycles. Consequently, a fundamental understanding of water vapor flows during drying in a freeze-dryer is essential for the construction of an accurate model. In this thesis, the primary drying step during freeze-drying of *Streptococcus thermophilus* was investigated based on Computational Fluid Dynamics (CFD) techniques. A scale-up approach, going from the small scale of a single particle where only product characteristics are addressed, to the laboratory/pilot scale where both product and equipment characteristics are taken into account, was implemented.

The established model represents a good strategy to determine the effect of different operating conditions during the freeze-drying of pellets in open trays. Additionally, it opens the possibility to better understand scale-up issues and to develop robust freeze-drying cycles that facilitate the transfer between apparatus.

Resumé

Mælkesyrebakterier er én af de mest benyttede starterkulturer grundet det store applikationsområde. Produktion af disse starterkulturer involverer gæring, opkoncentrering og nedfrysning. Efter nedfrysning kan produktet sælges. Alternativt kan produktet gennemgå en tørringsproces og derefter salg. Disse produkter er at foretrække, da håndtering, transport, opbevaring og anvendelse er nemmere. Forskellige tørreprocesser kan benyttes afhængig af applikationsområde. Generelt anses frysetørring for at være en mere skånsom tørreproces med højere produktkvalitet.

Frysetørring, eller lyofilisering, er en tørreproces hvorved vand fjernes fra et produkt gennem et sublimerings- og desorptionstrin. Sammenlignet med andre tørreprocesser er denne mere skånsom. Stabiliteten af produktet forøges uden ændring af strukturelkarakteristika og form. Processen er dog dyr og tidskrævende, og bliver jævnligt drevet på en ikke robust og effektiv måde. Meget konservative frysetørrecykler og opskalering på baggrund af empirisk data kan have store negative konsekvenser. Disse er ikke bare økonomiske, men også produktkvaliteten kan påvirkes negativt. Derfor har procesoptimering og udvikling hovedsageligt været fokuseret på minimering af tørretid uden at gå på kompromis med produktkvalitet.

Frysetørreprocessen er både afhængig af den fysiske form på materialet som tørres, men også afhængig af fysiske parametre og karakteristika på frysetørreudstyret. Da størstedelen af studier indenfor dette område beskæftiger sig med frysetørring i den farmaceutiske industri, er data indenfor frysetørring af partikelformet materiale i åbne bakker til fødevareindustrien begrænset.

Frysetørring af frosset partikelformet materiale er karakteriseret ved en bimodal porestørrelsesfordeling, afhængig af det intrapartikulære- og interpartikulærefrirum. Porestørrelsesfordelingen i partikelbedden bestemt på baggrund af partikelstørrelse og hvordan disse partikler pakker sig i bedden, mens porestørrelsesfordelingen i partiklerne er afhængig af tørstofindholdet og hastigheden hvorved partiklerne nedfryses.

Lokale temperaturer og vandindhold i produktet er essentielle i forbindelse med design af effektive frysetørrecykler. Fundamental forståelse af flow af vanddamp under frysetørreprocessen er essentielt for udviklingen af en nøjagtig model. I denne afhandling er det primære trin under frysetørring af *Streptococcus thermophilus* undersøgt ved brug af Computational Fluid Dynamics (CFD). En ”Scale-up”-tilgang er benyttet, hvor produktkarakteristika blev undersøgt gennem forsøg med enkelte partikler, efterfulgt af laboratorie-/pilotskala undersøgelser, hvor der både blev taget hensyn til udstyrskarakteristika og produktkarakteristika.

Den udviklede model repræsenterer en god strategi til bestemmelse af virkningen af forskellige driftsbetingelser under frysetørring af partikler i åbne bakker. Derudover åbner den mulighed for bedre og mere effektiv forståelse af opskalingsproblemer, samt udvikling af mere robuste frysetørringscykler, der letter overførslen mellem udstyr.

Nomenclature

Roman Letters

A	Area	[m^2]
a_w	Water Activity	[-]
CFD	Computational Fluid Dynamics	[-]
CIP	Cleaning-in_Place	[-]
$D_{bulk,eff,bed}$	Effective Bulk Diffusion in the Bed	[m^2/s]
$D_{eff,bed}$	Effective Diffusion in the Bed	[m^2/s]
$D_{eff,chamber}$	Effective Diffusion in the Chamber	[m^2/s]
$D_{eff,particle}$	Effective Diffusion in the Particle	[m^2/s]
$D_{eff,porous}$	Effective Diffusion in the Porous Material	[m^2/s]
D_{ice}	Diffusion of the Ice	[m^2/s]
$D_{kn,eff,bed}$	Effective Knudsen Diffusion in the Bed	[m^2/s]
$d_{bed,pore}$	Pore Diameter of the Bed of Particles	[mm]
$d_{particle}$	Diameter of the Particle	[mm]
d_{pore}	Diameter of the Pore	[µm]
d_{sph}	Diameter of the Sphere	[mm]
Eff_{bed}	Bed Effectivity	[%]
$Eff_{particle}$	Particle Effectivity	[%]
F_{2-1}	View Factor between Two Bodies	[-]
FD	Freeze-Drying	[-]
FDM	Freeze-drying microscope	[-]
HTC	Heat Transfer Coefficient	[$W\ m^{-2}\ K^{-1}$]
L	Thickness / Characteristic Length Scale	[m]
LAB	Lactic Acid Bacteria	[-]
ΔH_{subl}	Enthalpy	[$J\ mol^{-1}$]
K	Heat Conductivity of the Gas	[$W\ m^{-1}\ K^{-1}$]
k_d	Desorption Rate Constant of Bound Water	[s^{-1}]
Kn	Knudsen Number	[-]
Kn_{bed}	Knudsen Number in the Bed of Particles	[m^2/s]
k_s	Solid Film Mass Transfer Coefficient	[s^{-1}]
m	Mass	[kg]
M_W	Molecular Weight	[$kg\ mol^{-1}$]

$Pack_{bed}$	Packing Factor of the Bed of Particles	[-]
PCA	Principal Component Analysis	[-]
p_c	Vapour Pressure Chamber	[Pa]
p_{ice}	Vapour Pressure Ice	[Pa]
p_{subl}	Vapour Pressure Sublimation	[Pa]
p_{tr}	Triple Point Vapor Pressure	[Pa]
p_w	Vapour Pressure Water	[Pa]
q_{rad}	Heat Flux Transferred through Radiation	[W m^{-2}]
$Q_{product}$	Energy Transferred to the Product	[J]
$q_{Fourier}$	Heat Flux Transferred through Conduction	[W m^{-2}]
R_{gas}	Gas Constant	[J mol^{-1} K^{-1}]
R_p	Product Resistance	[m s]
SEM	Scanning Electron Microscopy	[-]
SIP	Sterilization-in-Place	[-]
ST	*Streptococcus thermophilus*	[-]
T	Temperature	[-]
Ta	Acidification Time	[h]
T_g	Glass Temperature	[K]
T_g'	Glass Temperature for Maximally Freeze-Concentrated Solution	[K]
T_m	Melting Temperature	[K]
T_m'	Melting Temperature for Maximally Freeze-Concentrated Solution	[K]
T_{subl}	Temperature Sublimation	[K]
T_{tr}	Triple Point Temperature	[K]
t	Time	[s]
u_{creep}	Thermal Creep Velocity	[m s^{-1}]
$V_{pellets}$	Volume of Pellets	[m^3]
V_{tray}	Volume of Tray	[m^3]
X	Mass Fraction of Absorbed Water in Solid	[-]
y_W	Gas fraction	[-]

Greek Letters

α	Accommodation Coefficient	[-]
ε	Emissivity of the Surface	[-]
θ_{bed}	Porosity of the Bed of Particles	[-]
$\theta_{particle}$	Porosity of the Particle	[-]
λ	Molecular Mean Free Path	[m]
μ	Viscosity of the Gas	[Pa s]
ρ	Density	[kg m^{-3}]
σ	Stefan-Boltzmann Constant	[W m^{-2} K^{-4}]
σ_T	Thermal Slip Coefficient	[-]
$\tau_{particle}$	Tortuosity of the Particle	[-]

Contents

Chapter 1

Introduction

1.1 Background

Starter cultures are nowadays used for the production of fermented foods, since they allow standardized industrial processes and therefore improved products [1]. The production of starter cultures allows the reproduction of a selected strain or mixed population of microbes to a density that is likely to survive and be metabolically active in the process.

At the end of the production, starter cultures are often dried since it increases their viability and long-term preservation. Additionally, dried products allow easy and inexpensive handling, transport, storage and application. Different drying techniques are employed regarding their suitability, e.g. freeze-drying, vacuum drying, spray drying, drum drying, fluidized bed and air drying [2]–[4]. Compared with other conventional drying techniques, freeze-drying is generally considered to produce the dried products with the highest quality. Since the process operates at low temperature, thermal damage of the products is minimized, and the structural and shape characteristics are preserved.

Freeze-drying or lyophilization was for the first time described in 1906 by Bordas and d'Arsonval in an article for the Académie des Sciences in Paris [5]. However, it was not until during the Second World War that it started to be used at industrial scale for human plasma production [6]. Today the use of this technology has expanded for several different applications: high value foods, pharmaceuticals and sensitive biological material.

Freeze-drying consists in the removal of water from a frozen product through sublimation and desorption at high vacuum conditions. The target of the process is to get the desired value of residual moisture in the final product. Large amounts of energy are required during the process which makes it an expensive process when compared with other drying technologies [7]. Furthermore, the long production times also contribute to the increase of production costs. Therefore, process development in this area has been focused on minimizing drying times while maintaining product quality [8], [9].

The successful design of a freeze-drying cycle – identification of the optimal values of shelf temperature, chamber pressure and process duration – requires true understanding of the interrelation between product composition, process parameters and equipment capabilities. In order to maximize plant productivity and reduce the cost of the products, the rate of solvent removal should be maximized [10]. The problem arises when the increased sublimation rate causes damages in the product or increase of the pressure in the drying chamber due to lack of condenser capacity or choked flow on the duct. This

means that the successful design of a freeze-drying cycle starts with the characterization of both the product (identify the limit temperature and product morphology) and the apparatus (evaluate the duct and condenser capacity), followed by the monitoring of the residual amount of ice in the product, its temperature, and the sublimation flow rate.

The identification of the optimal values for the design of freeze-drying cycles is frequently obtained through an extensive amount of experimental work. This is an expensive and time consuming approach which does not guarantee the achievement of an optimal solution. Furthermore, the in-line measuring technologies for the important parameters involved in the optimization and control of freeze-drying cycles, present several challenges and inaccuracies [10].

Alternatively, model-based systems give tools for process design and optimization and have been increasingly developed in the last years. A particularly relevant application of mathematical modelling is the scale-up of the process. After the optimization of the process in laboratory scale, this needs to be transferred to production scale. Although, in freeze-drying the scale-up of a process is relatively simple since the product characteristics do not change drastically between scales (especially when the freezing step is performed outside of the freeze-dryer), there are still several challenges. Figure 1.1 summarizes the main challenges when scaling up a freeze-drying process of starter cultures.

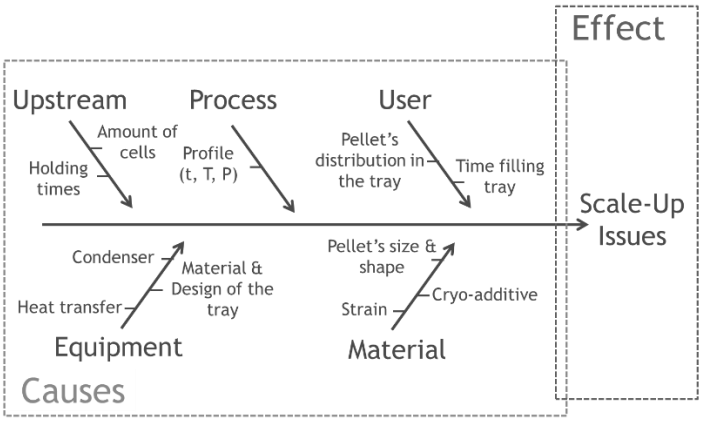

Figure 1.1 – Causes for scale-up issues of the freeze-drying process of starter cultures.

One of the biggest challenges when scaling-up a freeze-drying process is the variation in the apparatus characteristics. Therefore, understanding how the sublimation rate and the vapor flow are affected by the equipment design is essential in order to avoid problems during scale-up. A mathematical model coupling the product characteristics and the freeze-dryer design can be a useful tool in order to increase process knowledge by comparing a hypothesis with experimental findings. In this thesis, a mathematical model will be developed using Computational Fluid Dynamics (CFD) as a tool to reach a more fundamental understanding of the drying process during freeze-drying.

1.2 Scope

The overall focus of this project has been to address the main challenges of modelling the drying behaviour during freeze-drying of particulate material using computational fluid dynamics. The main focus has been on the development of modelling strategies based on scale-up approaches – going from the small scale of a single particle where only product characteristics are addressed, to the laboratory/pilot scale where both product and equipment characteristics are taken into account. The learnings at each step of the model development were considered in the subsequent steps increasing the complexity of the model. Furthermore, this project focused on the freeze-drying of lactic acid bacteria as a case study and aimed to predict its drying behaviour at a laboratory/pilot scale. A comprehensive investigation of product morphological characteristics and drying behaviour at different scales was performed at the start of the project.

1.3 Thesis Structure

The general outline of the thesis is presented in Figure 1.2and below as a brief overview:

Chapter 1 introduces freeze-drying and the challenges related to process transfer and scale-up. Furthermore, it introduces the scope and outline of the thesis.

Chapter 2 covers the theory associated with the freeze-drying process and its application to starter cultures. Furthermore, the chapter presents an extensive review of the mathematical models present in the scientific literature that describe the drying process during freeze-drying.

Chapter 3 investigates the freeze-drying process at Chr. Hansen. Four different production strains were investigated in detail in relation to their drying performance and morphological characteristics.

Chapter 4 illustrates the importance of the freezing step, product concentration and annealing on the drying behavior and on the final product morphology through experiments on a freeze-drying microscope (FDM). A mathematical model is developed using computational fluid dynamics techniques in order to simulate the drying process on the FDM.

Chapter 5 presents a theoretical study on the influence of the packing factor on the drying of particulate material. The study is made through numerical simulations.

Chapter 6 implements the developed CFD model for the prediction of the drying behavior during freeze-drying at laboratory/pilot scale. The simulations are compared with the measured values from the laboratory/pilot scale.

Chapter 7 provides the major conclusions and perspectives for future work.

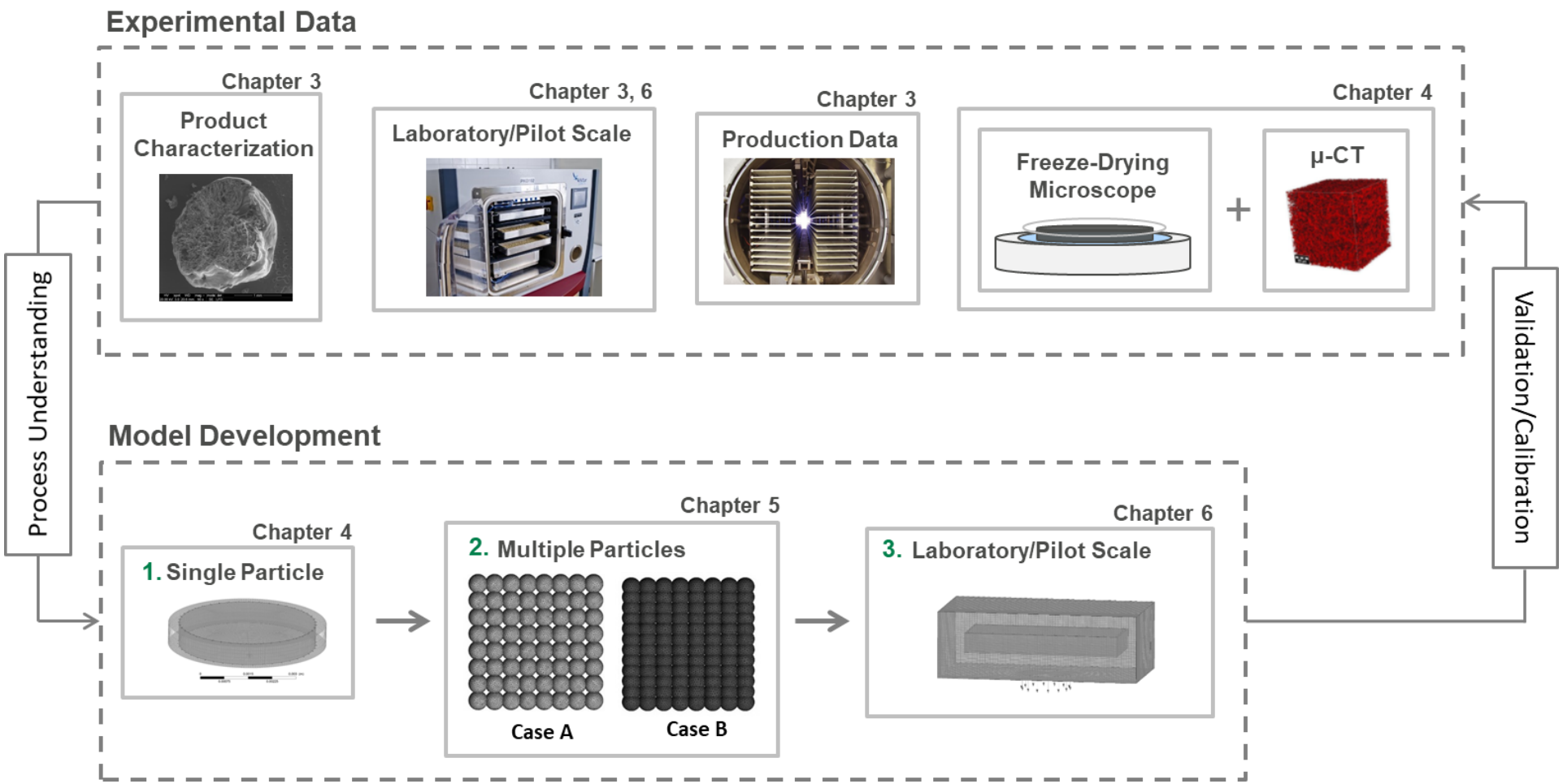

Figure 1.2 – General outline of the thesis.

Chapter 2

Freeze-Drying of Lactic Acid Bacteria as Starter Cultures

The production of fermented foods is nowadays based on the use of starter cultures which contribute to product characteristics, sensorial and safety attributes. The great advantage of starter cultures is that they can provide controllable and predictable fermentations, leading to improved products and standardized industrial processes [1].

Lactic acid bacteria (LAB) are the main microorganisms responsible for fermentation of fermented food products, and therefore also one of the most common starter cultures used in the production of fermented food products, e.g. dairy, meat, vegetables, wine, sourdough and fish [4], [11]. *Lactococcus*, *Leuconostoc*, *Lactobacillus*, *Streptococcus* and *Pediococcus* are members of the LAB [12]. LAB starter cultures are primarily used because of their ability to produce lactic acid from lactose and consequent pH reduction, leading to important effects like inhibition of growth of undesirable organisms (due to low pH), improvement of sensorial and textural properties, as well as contribution to health benefits [1].

The production of starter cultures allows the reproduction of a selected strain or mixed population of microbes to a density that is likely to survive and be metabolically active in the process. The main phases of industrial starter culture production are: (1) fermentation, (2) centrifugation, (3) addition of cryo- and lyo- additives, (4) freezing, (5) freeze-drying and (6) packing. Nowadays concentrated starter cultures are supplied in frozen (skipping step 5) and dried forms for direct incorporation into a food formulation. Frozen starter cultures must be transported and stored at very low temperatures, and therefore drying is nowadays the dominant preservation technique. Different drying techniques are employed in food production, e.g. freeze-drying, vacuum drying, spray drying, drum drying, fluidized bed and air drying [2]–[4]. Each of these drying techniques can be useful for a range of applications. This thesis will focus on freeze-drying since this is the conventional and preferred method used for drying starter cultures and the method used at Chr. Hansen.

2.1 Fundamentals of Freeze-Drying

Freeze-drying or lyophilization is a drying process in which water is removed at low pressures providing a product with increased shelf stability and that it is quickly and completely rehydrated upon addition of a solvent. The process requires three different steps: freezing, primary drying (sublimation step) and secondary drying (desorption step).

Freeze-drying of starter cultures allows their easy and inexpensive handling, storage and application, coupled with long-term preservation. However, different factors can influence the viability of lyophilized starter cultures during production and storage: the composition of the growth medium during fermentation, freezing rate, drying temperature and pressure, presence of lyo- and cryo-additives, water activity, oxygen content, pH, storage temperature, headspace composition above the product, light exposure, relative humidity and packaging material [13]. Therefore it is important from a technological and economical point of view to increase the survival to a level that is as high as possible during freezing, drying and storage steps [14].

The next sections describe the three different freeze-drying steps and their role in the production of viable and stable final products.

2.1.1 Freezing

Freezing is the phenomenon in which the water present in the concentrated cell suspension is frozen under atmospheric pressure. This step will determine the porosity, specific surface area and dissolution behaviour of the final product formed during the removal of ice crystals [15]. Thus, the freezing process plays a significant role on the later drying behaviour of the sample.

The freezing process starts above the freezing line by cooling a liquid sample from room temperature to below its freezing temperature (Figure 2.1). Usually, ice formation starts several degrees below the freezing line due to nucleation. The temperature interval between the freezing line and the moment ice starts forming is called the degree of supercooling and depends on several factors like cooling velocity, sample formulation, sample purity, sample size and the type of freezing container [15], [16].

Depending on the final temperature and cooling velocity required, freezing can be performed inside or outside the freeze-drying equipment. Fast freezing rates, meaning a high-degree of supercooling, lead to small ice crystals and can induce lethal ice formation inside the cells [17], [18]. On the other hand, slow freezing rates, meaning a low-degree of supercooling, lead to large ice crystals which are preferable to ensure rapid drying and facilitate the movement of the vapour during drying. However, large crystals can induce cell damage due to mechanical stress, eutectic crystallization of buffer salt components and osmotic stress by solute concentration [19].

The response to different cooling regimes depends on the cell type, where small cells such as bacteria are more resistant to freezing than larger yeast and mammalian cells [20], [21]. Therefore, optimum freezing rates are strain dependent and result from the strain's ability to release water, which is dependent on the presence/absence of a cell wall, cell size and shape, and the permeability to water of the cell membrane [20]–[23]. Optimum freezing conditions involve a compromise between the requirements of the bacteria and the drying performance.

The maximum amount of water that can be frozen is usually 70% to 90% of the amount present in solution [24], [25]. The remaining water is called unfreezable water. Between the melting transition temperature (T_m) and the glass transition temperature (T_g), the freeze-concentrated solution is in a rubbery state, characterized as being highly viscous, visco-elastic and unstable. Further decrease in temperature will lead to a transition from the rubbery state to a glassy state. This phenomenon happens at the glass transition temperature (T_g or T_g' for a maximally freeze-concentrated solution) [26], [27]. The glassy state is an amorphous metastable state that resembles a solid but without a long-range lattice order [17]. An amorphous glass has extremely high viscosity (typically ≥ 10^{12} Pa.s) which can inhibit diffusion and slow down deterioration reactions because water is immobilized and unavailable. Therefore, it is common practice to freeze at temperatures below T_g' since the frozen solution will be characterized for long-term stability in the frozen state, with maximum ice formation and structure stability during sublimation. The state diagram presented in Figure 2.1 shows the different regions and states of a matrix at different temperatures and solute concentrations.

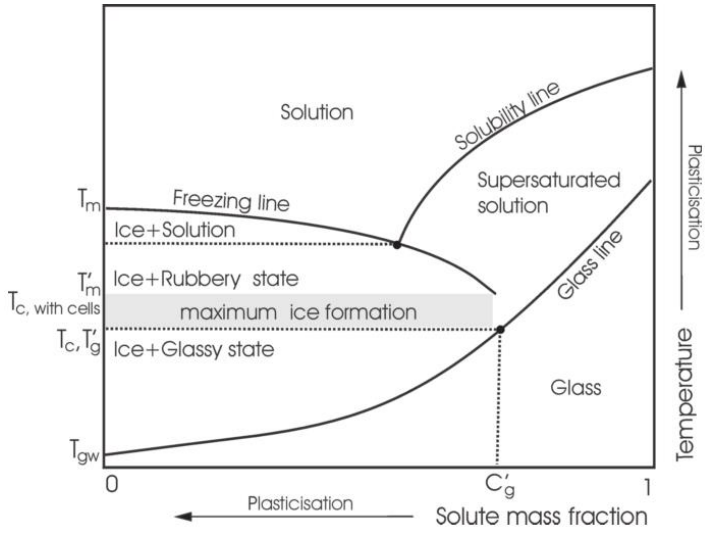

Figure 2.1 – State diagram for an aqueous sugar solution showing different regions and states of the drying matrix [17].

The formation of a maximally freeze-concentrated solution with entrapped microbial cells is crucial for the survival of the cells during drying [27]. For the production of starter cultures, freezing is mostly carried out by immersion in liquid nitrogen (-196 °C) of the cell suspension, but in the form of liquid droplets, which is

a process characterized by high cooling rates (300°C/min) [28]. Given the T_g' of the most common components of the medium in the production of starter cultures - skim milk (-50 °C), sucrose (-46 °C), trehalose (-40 °C) – and of pure water (-135 °C), the formation of a maximally freeze-concentrated matrix should be achieved by this freezing method [27].

2.1.2 Primary Drying

During primary drying the frozen water, which constitutes 70 to 95 % of the sample, is removed through sublimation [29]. By decreasing the partial pressure below the triple point (T_r), water can directly change from solid to gas state, which avoids undesired melting, foaming or softening of the product (Figure 2.2). This step requires very low pressures; therefore, it is always performed inside a drying chamber. The heat source, condenser and vacuum pump will assure the correct pressure and temperature that allow the chamber to be below the triple point (Section 2.2 will focus more on equipment design).

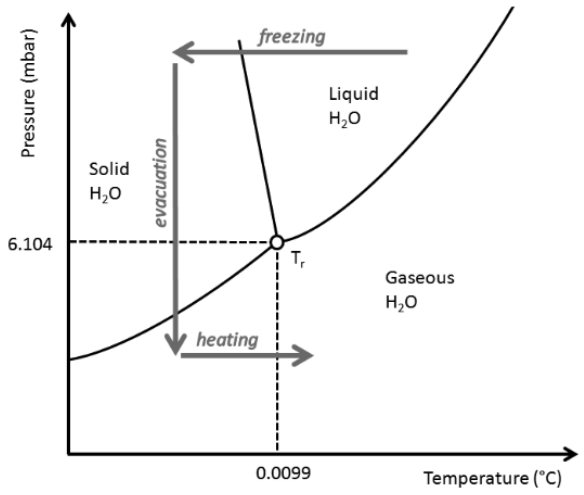

Figure 2.2 – Water state diagram showing the different aggregate states dependent on temperature and pressure. The arrow represents a typical freeze-drying process [30].

The difference in water vapour pressure between the sublimation front and the chamber is the driving force for the sublimation process (Equation (2.1)) [31]. The condenser plays an essential role during the drying process since it continuously removes the water vapour from the drying chamber, thereby increasing the partial pressure difference between the sublimation front and the drying chamber. Low condenser temperatures result in water condensation and immediate freezing at the condenser surface. Therefore, a low condenser temperature and a large surface area result in a more efficient process.

$$\frac{dm}{dt} = \frac{p_{ice} - p_c}{R_p} \tag{2.1}$$

The vapour pressure at the sublimation front is dependent on the product temperature (Equation (2.2)). Low product temperatures during primary drying result in low partial pressures at the ice front. Thus, higher product temperatures guarantee a higher sublimation rate since the vapour pressure difference is higher between the sublimation front and the chamber. However, the target product temperature during freeze-drying cannot be established by only considering process efficiency but should also consider the desired product characteristics. In order not to suffer structural changes due to a drop in viscosity, the product temperature should not exceed the collapse temperature (T_c) which is located between T_g' and T_m', usually just some degrees above T_g'. The effect of collapse in terms of product quality is not consistent. It has been reported that the loss of product structure may have beneficial as well as detrimental effects [31]–[34].

$$ln\frac{p_{subl}}{p_{tr}} = -\frac{\Delta H_{sub}}{R}\left[\frac{1}{T_{subl}} - \frac{1}{T_{tr}}\right] \tag{2.2}$$

The rate of sublimation is not only influenced by the vapour pressure difference but also by the cake thickness, total solid content, ice crystal distribution and surface area [35]. During drying, the sublimation front will move inwards the product leaving a porous matrix, which is dependent on the solid concentration, the solids composition and on the cooling rate. The formation of a dry porous matrix will increase the resistance to vapour movement over time.

Coupled to mass transfer, there are also heat transfer phenomena to be considered. An additional heat source is essential since the product temperature decreases with the start of sublimation. The amount of heat transferred to the product comes from different sources: radiation, conduction (solid/solid interfaces) and convection (solid/gas, liquid/gas, liquid/liquid) [26], [28], [35]. During drying the heat is mostly transferred through radiation from heated surfaces and conduction from heated plates/trays. Due to the coupled heat and mass transport, the product temperature (T_p) changes throughout the entire sublimation process. The heat transfer mechanisms are strongly dependent on the chosen drying profile (temperature and pressure), the loading of the dryer and the design of the dryer equipment.

2.1.3 Secondary Drying

As mentioned in Section 2.1.1, not all the water shifts to the solid state during the freezing step. Between 5 to 30% of non-freezable water is still present at the end of primary drying [36]. To achieve high storage stability the water activity of the sample has to be further reduced. A moisture content of 2-5% is considered optimal for storage stability [37], [38]. However, it is still debatable which is the optimal water content, yet there is a general agreement that it is dependent on the substance being freeze-dried and on the storage conditions [37], [39]. Over-drying might be harmful to bacterial survival or activity due to removal of free and unfreezable/structural water from the cellular components [15].

Water activity is defined as the vapour pressure of the substance (p) divided by the vapour pressure of water (p_w) at the same temperature [40].

$$a_w = \frac{p}{p_w} \tag{2.3}$$

Residual water can be bound as hydrate water in crystalline form, adsorbed on surfaces, or bound in the amorphous matrix. Water removal during the secondary drying step involves diffusion of the water in the amorphous glass, evaporation of the water at the solid/vapour boundary, and water vapour flow through the pore structure of the dry product [15].

Contrary to the sublimation step which is highly dependent on the chamber pressure, the main influencing parameter for the desorption process is the temperature of the product [41]. Once again not only the product temperature will influence the rate of secondary drying but also the product structure. Indeed, the higher the specific surface area of the sample, the shorter is the secondary step [32], [35]. T_g' stays constant during primary drying, yet during secondary drying it continuously increases due to desorption (Figure 2.3). The shelf temperature can be adapted throughout secondary drying since the stability of the amorphous sugar matrix increases with time [30].

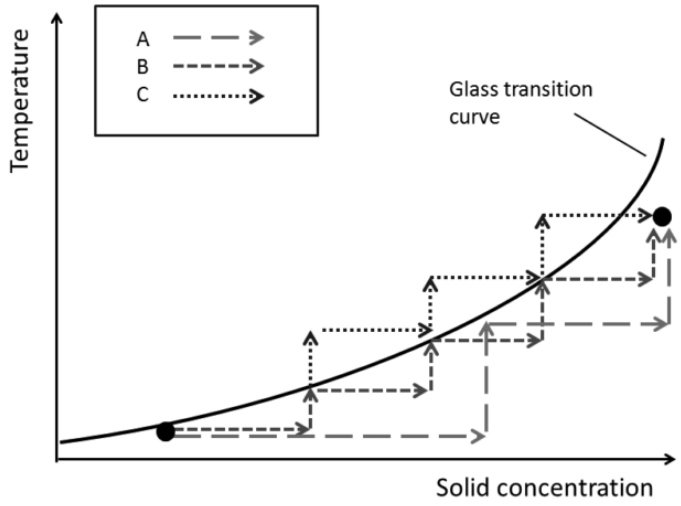

Figure 2.3 – State diagram representing the glass transition curve dependent on solid concentration and temperature. The dashed lines show three different stepwise drying profiles [30]**.**

2.2 Equipment Design

Typical freeze-drying equipment consists of three main components: a freeze-drying chamber, a condenser and a vacuum pump [26], [42]. Depending on the size and on the application, freeze-dryers have different designs. The main differences are the location of the condenser, the design of product containers and the heat source.

The freeze-drying chamber provides the necessary temperature and pressure to conduct freezing (optional), primary and secondary drying. The product is loaded in this section either in vials, trays, syringes or in other types of containers [43], [44]. The product can be loaded directly on top of the heating shelf (contact freeze-dryer) or suspended between drying shelves (radiation drying).

The vacuum pump evacuates the chamber in the beginning of the process and eliminates air that may leak into the dryer during operation. However vacuum pumps are not able to continuously remove water vapour from the chamber, so there is the need of a condenser.

The main function of the condenser is to remove the water vapour from the drying chamber, thereby assuring a vapour pressure difference between the sublimation front and the chamber. It can be placed in the drying chamber (internal condenser) or located in a separate chamber between the chamber and pump (external condenser). In the case of external condensers there will also be a duct that will connect the chamber and the condenser, allowing the transport of the water vapour between the two sections. The temperature of the condenser and its surface area can greatly influence its efficiency.

2.3 Protection Strategies

During freeze-drying cells are exposed to various stresses, especially dehydration, compromising the cell survival. The formation of ice crystals during freezing and the removal of water during drying is detrimental since water plays an important role in cell integrity and stability. When water crystallizes, the solutes in the remaining unfrozen fraction concentrate, which can lead to chemical and osmotic damage. Furthermore, the removal of water from the cells can cause damages to surface proteins, cell wall and cell membrane, decreasing the cell viability after drying.

Many protection strategies have been developed to enhance the bacterial viability during freeze-drying: addition of excipients to the drying medium, control of process parameters, pre-stressing prior to freeze-drying and change of fermentation conditions [45]. This section focuses on the addition of protective agents. The efficiency of these strategies is strain dependent, since the tolerance to freezing and drying processes depend also on the studied strain.

2.3.1 Protective agents

The addition of suitable protective agents during growth, or prior to freezing, is necessary to successfully preserve cells from freeze-drying [46], [47]. The choice of suitable protective agents is organism dependent but there are some which seem to work with many species: mono- and disaccharides (trehalose, sucrose, glucose, lactose), sugar alcohols (glycerol, sorbitol), skim milk, peptones, polymers (polyethylene glycol, polyvinylpyrrolidone, dextrane), and different amino acids and derivatives [14], [48], [49]. Cryoprotectants are used for stabilization during freezing and lyoprotectants for stabilization during drying. The molecular protection mechanisms differ depending on the nature of the solute and the available amount of water. A specific solute might be able to act as cryoprotectant and lyoprotectant dependent on the mode of action.

Cryoprotectants are water soluble substances that lower the melting point of water and increase the unfrozen part of the sample. Consequently, the cell will be less damaged due to mechanical or osmotic stress when a cryoprotectant is added before freezing. All non-toxic, low-molecular weight solutes can be used as protection for cells by minimising, via colligative effects, the percentage of water converted into extracellular ice and the extent of cell volume reduction. Furthermore, some viscous cryoprotectants (glycerol, sugars and polymers) increase the viscosity of the freeze-concentrated solutions or cytoplasm, and consequently the glassy state can be reached at lower cooling rates and higher freezing temperatures [17], [50].

Oxidation of membrane lipids, changes in cell wall and, DNA and protein damage are some of the factors reported to be the cause of cell death during drying and storage [51]. Therefore, it is crucial to maintain the fluidity and structure of the cell membrane. Lyoprotectants (especially disaccharides) are added to form an amorphous sugar matrix around the individual bacterial cells. The excellent performance of sugars in lyoprotection has been proposed to be a combination of two mechanisms: 1) the ability to form a glassy structure where biomolecules are embedded; and, 2) the ability to form hydrogen bonds between sugars and biomolecules to replace water bonds (water replacement hypothesis) [17], [52]–[54]. Both the intracellular and extracellular concentrations of lyoprotective agents are important for achieving optimal desiccation tolerance [55], [56]. It has been shown that complex mixtures of lyoprotective agents can stabilise better than one agent alone [39].

2.4 Modelling of the freeze-drying process

In the last years, an increase in the development of mathematical models describing the freezing and the drying steps during freeze-drying has been observed in order to support the development of optimal freeze-drying cycles that produce quality products in a robust process. Suitable mathematical models for the design and scale-up of freeze-drying cycles should reliably describe the dynamics of the process, have short calculation times, have few model parameters and be easy to validate with experimental data [57].

A mathematical model is an abstract and simplified representation of reality that summarizes available process knowledge and attempts to increase the fundamental scientific understanding of a process; it is therefore suited to explore available knowledge in order to improve or design a process [58]. There are two main categories of mathematical models: white-box and black-box models. A white-box model, also called “mechanistic” or “deterministic” model, is derived from first principles, like mass balances, energy balances, etc. Black-box models offer an empirical representation of the system’s behaviour, since measurement data of system inputs and outputs is used to build a process model. However, in most cases, some a priori knowledge is incorporated into the black-box model (for example a mass balance) or some black-box elements are incorporated in the white-box model, resulting in semi-mechanistic models or grey-box models [58], [59]. Nowadays, the term ‘hybrid model’ is also frequently used to indicate this type of models [60].

2.4.1 Physics-Based Models

Most attention in the literature is devoted to optimization of primary drying [43], [61]–[67], though secondary drying also occupies a significant fraction of the process time [39], [61], [68]–[70]. Modelling at the scale of the product being freeze-dried can be the starting point for a detailed model that can predict the freeze-drying sublimation rate and the product temperature profile. In the development of first principles models for the drying process during freeze-drying it is essential to understand the mass and heat transfer associated with the mechanisms of sublimation and desorption during primary and secondary drying, respectively.

During drying the thickness of the frozen product (L_{prod}) is reduced while the depth of the dried layer increases. Throughout primary drying the crystallized water is removed by sublimation. The sublimation rate is mainly dependent on the chamber pressure, shelf temperature, product thickness, product container surface available for heat transfer and product area and temperature [71]. Fundamental mass and energy conservation equations, Equation (2.4) and (2.5) respectively, describe the sublimation phenomena at the sublimation front.

$$\frac{dm}{dt} = A \cdot \sqrt{\frac{M_w}{2\pi \cdot R \cdot T_{sub}}} \cdot [p_{tr} - p] \quad (2.4)$$

$$\frac{dQ_{sub}}{dt} = \frac{\Delta H_{sub}}{M_w} \cdot \frac{dm}{dt} \quad (2.5)$$

During secondary drying residual water molecules tightly bound to the solid matrix through hydrogen bonds (forming a monolayer) and loosely bound water (forming a multilayer) are eliminated. The energy balance during desorption is described by Equation (2.6).

$$\frac{dQ_{sub}}{dt} = m \cdot \frac{\Delta H_{des}}{M_w} \cdot \frac{dX}{dt} \quad (2.6)$$

Here X is the mass fraction of absorbed water in the solid and can be described through two different rate mechanisms described by Equation (2.7) and (2.8), respectively.

$$\frac{dX}{dt} = k_s \cdot (X^{equ} - X) \quad (2.7)$$

$$\frac{dX}{dt} = -k_d \cdot X \quad (2.8)$$

In Equation (2.7) the variable X^{equ} represents the weight fraction of absorbed water in the solid which is in local equilibrium with the partial pressure of water vapor. A large number of physical models are proposed in the literature to describe moisture sorption isotherms [72]. The most frequently used ones are the Brunauer-Emmett-Teller (BET) model and the Guggenheim-Anderson-Boer (GAB) model, given, respectively, by Equation (2.9) and (2.10). In most cases, the BET equation is appropriate for lower ranges of water activity ($0.10 < a_w < 0.40$) and the GAB equation is applicable for a wider range of water activity values ($0.10 < a_w < 0.90$).

$$X^{equ} = \frac{X_M C a_w}{(1 - a_w)(1 + a_w(C - 1))} \quad (2.9)$$

$$X^{equ} = \frac{X_{MG} K_G C_G a_w}{(1 - K_G a_w)(1 + K_G a_w(C_G - 1))} \quad (2.10)$$

Here X^{equ} is the moisture content adsorbed per dry weight, a_w is water activity, X_M is a constant representing the amount of water needed to surround the material surface with just one layer of water molecules, and C is a constant related to the heat liberated in the monolayer sorption process. Furthermore, in Equation (2.10), X_{MG} is a constant representing the monolayer moisture content, and C_G and K_G relate to the interaction between the first layer and further layers of water molecules at the sorption sites [73].

2.4.1.1 Steady State Approach

Primary Drying

Several authors have attempted to approximate the drying process during freeze-drying with a simple steady state model, since for most of the primary drying step the process is in a pseudo steady state. In these models it is considered that the sensible heat (energy needed to change the temperature of the product) is negligible, meaning that the heat input to the product equals the heat removed by sublimation at the interface (Equation (2.11)).

$$\frac{dQ_{ext}}{dt} = \frac{-\Delta H_{sub}}{M_w}\frac{dm}{dt} \tag{2.11}$$

These models have been proven to accurately predict drying times and product temperature profiles, thus being of great use to investigate the operating conditions - plate temperature and chamber pressure - that minimize the time required for primary drying [64]. Furthermore they have shown good results with respect to the prediction of the impact of different product resistances [65] and for the prediction of freeze-drying kinetics when sublimation progresses multi-dimensionally in a product [66]. They have also been implemented in the investigation of the effect of vapor fluid dynamics and of other sources of heterogeneity — e.g., non-uniform shelf temperature and inert distribution [67] and to achieve a better understanding of the heat and mass transfer in novel container systems [43].

Secondary Drying

Regarding the secondary drying a recent method was developed by Sahni and Pikal [74] where the authors describe the drying phenomena in vials through an excel-based model. In this approach secondary drying is approximated by a series of steady state calculations of heat and mass transfer and the output corresponds to the variation of moisture content and temperature with time. The results of this simplified approach are fairly satisfactory although further studies with different formulations are required to further validate the approach.

2.4.1.2 Dynamic Approach

While it has been shown that steady-state approaches can accurately describe primary drying, there is a lack of accuracy when applying the steady-state model for big heat loads [75] showing that this type of models cannot give a complete description of the process. Steady-state models do not predict residual moisture as a function of time or the product temperature change immediately after a variation in shelf temperature [76]. Therefore, several researchers developed dynamic heat and mass transfer models to achieve a more complete description of the drying process [64], [77]–[80].

Primary Drying

Velardi and Barresi [64] developed a one-dimensional dynamic model for primary drying that introduces a dynamic energy balance to describe the heat transfer in a glass vial. Through a comparison with experimental data they concluded that shorter drying times and higher product temperature were obtained when considering the heat exchange with the environment due to radiation and heat transfer with the sidewall, and therefore this contribution should not be neglected. Later, the same research group proposed a control system based on dynamic parameter estimation using a mathematical model that allows in-line optimization and control of the freeze-drying process of pharmaceuticals in vials [8]. The proposed control strategies based on feedback and a simplified dynamic model, indicated efficiency for a wide range of operating conditions.

Secondary-Drying

Mechanisms of moisture desorption for amorphous and crystalline solutions, with specific solid-gas contact areas, have been discussed in the scientific literature [41], [81]. Liapis and Bruttini concluded that simultaneous adsorption and desorption at the interface between the solid and gas, convective transport and gas diffusion in pores were the three mechanisms that were rate limiting in the considered amorphous system [81]. In previous models the adsorption of bound water during primary drying was considered, which added increased complexity to the models. Therefore, Sadikoglu and Liapis [9] investigated the possibility of neglecting this term based on comparison of model predictions with experimental data. They verified an equally good measure of the residual moisture kinetics.

Most proposed models of the desorption step assume a single desorption stage [82]–[85], although it was demonstrated [41] that this step in reality consists of two different stages due to the different states of water molecules (mono-layer and multi-layer) and the corresponding limiting mass transfer mechanisms. Pikal et al. [41] showed that a fast desorption is observed in the first hours and a slower one when the residual moisture content becomes very low, which can lead to cake shrinkage and collapse, resulting in an increase of desorption time when approaching the mono-layer state is ignored in the setup of the model.

Trelea and co-workers [86] developed a dynamic model that considers different desorption kinetics and is able to accurately describe the temperature dependence during desorption. Although this dependence has been proven, most of the models in the scientific literature do not consider it which represents a model simplification and therefore a limitation [9], [62], [64], [82], [87], [88].

Primary & Secondary Drying

One of the first works where a dynamic model was designed in order to describe both primary and secondary drying was made by Litchfield and Liapis [89]. An extension of this model was made by Millman and co-workers [90] where heat transfer from both top and bottom was considered, and a one-dimensional moving sublimation interface and a top-down variation of temperature as well as moisture in the porous product layer was assumed. Different heat transfer modes and operating conditions (chamber pressure and shelf temperature) were tested in order to study moisture content profiles [90]–[92]. Based on a previously developed model [9], Sadikoglu et al. [92] studied the effect of a dynamic optimization considering the maximum allowable product temperature. Dynamic shelf temperature and chamber pressure profiles showed decreased process times and lower product moisture content. Jafar and Farid [93] studied the drying profile when both plate heating and radiation heating are applied and concluded that drying occurs from the material surface close to the heating source irrespective of the heating method.

Liapis and Bruttini [94] developed an extension of the one-dimensional model [90] for vials where both axial and radial movement was considered for the sublimation interface. Sadikoglu [95] repeated the study of the effect of a dynamic optimization [92] but considered a multi-dimensional system, arriving to the same conclusions as previously. An optimization study of the vial position and geometric arrangement was elaborated by Gan et al. [96] showing the number and location of vials that should be monitored in real time. Mascarenhas and Pikal [82] also designed a three-dimensional model using a 2D approach with axis symmetry where both sublimation and desorption were accounted for. Later, the same group performed a study that provides a validation of the model with experimental data providing a physical set of boundaries closer to reality [76].

2.4.2 Computational Fluid Dynamics

Computational Fluid Dynamics (CFD) is a branch of fluid mechanics that applies numerical methods for the modelling of physical problems involving fluid flows. A CFD model consists of mathematical expressions that describe the conservation laws for momentum, mass and energy. Partial differential equations (PDEs) are derived and simplified using a discretization technique, which transforms the continuous equations into discrete formulations. CFD models are thoroughly explored for single-phase flow, however for multi-phase flow or complex geometries they are more difficult to handle. In the specific case of freeze-drying, the application of CFD is limited by the description of the sublimating gas as a continuum flow, due to a pressure close to vacuum during process operation [97].

CFD models are useful tools for freeze-drying process investigations since they can give an accurate quantitative description of all variables involved in the process. The drawback is that assumptions must

be made in order to allow a mathematical description of the complex investigated processes, and stability problems may arise in numerical simulations.

CFD can be used to simulate pseudo-stationary conditions at a certain time or for the entire freeze-drying cycle, and the analysis can be done for specific parts of the equipment (i.e. chamber, condenser, duct and valve) or for the entire apparatus.

2.4.2.1 Flow Regime

Three types of flow are mainly encountered in vacuum technology: viscous or continuous flow, molecular flow and – at the transition between these two – the so-called Knudsen flow. The continuum fluid hypothesis states that fluid flow properties such as density and velocity can be defined as averages over volume elements large enough in comparison to the microscopic structure of the fluid, but small enough in comparison to the scale of the macroscopic flow phenomena. Due to the very low pressure in freeze-drying chambers it is possible that this assumption of continuity is no longer applicable and the choice of the numerical modelling approach for heat and mass transfer in freeze-drying will be governed by the significant rarefied flow effects.

The dimensionless parameter Knudsen number (Kn) is equal to the ratio of molecular mean free path (λ) to the characteristic length scale (L) and it characterizes the influence of rarefied effects in a gas flow (Equation (2.12)) [57].

$$Kn = \frac{\lambda}{L} \tag{2.12}$$

In the transitional regime (0.01 < Kn < 0.1) CFD can still be used with specific boundary conditions imposing gas velocity at the wall (i.e., partial-slip boundary condition). In the so-called molecular regime (Kn>1), the flow is no longer dominated by collisions between gas molecules, and non-equilibrium effects gain importance, resulting in velocity distributions far away from the Maxwellian distribution. In these cases, it is necessary to resort to alternative simulation frameworks, such as the Lattice-Boltzmann scheme [56]. In conclusion, flows under continuum gas conditions can be analyzed using the solution of the Navier-Stokes equations whereas the rarefied flow solutions can be obtained by the direct simulation Monte Carlo (DSMC) method for the Boltzmann equation [58].

2.4.2.2 Modelling at the Product Scale - Condensation Phenomenon

The majority of freeze-dried products are porous materials where condensation occurs frequently. In the models presented in Section 3 the saturation change of the frozen region caused by recondensation was not considered which leads to model uncertainty. Thus, studies were made to investigate the condensation phenomenon of unsaturated capillary porous media [98]–[103]. Ghajar and Hashemabadi

[104] investigated the condensation in an idealized porous medium using a cavitation model with a two-phase mixture multi-phase flow. They developed CFD methods where slip flow, buoyancy, and capillary forces in micropores were analysed with adequate boundary conditions. From this study it was concluded that porosity and vapor flow rates are the main parameters that influence condensation kinetics. When vacuum pressure is greater than saturated vapor pressure the condensation rate will increase, and condensate in the porous material will block the pores. However, the influence of non-homogeneous porous media has not been investigated in this study.

2.4.2.3 Modelling at Equipment Scale

In the past, the role played by vapor fluid dynamics once the vapor leaves the product was assumed to be negligible due to the difficulty to identify and isolate its effects in the experimental results. Batch heterogeneity problems and issues to evacuate the requested water vapor flow are frequent during a freeze-drying process, and therefore, when designing a freeze-dryer critical features dependent on equipment design and water vapor flow must be addressed. Typical design parameters that affect the overall performance of a freeze-dryer are the geometry of the condenser and, for freeze-dryers with condensers separated from the freeze-drying chamber, the size of the duct and of the isolating valve. The experimental investigation of these issues is costly and time consuming, and therefore it is interesting to explore them through a computational approach like Computational Fluid Dynamics (CFD).

2.4.2.4 Duct

Studies were carried out with focus on the resistances to vapor flow from the chamber to the condenser pathway when the condenser is placed outside the drying chamber [105], [106]. A primary cause of loss of pressure control is a phenomenon described as “choked flow”. This phenomenon happens under aggressive operating conditions where the required mass transfer through the duct connecting the drying chamber and the condenser cannot be maintained at the controlled pressure. The water vapor flow rate increases as the condenser pressure decreases until the velocity of the water vapor reaches the speed of sound at the duct exit. From that moment any further increase in water vapor flow rate results in an increase in chamber pressure. This problem does not happen frequently in more conservative processes where slow and suboptimal freeze-drying cycles are employed. However, since the need for increased capacity has driven the design of new freeze-drying systems, it is essential to find the conditions (combinations of dryer load, dryer capacity, shelf temperature and chamber pressure) under which choked flow occurs. Studies were carried out to identify the critical parameters responsible for the discrepancy when scaling up from laboratory to industrial freeze-dryers [106]. It was found that the presence of a Cleaning-in-Place (CIP) and Sterilization-in-Place (SIP) piping in the duct lead to significant changes in the mass flow rate predictions and the velocity profile in the duct (Figure 2.4). Thus, the fluid dynamics of vapor and non-condensable gas in a low-pressure environment forms an important factor affecting the energy and time costs of a freeze-drying unit operation.

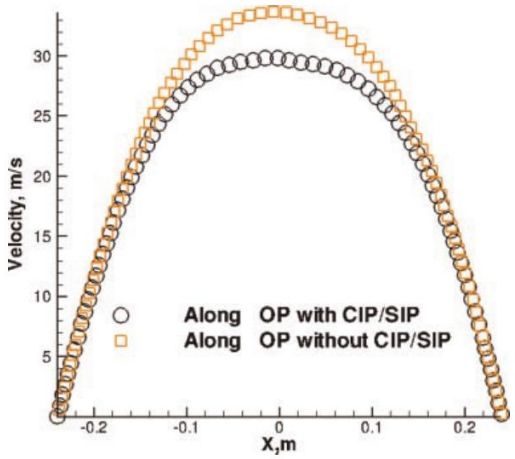

Figure 2.4 – Comparison of velocity profile along the TDLAS optical path (OP) in the duct with and without the presence of a CIP/SIP piping. [54]

2.4.2.5 Condenser

Models were also developed in order to improve condenser efficiency. These models describe the fluid dynamics, the process and patterns of ice deposition in freeze-dryer condensers. Studies revealed that the presence of a duct connecting the product chamber and condenser increased non-uniformity on ice growth, and that the presence of non-condensable gases increased the effective resistance in the condenser, preventing the vapor from condensing on the coils away from the duct exit [107], [108]. Ganguly and Alexeenko [107] have also shown that the location and topology of the condensing coils significantly alter the ice growth and uniformity. They concluded that the hardware and the design of the dryer and of the condenser could significantly alter the flow structure and vapor path (Figure 2.5).

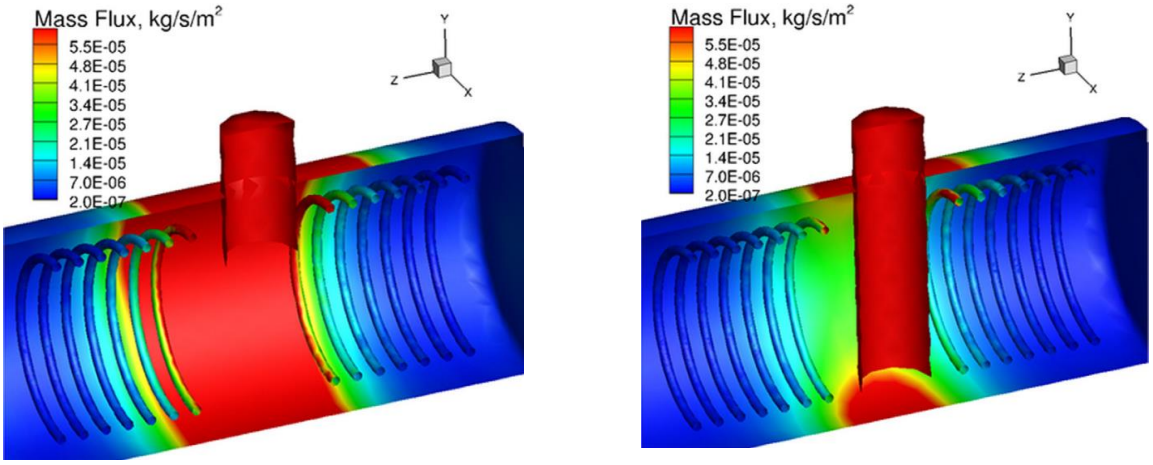

Figure 2.5 – Left: Mass flux contours in the condenser for Case 1 with a duct extending by 9.5 cm into the condenser reservoir. Right: Mass flux contours in the condenser for Case 2 with a duct extending by 28.5 cm into the condenser reservoir. [55]

2.4.2.6 Dual-Scale Model – Coupling Product and Equipment Attributes

In the previous sections, models describing the effect of the product characteristics on product temperature and sublimation rate on the one hand, and the effect of the equipment capabilities on flow dynamics on the other hand, were considered in separate models. However, it is critical to build a framework that couples both equipment design and product attributes in a single model. Including first-principles models for heat and mass transport as well as models for vapor transport in the drying chamber and for ice deposition in the condenser, it is possible to develop, implement and validate a simulation framework that describes the freeze-drying process. Ganguly and co-workers [71] presented a framework where a system-level coupled sublimation-condensation model was used to determine the effect of equipment design on the dynamic process/product characteristics and the effect of dryer hardware and restrictions in the duct on the onset of choking. Similarly Rasetto et al. [109] introduced an important model in process scale-up and transfer which allowed evaluating quantitatively the influence of the size of the equipment, of the geometric characteristics of the chamber, and of the operating parameters.

2.4.3 Black-box Models

In the previous sections the application of mechanistic models to both optimize and monitor the process was highlighted. However, first-principles based models are time consuming to develop, which can make the in-line optimization unfeasible and/or increase significantly the required time for the off-line optimization. Therefore, advantages could be obtained by using black-box models. As mentioned before, black-box models are models where no physical insight is needed but where inputs and outputs can be measured. These models can be either linear (e.g. linear input-output models, linear state-space models), or non-linear (e.g. artificial neural networks, wavelets, fuzzy models) [110].

2.4.3.1 Artificial Neural Networks and Fuzzy Models

An artificial neural network (ANN) is a mathematical model which mimics the behavior of the brain, and is composed of neurons organized into layers. This type of model is frequently used to estimate or approximate functions that can depend on a large number of inputs. Fuzzy models are able to represent process uncertainty and imprecision. In these models there are two fundamental functional components: input and output interfaces and the processing core [111]. Fuzzy models are an approach to form a system model using a description language based on fuzzy logic with fuzzy predicates. Fuzzy modelling is a qualitative modelling scheme by which system behaviours are qualitatively described through a natural language [112].

Based on a truncated Fuzzy-Neural Volterra Model, Todorov and Tsvetkon [113] presented a method for designing a non-linear model predictive controller for the control of product temperature in a lyophilization plant. The controller is based on a Volterra Fuzzy-Neural predictive model and a simplified gradient

optimization algorithm. Dragoi and co-workers [114] investigated a method for process modelling and monitoring using a new methodology for optimal neural network design. They developed a self-adaptive differential algorithm that allowed the simultaneous structural and parametric optimization of the network.

2.4.4 Novel Applications in Freeze-Drying

Different model strategies were highlighted in this chapter, leading to the conclusion that regardless of the modelling approach, it is essential to have a fundamental understanding of the heat and mass transfer phenomena for the selection of the correct freeze-drying conditions and the construction of an accurate model [20]. Additionally, in the scientific literature a particular focus on studies regarding applications using vials is notable since freeze-drying is primarily used in the pharmaceutical industry. Yet in the past few years lyophilization has received a growing interest for food and biotechnology applications. Therefore, in the future, freeze-drying can be expected to be performed in all different types of containers and new equipment designs are likely to be implemented at both small and large scale [43], [44], [115].

Although the physical phenomena behind the process are basically the same – a sublimation and a desorption phenomenon – there will be differences in the shape of the material being freeze-dried, in the different resistances affecting the sublimation rate and in the vapor flow dynamics due to the different equipment designs. Studies on the freeze-drying of food and of frozen pellets have shown how challenging it is to model such systems since they are not very well known [66], [116]. For instance studies for the drying of frozen pellets have been made where steady-state approaches have been described both for primary and secondary drying of frozen particles [85], [117], [118]; however it seems that different studies report different approaches for the way that particles dry in a freeze-drying process dependent on the size of the particle. It is important to highlight the presence of two different porosities on a bed of frozen particles – the inner porosity of each particle (changes with time) and the outer porosity of the bed (constant if no collapse is considered). Liapis and Bruttini [85] studied the drying of small frozen micro-particles (5-15 microns) and proposed a model where there is a sublimation front situated inside the slab, where all the pellets above the front are dry and the ones below are frozen. Trelea et al. [117] instead studied bigger particles (2000 microns) and proposed a model approach where sublimation occurs simultaneously at different rates in all the pellets present in the tray; therefore there will be a dry part situated at the periphery of the pellet and a frozen part at its core.

2.4.5 Measurement Techniques for Model Calibration & Validation

As described before mechanistic models have been successfully applied for freeze-drying cycle development and optimization. However, to ensure constant product quality, the development of a design space and a control strategy are essential. Based on the available potential combinations of shelf temperature and chamber pressure the Design Space can be constructed for a specific formulation [119]. The Design Space is defined in ICH Q8 [120] as the multi-dimensional combination and interaction of

input variables and process parameters leading to the acceptable product quality with a controlled probability [121]. The limits of this Design Space are determined by the efficiency of drying, the equipment limitations and the Critical Quality Attributes (CQAs) identified for the specific product (e.g. the dried cake appearance) [122]. Thus Quality by Design can be incorporated into formulation and process development, and also in process scale-up [57], [119], [123].

Before model predictions are useful to draw conclusions or decide on a Design Space, the model should be a reliable representation of the reality. Therefore, an uncertainty analysis [124] and a verification of the models using experimental data are essential. The literature reveals an extensive variety of measurement techniques that have been applied in order to measure and understand the variables that are being modelled. An overview of the most frequently used measurement techniques is presented in Table 2.1. Furthermore, this table also highlights the disadvantages of each method.

Physical characterization of different formulations in both frozen and dried solid states provides relevant information for formulation and process development. Table 2.1 shows an overview of different techniques for measuring different physical characteristics of materials in both states. Porosity, density and specific surface area will greatly influence the sublimation rate and are mostly influenced by the solid concentration and composition, the freezing rate and size of the particles (when applied to bulk freeze-drying). Glass and collapse temperature are critical product parameters in the determination of process temperature and pressure since the product should be kept below these values in order to prevent modifications in its structure.

In order to follow and control the process variables such as chamber pressure and shelf temperature, these variables are normally measured during the course of the freeze-drying process. In addition, when developing or improving a process it is relevant to measure the product temperature and the vapor flow, yet these variables are not standard measurements since they are not accurate and reliable. It is challenging to set the correct position for both probes since measurements will considerably differ with the position selected, and furthermore the placement of the probes can disturb the process. Table 2.1 summarizes different on-line techniques for the measurement of these variables.

The performance of drying technologies is mainly evaluated by the reduction of water activity in the freeze-dried products. Water activity and residual moisture content are variables used to control the quality of the products being freeze-dried. Table 2.1 presents different methods used for the measurement of these variables.

In summary, process methods can be divided in two groups where the first group comprises measurements related to the product which include both on-line and off-line measurements, and the second comprises measurements related to the entire batch. The application of developing technologies for process monitoring (e.g. wireless product temperature monitoring, tuneable diode laser absorption

spectroscopy at manufacturing scale, heat flux measurement, and mass spectrometry) is a very important step towards reaching a better understanding of the process and a way to optimize freeze-drying cycles [125].

Table 2.1 – State variables in freeze-drying and their measurement basis.

	State Variable	Measurement Basis	Mode	Ref.	Description	Disadvantages
Material	Porosity	Mercury Intrusion Porosimetry	Off-line	[126]	Determination of pore size distribution by mercury intrusion. Pressure is applied to force mercury into the pores. By measuring the intrusion volume and the applied pressure it is possible to calculate the pore size distribution	
		Scanning Electron Microscopy (SEM)	Off-line	[126] – [128]	Method where images of a sample are produced by scanning with a focused beam of electrons. Image analysis is used in order to estimate the pore size distribution.	• It can damage the sample; • Sample preparation can modify the sample structure;
		Bulk Density vs True Density	Off-line	[59]	$\epsilon = 1 - \frac{\rho_{bulk}}{\rho_{true}}$	
		X-ray micro-CT	Off-line	[129] , [130]	Micro-focus X-ray source illuminates the object and a planar X-ray detector collects magnified projection images. The structure is analyzed by interpolating different sections.	• Lower resolution than SEM; • It can damage the sample;
	Density	Gas Pycnometer	Off-line	[127]	Technique that uses gas displacement method to measure volume	
		Bulk Density	Off-line	[127]	Dry weight of a material related to a specific volume. Considers both the volume of the material and the air trapped between particles	
	Specific Surface Area	BET surface area analysis	Off-line	[41]	Specific area evaluation of materials by nitrogen multilayer adsorption measured as a function of relative pressure using a fully automated analyser	• Not accurate for pore size analysis; • Not applicable to all types of isotherms;

	State Variable	Measurement Basis	Mode	Ref.	Description	Disadvantages
	Glass Temperature	Differential thermal analysis (DTA)	Off-line	[61]	Compares the difference in thermal properties of the product with a reference substance	• Low accuracy; • Difficult to determine the conversion factors from temperature difference to enthalpy change;
		Differential Scanning Calorimetry (DSC)	Off-line	[26], [131]	Compares the difference in heat flow between the sample and the reference temperatures	• Low accuracy; • Difficult to choose the right temperature scanning rate; • Low sample mass that can lead to contaminations;
		Modulated Temperature DSC	Off-line	[132]	Recently developed extension of DSC in which sine wave modulation is applied to the standard linear temperature program	• Difficult to evaluate the data; • Great number of experimental variables needed;
		DTA – Electrical Impedance	Off-line	[64]	Based on conventional electrical resistance analysis adding the use of derivative impedance analysis ($Z\sin\varphi$)	
	Collapse Temperature	Freeze-Drying Microscope	Off-line	[34], [133]	Microscope where the freeze-drying of a small sample can be observed. Increasing/decreasing the temperature of the sample allows the visualization of structure collapse	• Not accurate;
Process	Product Temperature	Infrared Thermography	On-line	[134]	Monitors spatial temperature distribution on materials or between vials placed inside the freeze dryer	• Change in the apparatus. • Wrong temperature readouts when the material has low emissivity

	State Variable	Measurement Basis	Mode	Ref.	Description	Disadvantages
		Thermocouple	On-line	[28], [125], [135]	Monitors temperature at a specific position of the sample and tray. Temperature measurement principle based on the Seebeck effect	• Invasive temperature measurement; • Difficult to sterilize; • Cannot be used in automatic loading systems; • Not representative of the average batch temperature;
		Resistance Thermal Detector	On-line	[28], [125]	Monitors temperature at a specific position of the sample and tray. Temperature measurement principle based on the temperature dependence of the electrical resistance of metals	• Invasive temperature measurement • Difficult measurements at one point of the sample due to large thermo-sensitive region • Requires power source • Produces heat • Not representative of the average batch temperature;
		Manometric Temperature Measurement (MTM)	On-line	[136], [137]	Records the pressure versus time data and analyses the data to calculate the temperature at the sublimation interface	• Does not consider temperature heterogeneity, just yields one temperature value.
		Temperature Remote Interrogation System (TEMPRIS)	On-line	[125], [138]	Wireless and battery free probes. Temperature monitored in real-time and displayed and recorded in a computer	• Invasive temperature measurement (possible differences of the freezing behaviour)
		TrackSense Pro sensor	On-line	[139]	Temperature is measured and transmitted on the ISM band to a data collector	• Invasive temperature measurement • Dependent on the battery life time • Data not available in real-time
	Chamber Pressure	Pirani Gauge	On-line	[140]	Measures the pressure in the drying chamber, measurements are highly influenced by gas composition	• Low accuracy
		Capacitance Manometer	On-line	[125], [140]	Measure the absolute pressure in the drying chamber	

	State Variable	Measurement Basis	Mode	Ref.	Description	Disadvantages
		Thermocouple Gauge	On-line	[125], [141]	Similar to Pirani Gauge	• Type of surrounding gas and its heat capacity influences the measured pressure
		Mass Spectrometry	On-line	[125], [142]	Technique that ionizes chemical species and sorts the ions based on their mass-to-charge ratio. Able to monitor the partial pressure of water vapor	• Electronics do not allow sterilization;
	Shelf Temperature	Thermocouple	On-line	[28]	Measures temperature of the heating fluid in the inlet manifold of the shelf. Temperature measurement principle based on the Seebeck effect	
		Resistance Thermal Detector	On-line	[28]	Measures temperature of the heating fluid in the inlet manifold of the shelf. Temperature measurement principle based on the temperature dependence of the electrical resistance of metals	
		Infrared Thermography	On-line	[134]	Monitors spatial temperature distribution on the shelf inside the freeze dryer	• Difficult to observe more than one shelf;
	Vapor Flow	Tuneable Diode Laser Absorption Spectroscopy	On-line	[125], [140]	Measurement based on spectroscopic principles measuring absorption of radiation by water vapor. Measures the water vapor concentration in the duct connecting the chamber and the condenser	• Expensive; • Difficult to determine the offset of dew point as it reaches the plateau value asymptotically;
		Gas Plasma Spectroscopy (Lyotrack)	On-line	[140]	Measures water vapor concentration based on optical emission spectroscopy. Can be placed in the duct or in the drying chamber	• Expensive; • When placed in the drying chamber, it can cause product degradation via oxidation;

	State Variable	Measurement Basis	Mode	Ref.	Description	Disadvantages
	Heat Flux	Heat Flux Sensor	On-line	[125], [143]	Heat transfer can be measured in discrete locations. Thin-film differential thermopile that generates an electrical signal proportional to the total heat applied to the surface of the sensor.	• Not suitable for secondary drying. Desorption heat is below the limit of detection of the sensor;
Quality	Water Activity	Chilled Mirror Dewpoint	Off-line	[144]	Water activity is measured by equilibrating the liquid phase water in the sample with the vapor phase water in the headspace of a closed chamber and measuring the relative humidity of the headspace	
		Electric Hygrometers	Off-line	[144]	Uses resistance or capacitance sensors to measure relative humidity	• Needs calibration; • For accurate measurements a good temperature control or measurement is needed;
	Residual Moisture Content	Gravimetric Method	Off-line	[28], [145]	Measures the maximum loss in weight of a sample equilibrated to constant weight over anhydrous P_2O_5 at a pressure below 1 mm Hg and a temperature between 20-30 °C	
		Karl-Fisher Method	Off-line	[28], [145]	Weighted product is dissolved in methanol and titrated with Karl-Fisher solution until the colour changes from brown to yellow	• Cannot be used if the product reacts with iodine; • Cannot be used if the product dissolves in methanol;
		Thermogravimetry	Off-line	[28], [145]	Weight loss of the product is measured at constant temperature or at a temperature-time profile	

	State Variable	Measurement Basis	Mode	Ref.	Description	Disadvantages
		Near-Infrared (NIR) Spectroscopy	On-line	[146]	NIR spectra are measured noninvasively with the assistance of a hyperspectral camera, a multichannel fiber-optic light source and fiber-optic noncontact diffusion reflectance probes	• Needs a reference method; • Probes interfere with the tray disposition;

2.4.6 Summary

This review provides an overview of the current state of mathematical modelling of the drying step during a freeze-drying process. In this chapter the following key points have been identified:

- Freeze-drying is an expensive and very time-consuming process with high investment, operating and maintenance costs. Modelling can be helpful for achieving a better overview and understanding of the process and for the development of a Design Space;
- Steady state and dynamic state models to describe primary and secondary drying are reviewed. Dynamic models are necessary for a more complete description of the drying considering both sublimation and desorption;
- The use of CFD to simulate and study the water vapor flow in the duct and in the condenser was reviewed. These models assess critical issues like batch heterogeneity problems or the capability of the freeze-dryer to evacuate the requested water vapor flow;
- Dual-scale models describe frameworks that couple both equipment design and product attributes. Including first-principles models for heat and mass transport as well as models for water vapor flow it is possible to develop, implement and validate a simulation framework that describes the freeze-drying process;
- Black-box models are based on empirical observations of the system's behaviour; therefore, measurement data of the inputs and outputs is used to build a process model. In industry this type of models can be very useful due to the large amount of data available, yet it is necessary to assure data validation to avoid potential errors;
- First-principles and data-driven modelling approaches can play an important role in process design, optimization and control of critical quality parameters in freeze-drying: however they still require a high degree of development for novel types of containers due to an increased use of freeze-drying in different applications;
- Model validation is essential to ascertain whether the assumptions made are reasonable with respect to the real system;
- In order to increase process knowledge that can lead to improvements in equipment design, process control and processing efficiency a compromise between an experimental and a model-based approach should be chosen.

The future requirements and developments in modelling and measurement techniques that should be prioritized for the freeze-drying process are as follows:

- Further studies on fundamental understanding of heat and mass transfer phenomena on novel containers and new equipment designs;
- Better understanding of the secondary drying phenomena through the introduction of PAT tools for the monitoring of these phenomena (e.g. mass spectrometry);

- More detailed understanding of vapor flow in a freeze-dryer both through PAT tools and though modelling;
- One of the main challenges of this area is the development of new measurement techniques, which are able to measure the product temperature without interfering with the drying process.

2.5 Conclusions

The above description of the different steps of the process leads to the conclusion that freeze-drying is a complex process that involves both heat and mass transfer to remove water from a frozen product. The removal of water through sublimation at low pressures increases the stability of products during storage and preserves their physical structure. However, it is an expensive and very time-consuming process with high investment, operation and maintenance costs. Therefore, process development in this area is focused on minimizing drying times while maintaining product quality. The successful development of a freeze-drying cycle requires the combined knowledge of product properties and equipment design.

Enhanced process understanding can result in improvements of the equipment design, process control, process efficiency, and potentially also the quality of the final product. To improve process performance and get an increased knowledge and understanding of the phenomena happening during freeze-drying, the development of mathematical models is an important tool. Mathematical models describing the freezing and the drying steps are available in literature mainly for pharmaceutical applications where the product is loaded into vials and frozen and dried inside the freeze-drying equipment. Nowadays, different types of containers and new equipment designs have been implemented at both small and large scale due to the implementation of this process in new applications. Although the physics involved in the process are basically the same – a sublimation and a desorption phenomenon – there will be differences in the shape of the material being freeze-dried, in the resistances affecting the sublimation rate and in the vapor flow dynamics.

A combined simulation that allows quantifying the effect of dryer design on the freeze-drying rate and product attributes requires advanced models that describe the dynamics of the fluid in the drying chamber. CFD allows predicting dynamic process conditions that take into consideration the design of the dryer. The combination of product attributes and equipment capabilities in the same model has great potential in both optimization of the current processes and introduction of new processes.

Chapter 3

Scale-up Investigation – *Streptococcus thermophilus* at Chr. Hansen

Chr. Hansen develops and produces starter cultures, enzymes, probiotics and natural colours for several different applications. Different species of lactic acid bacteria are produced at Chr. Hansen for later application in the production of fermented dairy products, yet this chapter will focus on *Streptococcus thermophilus* as the model organism. *Streptococcus thermophilus*, is one of the most important species at Chr. Hansen since it is used for the manufacture of several important fermented dairy foods, like yoghurt and cheese [147].

A detailed understanding of the principal characteristics of the products being freeze-dried and of the freeze-drying equipment itself, is a prerequisite for a rational development of a mathematical model. Therefore, this chapter focuses on the application of different methods for achieving a better and deeper understanding of the main characteristics of the product and the equipment that might affect the drying process.

3.1 Principal Component Analysis (PCA)

Multivariate Data Analysis (MVDA) is a strong and relatively easy to use tool to analyse large amounts of data, enabling analysis of all associated variables at once.

MVDA finds the typical data pattern for one or more classes of observations. Principal component analysis (PCA) is a multivariate technique that reduces the dimensionality of large datasets but at the same time increases its interpretability and minimizes the loss of information [148]. PCA can reveal groups of observations, trends and outliers.

This thesis focuses on the scale-up of the freeze-drying process. However, not only the scale has an effect on the process, but also different physical properties of the product and the design of the equipment. Therefore, through an exploratory analysis, this section intends to investigate the effect of the product and the equipment on the end properties of the product.

3.1.1 Production Data at Chr. Hansen

Data from six years of production was collected (2012-2017). Eight different production strains of *Streptococcus thermophilus* were selected. The selected production strains originated from different Chr. Hansen sites, and are either freeze-dried in the same or in a different site from where the fermentation step took place. Since this work focuses on the freeze-drying step, data from before and after freeze-drying was used in the PCA analysis. All the selected bulk production runs are dried under the same process conditions (temperature and pressure), yet the drying time is dependent on the site where freeze-drying takes place.

The quality and performance of each produced batch of bulk culture is evaluated through different steps before it is released. Each production strain has its own minimum and maximum specification. If the batch meets the specifications, the culture is internally approved, and immediately released for further processing. The different tests are described below and Table 3.1 indicates the different parameters used for the PCA analysis.

- **Ta, ph–4h, ph-6h and ph-12h -** measured using a CINAC (Alliance Instruments) equipment and software. The method consists in the inoculation of the culture in milk, and the continuous measurement of the pH in milk for 24 hours. Acidification curves are obtained which can be used to determine pH after 4, 6, and 12 hours of fermentation and the time of acidification;
- **Active Cells, Total Cells –** measured through flow cytometry;
- **Yield -** is calculated by measuring the mass of product that comes out of the process;
- **a_w -** water activity is measured with a chilled mirror dewpoint equipment.

Table 3.1 – Parameters used to evaluate the starter cultures before freeze-drying (PFD) and after freeze-drying (FD).

Parameters	Description	Application
Site	Site where a certain batch was fermented and/or freeze-dried.	PFD, FD
Equipment	Fermenter or freeze-dryer chamber where the process took place.	PFD, FD
Type of FD	Type of heat transfer in the freeze-dryer (Radiation, Contact)	FD
Yield	Mass of product that goes out of the process	PFD, FD
Active Cells	Number of active cells	PFD, FD
Total Cells	Number of total cells, including dead and active cells	PFD, FD
pH-6h	pH measurement after 6 hours of fermentation	PFD, FD
Ta	The initial time required to reach an acidification of the medium of 0.1 pH units	PFD, FD
a_w	Is the partial vapour pressure of water in the product after FD divided by the standard state partial vapor pressure of water	FD

3.1.2 PCA of *Streptococcus thermophilus* at Chr. Hansen

A PCA was performed to 1804 batches of the eight different strains in order to choose strains for further investigation. An exploratory analysis of the data was intended. Raw data was inspected in order to remove batches where data was inserted wrongly or had missing values. Since the different variables have different scales it is necessary to pre-process the data as a first step. Autoscaling subtracts the mean value from each sample and then the variable is divided by its standard deviation [149].

Four components were chosen for the PCA model since their eigenvalues exceed one (Kaisers' rule). Outliers were detected through Hotelling's T^2 statistic, and were removed after further investigation.

Figure 3.1 shows the scatter plot of principal components 1 and 2, which explain 46.38 % of the variation in the data. Groupings of the data were observed and four strains representative of each group were chosen for further investigation – ST-B, ST-C, ST-D and ST-H.

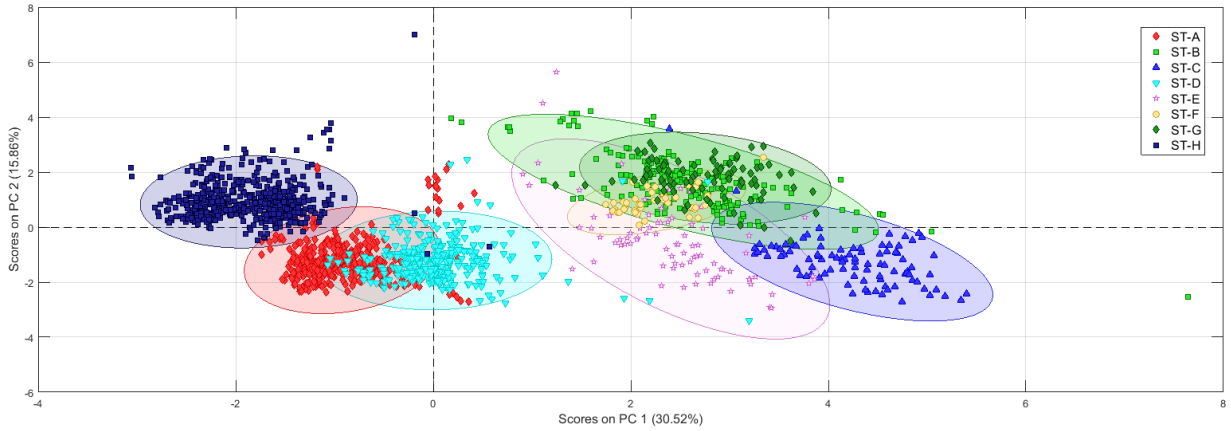

Figure 3.1 – PCA score plot of the first and second principal components of production data of *Streptococcus thermophilus*. The first and second principal components explain 46.38 % of the variation in the dataset.

3.1.3 PCA of the selected *Streptococcus thermophilus*

The same process as described before was applied to the four chosen strains. Once again autoscaling was performed for pre-processing of the data but only 3 components were chosen instead. In addition to the previously studied parameters, the composition of the fermentation media and of the eluate post-centrifugation were now also included in the analysis.

Figure 3.2 shows the bi-plot of principal components 1 and 2, which describe 56.78% of the variation in the dataset. Strains close to each other have similar properties, whereas the ones far from each other

have dissimilar properties. Furthermore, when looking at the loadings, it is known that variables are inversely correlated if they are positioned on opposite sides of the plot origin. For example, it is possible to see that the concentration of lactose in the fermentation broth and of glucose and galactose in the eluate is inversely proportional to the number of active cells before and after freeze-drying. It is also observable that strains with the same lyo- and cryo- additives (ST-B and ST-C) have the tendency to group. However, further investigation is needed in order to understand if there is any correlation between these factors.

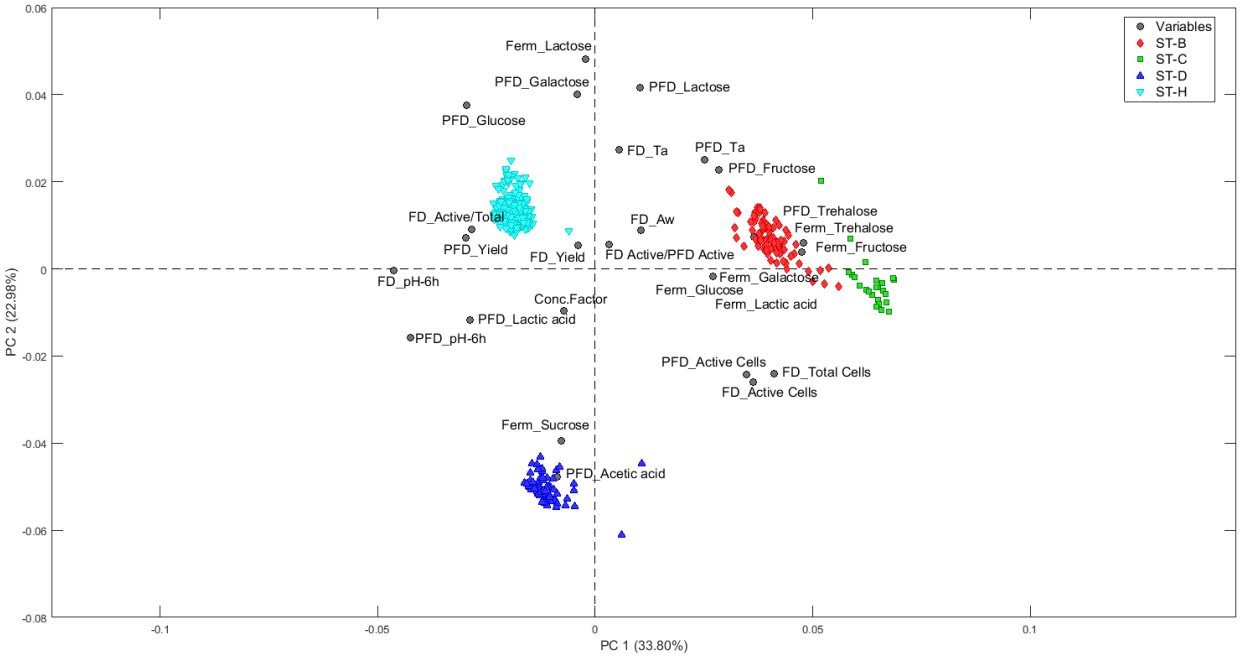

Figure 3.2 – PCA bi-plot of the first and second principal components of production data of the selected strains of *Streptococcus thermophilus*. The first and second principal components explain 56.78 % of the variation in the dataset.

3.1.4 Freeze-drying the same strain at different Chr. Hansen sites

The same process described before was applied to the four chosen samples. Once again autoscaling was performed for pre-processing with 3 components. In addition to the previously studied parameters, the composition of the fermentation media and of the eluate post-centrifugation were also included in the analysis.

As it was previously mentioned, the fermentation step of a certain strain can be performed on one production site and the same batch can be freeze-dried on a different site or even be freeze-dried on several different sites. Therefore, it is relevant to study the effect of different sites on the freeze-drying process. Figure 3.3 shows data from the same strain, ST-H, being freeze-dried in different sites. A

grouping of the data by freeze-drying site is not observed, leading to the conclusion that the freeze-drying site is not affecting the end characteristics of the product. Figure 3.3 shows the principal components 1 and 2, which explain 43% of the variation in the data set.

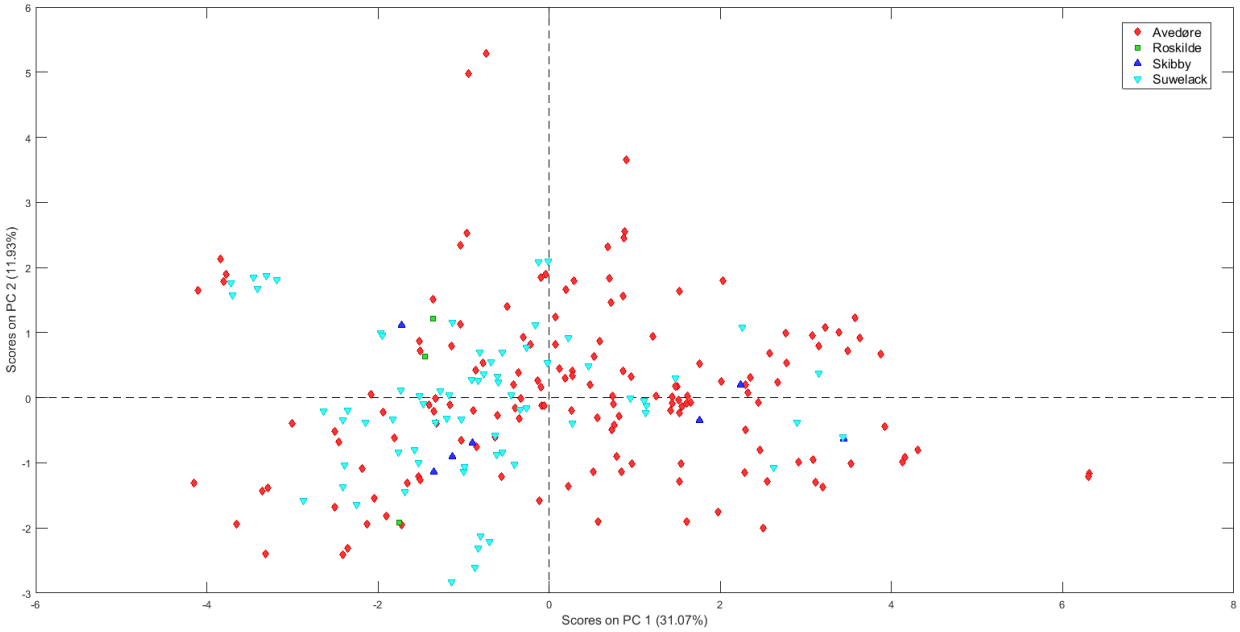

Figure 3.3 – PCA score plot of the first and second principal components of ST-H data on different sites. The first and second principal component explain 43 % of the variation in the dataset.

Furthermore, it is also important to investigate the influence of different types of heat transport during freeze-drying (contact, radiation) on the end product. Once again, from Figure 3.4 it can be observed that there is no grouping of the data for the same strain according to the type of heat transport that was applied.

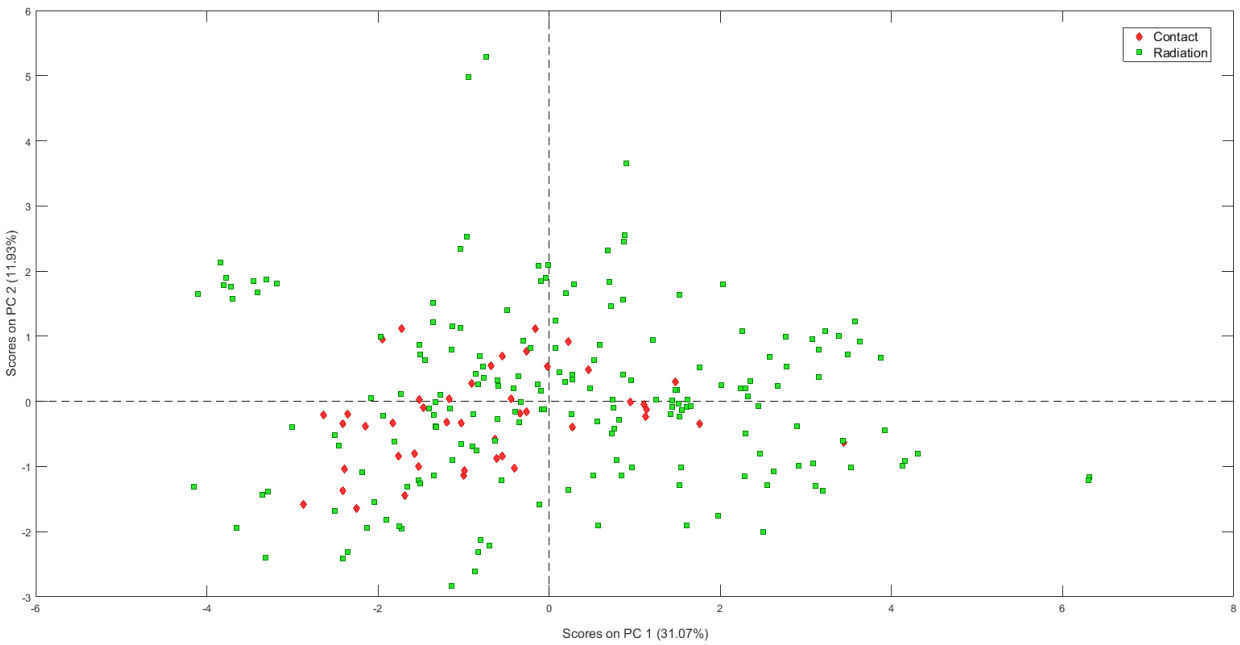

Figure 3.4 - PCA score plot of the first and second principal components of ST-H data on freeze-dryers with different heat transfer methods (radiation/contact). The first and second principal components explain 43 % of the variation in the dataset.

3.2 Product Characterization

Through PCA it was observed that strains with the same cryo-additive have the tendency to group in the scatter plot. Furthermore, it was shown that there exists a correlation between the product composition and the number of active cells. The fermentation medium, the non-consumed substrate and the formed products during fermentation and the added cryo-addictive differ from product to product and will affect the final characteristics of the product. The next section intends to study the physical state of the freeze-dried matrix and its effect on the drying behaviour of the different products. The composition of the growth media in the beginning and at the end of the fermentation step, the composition of the cryo-additives added to the media, the percentage of drying matter present in the product, the glass temperature before and after the addition of cryo-additives, the particle size distribution and the visual morphology of the product will be some of the characteristics analysed in this section.

3.2.1 Methodology

3.2.1.1 Freeze-drying

The four chosen strains were produced and pelletized in the production site Chr. Hansen in Avedøre. The freeze-drying experiments were carried out in a lab scale freeze-dryer (LyoBeta-15, TELSTAR). The product after pelletizing was stored at -55 °C. The freeze-drying chamber and the metal trays used for freeze-drying experiments were cooled down to -55 °C approximately 2 hours before a freeze-drying

experiment. The pellets were loaded onto the metal trays as quick as possible to prevent melting. Only one tray was loaded to the freeze-dyer, which corresponds to approximately 600-700 grams of product. The chamber pressure was set to 0.5 mBar and the shelf temperature to 32 °C.

During all freeze-drying cycles the on-line measurements are the fluid-inlet temperature, the temperature at the condenser, the chamber pressure and total weight. In some experiments the temperature of the product was also measured at different heights with TrackSense Pro data logger (Ellab).

3.2.1.2 Composition of the fermentation broth and eluate

The composition of the fermentation broth and eluate was measured through HPLC analysis with an in-house method developed at Chr.Hansen.

3.2.1.3 Differential Scanning Calorimetry (DSC)

Glass transition temperatures (T_g') were determined through differential scanning calorimetry (DSC, Mettler Toledo DSC822). 40 µl of sample were loaded into an aluminium cup and heated from -100 °C to 0 °C at 7 °C/min.

3.2.1.4 Scanning Electron Microscopy (SEM)

Freeze-dried samples were cut and observed with a scanning electron microscope (SEM, FEI Inspect S). Samples were cut, and applied on an inert carbon adhesive tab and coated with 20 µg of gold for 15 s. The images were produced with an electron beam under vacuum.

3.2.1.5 Dry matter content

The percentage of dry matter present in samples after the addition of lyo- and cryo- additives was measured with a moisture analyser (Sartorius Model MA35). Around 4.8 to 5.2 g of each sample were distributed evenly on a filter paper and the temperature was set to 120 °C. This method removes moisture using heat and it can therefore be applied to measure the amount of dry matter present in the sample.

3.2.1.6 Ice Sublimation tests

Sublimation tests were performed in a laboratory/pilot freeze-dryer (Telstar LyoBeta-15) and a production freeze-dryer (RAY 2, GEA). The trays were filled with ice pellets and inserted in the freeze-dryer. The laboratory/pilot freeze-dryer was loaded with 6 trays, which corresponds to the maximum loading. The production freeze-dryer was loaded with 26 trays, which does not correspond to the maximum loading. Sublimation rates were determined gravimetrically by an on-line scale.

On the laboratory/pilot freeze-dryer, drying was performed at different shelf temperatures (30, 50 and 75 °C) and different pressures (0.2, 0.35 and 0.5 mBar). The freeze-dryer was loaded before each cycle. On the production freeze-dryer drying was performed at different shelf temperatures (30, 50 and 75 °C) and a pressure of 0.5 mBar. Between the cycles at 30 °C and 50 °C the freeze-dryer was not loaded with a new batch of pellets, being at 30 °C for 2 hours and afterwards the shelf temperature was increased to 50 °C.

3.2.2 Results

The first step in the production of lactic acid bacteria cultures is to generate a large number of cells by fermentation. Lactic acid bacteria require complex substrates for growth. Figure 3.5 shows the sugars and acids present in the growth medium of ST-B, ST-C, ST-D and ST-H, confirming that the composition of the growth media is strain dependent.

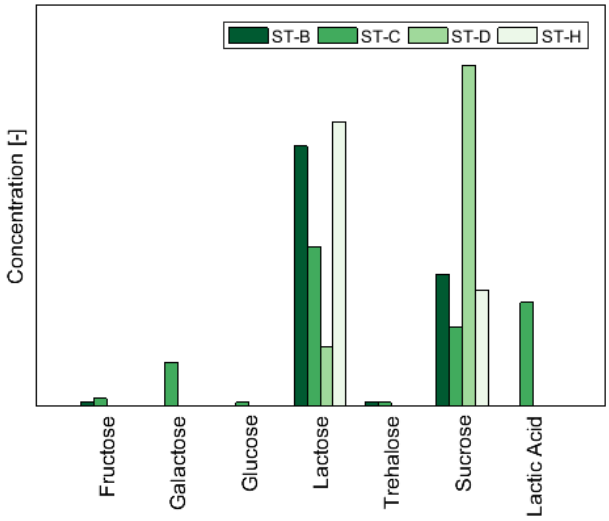

Figure 3.5 – Sugar and acids composition in the fermentation broth of different strains of *Streptococcus thermophilus*. Only relative differences between media are shown for proprietary reasons.

The majority of lactic acid bacteria convert over 50% of the sugar carbon to lactic acid and can be either homo- or heterofermentative [150]. Figure 3.6 shows which components were left in the eluate after centrifugation, where both non-consumed components and components formed during the fermentation step are present. Bacteria do not need to metabolize the carbohydrates in order for them to act as protective agents during drying, therefore it can be relevant to analyse the composition of the eluate since the survival rate can also be influenced by these compounds [14], [39].

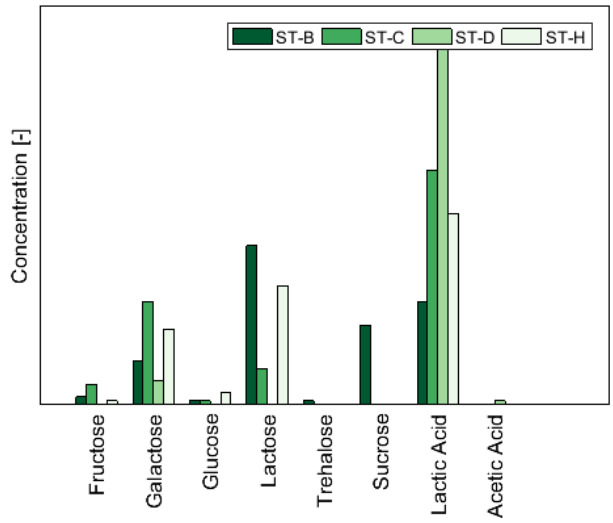

Figure 3.6 – Composition of the eluate after centrifugation of different strains of *Streptococcus thermophilus*. Only relative differences between media are shown for proprietary reasons.

Freeze-drying survival is dependent on fermentation process conditions, such as growth medium and time of harvest [151]–[153]. It is frequently assumed that the optimum growth conditions for the production of biomass also prepare the cell to survive the freeze-drying process, but this is not always the case. Further studies are needed to better understand the effect of growth media, temperature, redox potential, pH, and type of alkali on the survival of the cells in the different strains [154].

The last step before freezing and drying of the product it is the addition of cryo- and lyo- protectants to the media. As it was already discussed in Chapter 2, different components will have different mechanisms of protection. Furthermore, the protection mechanism is also strain dependent. ST-B and ST-C have the same protection additives which are mainly sucrose and maltodextrin. To ST-D mainly skim milk powder is added, and to ST-H sodium caseinate and ascorbate.

Skim milk has been extensively used when freeze-drying lactic acid bacteria since it is easy to dry. The whey and lactose contained in the milk increase the survival of lactic acid bacteria to freeze-drying and the proteins which are also present provide a protective coating for the cells. Lactose, sucrose and maltodextrin have also shown to improve the survival by inhibiting free radical production, forming hydrogen bonds with the protein and increasing the collapse temperature. Ascorbic acid helps to increase recovery rates although it has also been proved to be toxic to the cells in some cases. Through Figure 3.5 and Figure 3.6 and knowing the composition of cryo- and lyo- protectors added, it is possible to know the final composition of the product being dried. However, further studies are needed in order to know the exact effect of each component on the protection of the bacterial viability and on the product structure. Furthermore, the protection mechanism is not only dependent on the components present but also on their concentration [34].

Chapter 2 mentioned the importance and relevance of glass temperature. For aqueous solutions, it has been shown that glass and collapse temperatures have approximately the same value, with less than 3 °C of difference. When observing the thermograms of the different strains it can be seen that it is difficult to identify the step change in the heat flow curve that corresponds to the glass transition temperature. Instead the heat curve decreases over time until it reaches the melting temperature. Table 3.2 shows the approximated measured values of glass temperature of the different strains before and after the addition of cryo- and lyo-protectors. As expected, the addition of cryo- and lyo-protectors increases the glass temperature of the different strains. Nevertheless, Fonseca et al. (2004) have shown that lactic acid bacteria cells give robustness to the freeze-dried product, resulting in increased collapse temperatures and allowing the use of higher sublimation temperatures during primary drying [34]. Therefore, the gap between glass and collapse temperature becomes much higher (about 10 °C) and the use of glass temperature as a first approximation to collapse temperature becomes obsolete. Collapse temperatures can be determined by freeze-drying microscopy. The accuracy of the measurements for bacterial suspensions is quite low and due to time limitations they have not been performed.

Table 3.2 – Glass temperature (Tg') of different frozen samples of *Streptococcus thermophilus* before and after the addition of cryo- and lyo-protectors.

	T_g' without cryo- & lyo- protectors [°C]	T_g' with cryo- & lyo- protectors [°C]
ST-B	- 47.54	- 45.04
ST-C	- 53.87	- 50.01
ST-D	- 57.20	- 52.32
ST-H	- 49.63	- 45.88

Solid-state characterization was carried out by scanning electron microscopy (SEM) and ocular inspection to detect melting, collapse or any change in the product morphology that can explain a change in the drying behaviour. A wide pore size distribution was observable in all the samples, which leads to inaccurate measurements and estimations of average pore size. Nevertheless, SEM analysis revealed that after freeze-drying ST-C, ST-D and ST-H present a less porous layer on the surface (Figure 3.7). The formation of this layer could be due to a micro-collapse of the product, meaning that the surface of the product was exposed to temperatures above its collapse temperature. On the contrary, ST-B presents a porous surface which leads to a facilitated transport of the water vapour.

Inside **Outside**

a)

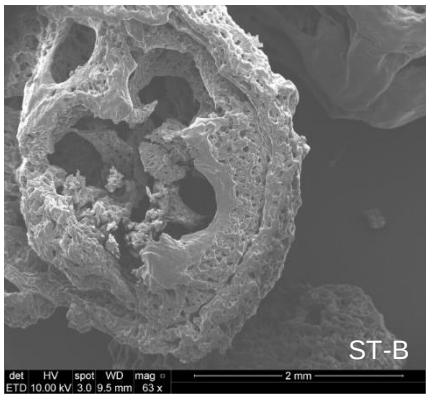

b)

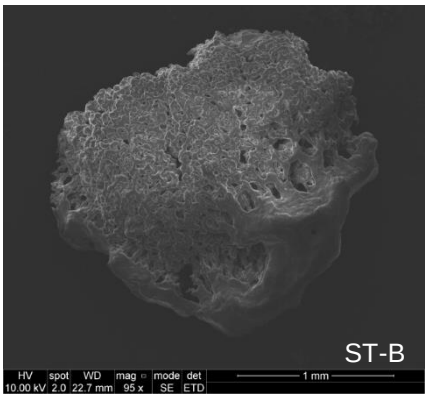

c)

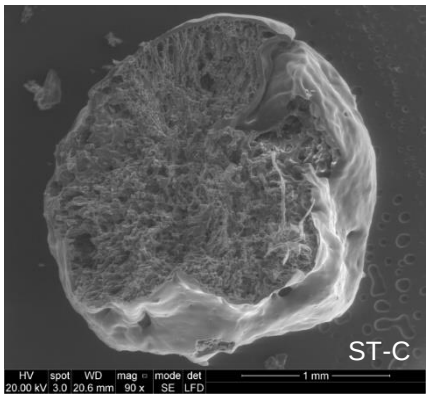

d)

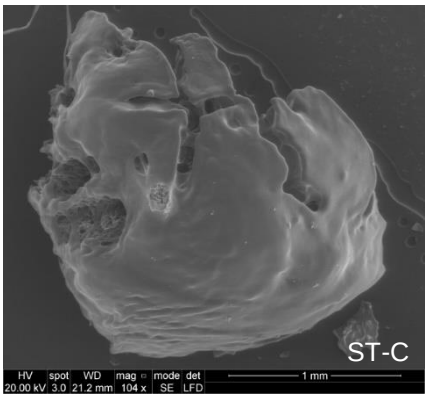

e)

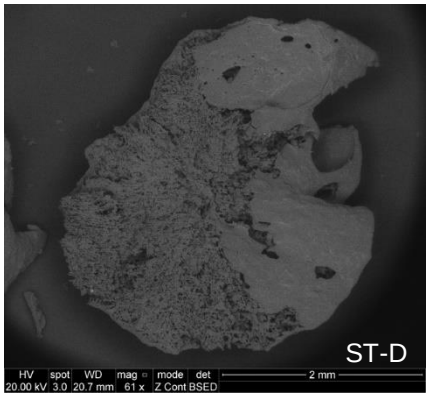

f)

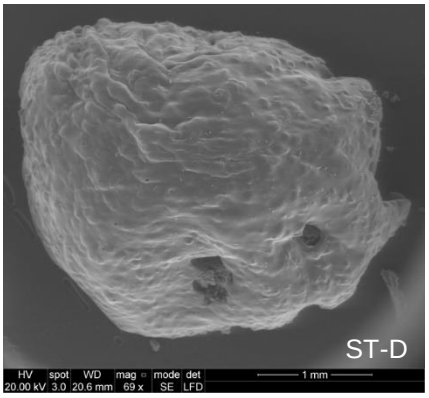

g) h)

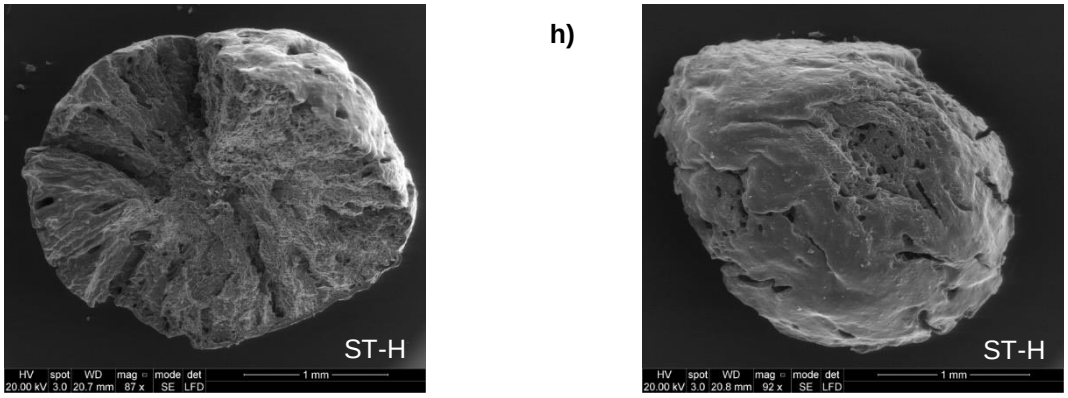

Figure 3.7 – SEM images of the inside and outside of freeze-dried samples of ST-B, ST-C, ST-D and ST-H. Freezing was done by quenching in liquid nitrogen.

Figure 3.8 shows the percentage of dry matter present in the frozen product. It is observed that ST-C is the strain with the highest percentage of dry matter and ST-D the one with the lowest. A higher percentage of dry matter in the product leads to a higher final weight fraction. Additionally, a higher amount of trapped water that cannot be dried will also lead to a higher final weight fraction. However, it cannot be stated that a higher percentage of dry matter results in faster drying since the physical morphology of the product will also influence the drying rate.

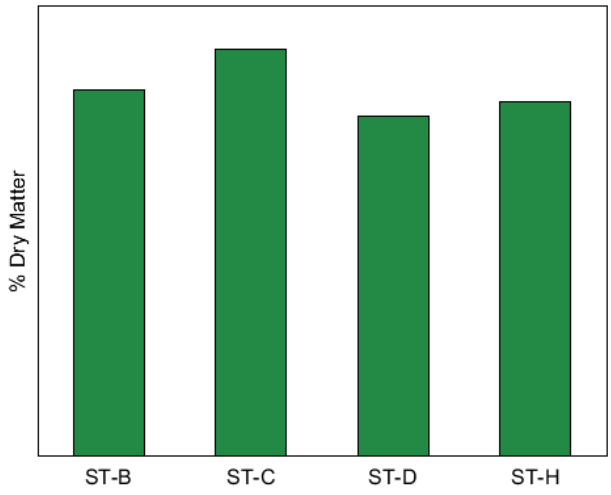

Figure 3.8 – Dry matter percentage of frozen samples of ST-B, ST-C, ST-D and ST-H.

Figure 3.9 shows how the weight fraction of the different strains evolves over time. Throughout this thesis it has been highlighted that drying time can be influenced by cooling rate, existence/absence of annealing, solid concentration, product composition, size and distribution of the pellets and selected process parameters (pressure and temperature). At Chr. Hansen the freezing step is done outside the freeze-drying equipment by dropping the product in liquid nitrogen, and therefore the cooling rate is

mostly constant for the different strains. Furthermore, the annealing process is not applied. Hence, cooling rate and annealing were not considered as influencing factors on the final physical state of the freeze-drying matrix of the different strains considered in this study. Comparing the drying behaviour of ST-C and ST-D, which correspond respectively to the strain with higher percentage of dry matter and the strain with lower percentage, it is possible to conclude that ST-C has a slower drying rate although it contains a lower amount of water. This observation follows the conclusions by Quast and Karel (1962) who showed that higher solute concentration leads to greater resistance of the dry layer to gas flow [155]. Figure 3.9 shows also that ST-B is the strain with the faster drying rate. ST-B and ST-H have an identical amount of dry matter in their composition. However, when comparing the drying profiles, it is observable that the drying rates are very different. Figure 3.7 shows a different morphology of the dried products, where ST-B presents a more porous outer layer and ST-H smaller pores and a melted outer layer. Since the drying conditions (pressure and temperature) were the same, the differences in their behaviour are most probably due to differences in their composition. It is well-known that the composition of the product will strongly influence the physical state of the freeze-dried matrix and the viability of dried lactic acid bacteria, yet further studies are needed to understand to which extent they are affected. Table 3.2 concludes that both strains have approximately the same T_g', however in starter cultures the robustness is increased due to the presence of lactic acid bacteria, and therefore it is the collapse temperature (T_c') that determines the occurrence/absence of melting/collapse.

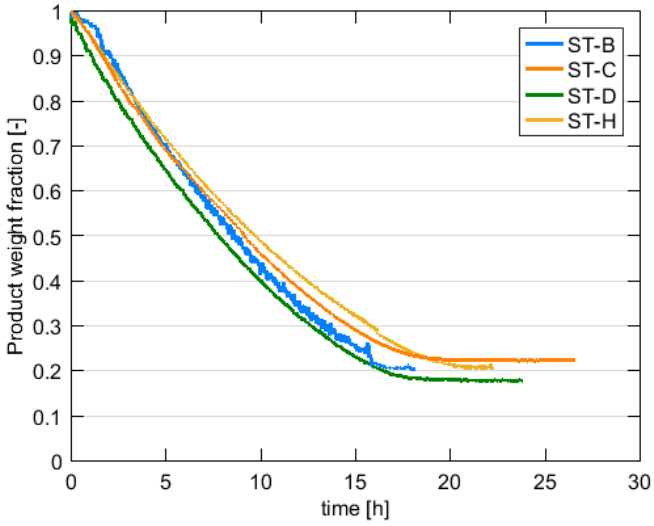

Figure 3.9 – Fraction of product weight per drying time. Measurements of one single tray of product loaded in a laboratory/pilot freeze-dryer. Different strains of *Streptococcus thermophilus* were investigated (ST-B, ST-C, ST-D, ST-H).

Therefore, it is possible to conclude from Figure 3.9 and through the different methods for product characterization that further studies are needed in order to better understand the drying behaviour of the different strains.

3.3 Equipment Characterization

Through PCA analysis it was shown that the same strain freeze-dried in different Chr. Hansen sites does not present considerable differences in terms of product quality. However, it is known that each site has a different freeze-drying equipment, and therefore the drying profiles had to be adapted to the characteristics of each freeze-dryer. Freeze-dryers can mainly differ in drying chamber size, condenser capacity and location (outside or inside the drying chamber) and heating method (contact or radiation). This section intends to characterize a laboratory/pilot scale freeze-dryer and a production freeze-dryer.

3.3.1 Design Characteristics

Heat and mass transfer are determinant success factors of a freeze-drying cycle. In order to account for scale-up factors related to freeze-drying equipment design and capacity, the equipment must be thoroughly characterized. The relevant performance components include shelves, chamber and condenser design.

The two characterized freeze-dryers are the laboratory/pilot freeze-dryer located at Chr.Hansen Hørsholm and the production freeze-dryer located at Chr.Hansen Avedøre. Table 3.3 summarizes some of the freeze-dryers' basic characteristics. The trapping rate of the condenser is an important parameter and is related to the design of the condenser (size and shape). The ratio between the condenser and the shelf surface shows the capacity of the condenser. From Table 3.3 both condensers seem to have similar capacity. However, it has been shown by Ganguly et al. [2012] that it is also important to consider the design of the condenser since it will influence the way that ice accumulates on the coils [71], [107]. Furthermore, also the position of the condenser might influence the sublimation rate. The temperature of the condenser is not as important as its design. However, it is essential to ensure that the temperature of the condenser is below the temperature of the chamber. The trapping rate might decrease as the ice builds up since the temperature of the ice surface is not as cold as the condenser surface.

Furthermore, it has been studied that in the case of vial freeze-drying the vials closer to the door and the walls have a higher drying rate due to additional radiation heat. In the case of bulk freeze-drying the same phenomena will happen [31]. Additionally, Table 3.3 shows that the laboratory/pilot scale freeze-dryer has a door made of transparent acrylic which can also lead to increased radiation heat since this material has a higher emissivity [115].

Table 3.3 – Properties of a laboratory/pilot freeze-dryer (Telstar) and a production freeze dryer (RAY).

	Telstar	**RAY**
Type of heating	Radiation	Radiation
Door	Transparent acrylic	Stainless steel
Surface area of shelves [m^2]	0.363	114
Maximum capacity of condenser [kg]	30	2200
Surface area of condenser [m^2]	0.171	57.64
Ratio between condenser and shelf surface area	0.471	0.506
Condenser temperature [°C]	- 80	- 47
Condenser partial pressure [mbar]	0.000547	0.055

3.3.2 Shelf heat transfer coefficient

Heat transfer into the product occurs through different mechanisms: radiation, conduction and convection. Sublimation tests were performed in order to calculate the shelf heat transfer coefficient. Pelletized deionized water was loaded into trays and Equation (3.1) was used to calculate the heat transfer coefficient.

$$HTC = \frac{\Delta H_{sub} \cdot dm/dt}{A_{shelf} \cdot (T_{heating\ plate} - T_{bottom\ tray})} \quad (3.1)$$

Figure 3.10 shows the estimated values of heat transfer coefficient for a laboratory/pilot freeze-dryer and a production freeze-dryer. It is concluded that, in the studied range, the heat transfer coefficient for the laboratory/pilot scale is not pressure dependent but temperature dependent. For the production equipment a constant heat transfer coefficient was observed which is not dependent on temperature and pressure. It was also observed that the production equipment has a six times lower heat transfer coefficient, which will result in a slower process.

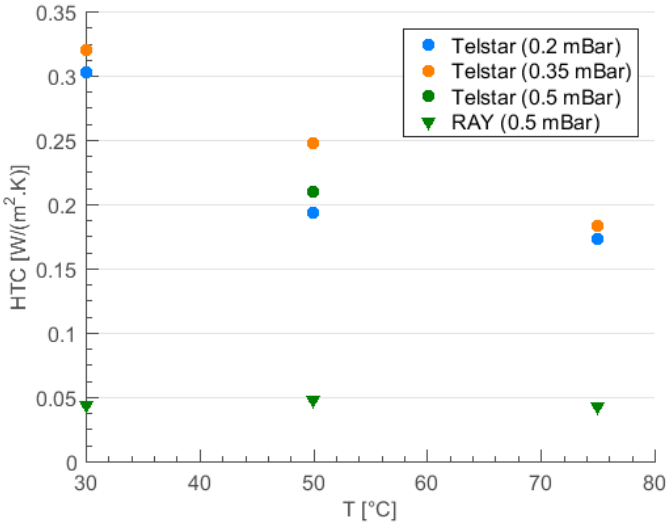

Figure 3.10 – Heat transfer coefficient for different temperatures and pressures for a laboratory/pilot freeze-dryer (Telstar) and a production freeze-dryer (RAY).

3.4 Conclusions

This chapter gave a general overview of the freeze-drying process and of the product and equipment characteristics at Chr. Hansen. Important considerations for the development of a mathematical model that describes the freeze-drying process were investigated and discussed. When modelling, it is not possible to fully represent all details of the real system, and some assumptions and approximations must be made.

Section 3.3 described different methods for product characterization and investigated some of the differences between different products dried under the same process conditions (temperature and pressure) and on the same freeze-drying equipment. The challenges to characterize freeze-dried lactic acid bacteria were discussed. A summary of the characteristics of freeze-dried lactic acid bacteria required to better describe the process can be found below.

- The average porosity and pore size diameter is not constant inside a single particle;
- The porosity between particles is dependent on the way that the trays are filled and on the average size of the particles;
- The matrix of the freeze-dried products and the absence /occurrence of melting and collapse is dependent on the product composition and process parameters;
- The survival of the bacteria during freeze-drying is dependent on protection mechanisms that are strain dependent and also composition dependent. The survival of the bacteria is also dependent on the process parameters.

However, it will not be possible to fully describe these characteristics in the mathematical model developed. An average pore size distribution and porosity inside the pellet and between pellets will be assumed for model development. Furthermore, the collapse of the pellet will change the morphology of the product which will lead to changes in vapour flow and consequently will influence drying rates. Since it is very difficult to quantify and predict these changes, the collapse phenomenon will be disregarded in the model. The model will only be able to predict physical properties of the process; therefore, it will also not be possible to predict the survival of the bacteria.

Section 3.4 described the main differences between a lab/pilot freeze-dryer and a production freeze-dryer. A summary of the main characteristics of the different scales that are relevant for the model development are described below.

- The position, design and capacity of the condenser might affect the freeze-dryer performance;
- The material of the freeze-dryer can influence the way that heat is transferred to the product;
- The transferred heat to the shelves and the sublimation rate will depend on their position;
- The heat transfer coefficient in the studied range is mainly affected by temperature. This effect is mainly observed in the lab/pilot freeze-dryer. The heat transfer coefficient decreases with the increase of temperature;
- The heat transfer coefficient is lower in the production freeze-dryer.

A simplified geometry of the equipment will be considered when developing the mathematical model. Furthermore, a constant heat transfer from the shelves will be considered throughout all the equipment.

Summarizing, this chapter gives an overview of different methods to characterize different products and equipment in order to better understand the assumptions and approximations made for the later development of the mathematical model.

Chapter 4

Drying of a Single Particle

Freeze-drying is both dependent on the physical form of the material to be dried and on the physical parameters and characteristics of the freeze-dryer itself. Different types of product containers (vials, trays, syringes, etc.) are used dependent on the physical characteristics of the product, and depending on its final application. As mentioned in the previous chapters, this work focuses on bulk freeze-drying where particles have irregular shapes and are randomly distributed in the trays.

Drying of frozen particulate matter is characterized by a bimodal pore size distribution: 1) Pore size distribution of the bed of particles which is determined by the particle size and packing, and 2) Pore size distribution inside each particle which is dependent on the initial solid concentration and on the freezing rate. The ratio between the two pore size distributions will influence primary drying rates.

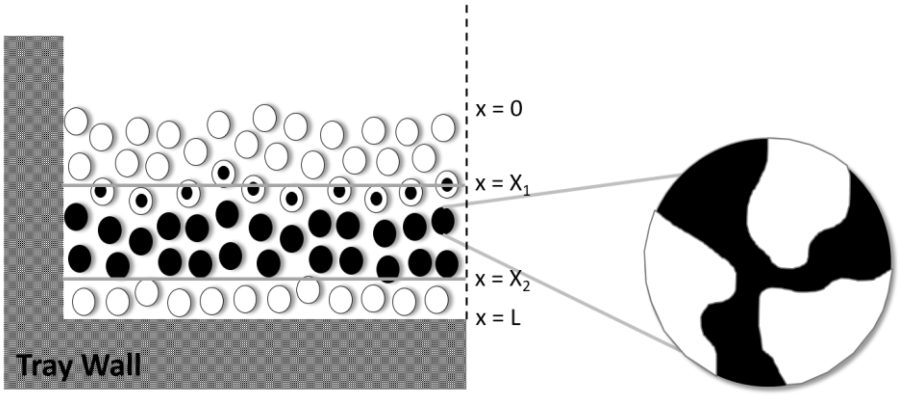

Figure 4.1 – Drying of a bulk tray characterized by a bimodal pore size distribution. 1) pore size distribution of the bed of particles; and, 2) pore size distribution inside each particle. Black represents frozen material and white dried material. X1 and X2 represent two moving sublimation fronts.

This chapter focuses on mass transfer processes occurring in a single particle during primary drying. A greater and more comprehensive understanding of the phenomena occurring at the product scale is the starting point for the development of a detailed model able to predict drying rates, product temperature and pressure profiles of a complete process.

Fundamental knowledge of the mass transfer process during primary drying of lyophilization was obtained using freeze-drying microscopy (FDM) and a micro-computed tomography (µ-CT) imaging system followed by image analysis. Total mass transfer is mainly determined by two types of flow: viscous flow which is driven by a total pressure gradient and described by Darcy's law, and molecular flow which is driven by a concentration gradient. In this study it will be assumed that the saturation pressure at the

sublimation front is equal to the chamber pressure, and therefore the contribution of the viscous flow is assumed to be negligible [156].

A model based on computational fluid dynamics (CFD) tools for the prediction of drying times of a single particle being freeze-dried will be developed. The developed model will be validated with experimental data obtained by use of a freeze-drying microscope (FDM).

4.1 Mechanisms of Mass Transport in Porous Material

Throughout primary drying the mass transfer is dominated by three different steps: 1) ice sublimation, 2) water vapour transfer from the interface between the frozen mass and the dried cake to the outer edge of the product, and 3) water vapour transfer from the edge of the product to the chamber and to the condenser [157]. The next sections will describe in detail the mass transport phenomena connected to each step.

4.1.1 Ice Sublimation

Sublimation is the process in which a substance transitions from the solid phase to the gas phase, without passing through a liquid phase. It is an endothermic phase change, meaning that heat is absorbed by the system. This phenomenon is given by Equation (3.1) developed by Heinrich Hertz and Martin Knudsen, typically known as the Hertz-Knudsen equation [158]. It is derived from the kinetic theory of gases assuming an equilibrium distribution of molecular velocity, and in its original form the dimensionless coefficient α is equal to 1.

$$\frac{dm_{ice}}{dt} = \alpha\, A_{surface} \sqrt{\frac{M_W}{2\pi RT}} (p_{sat} - p) \tag{4.1}$$

The difference of pressure between the vapour pressure (p) above the sublimation surface and the pressure (p_{sat}) corresponding to the phase equilibrium at the product temperature (T), will determine the sublimation/condensation rate. Sublimation takes place when $\Delta p < 0$ and condensation when $\Delta p > 0$. The saturation pressure will be determined by the Clausius-Clapeyron equation and it will be dependent on the product temperature.

$$ln\frac{p_{sat}}{p_{tr}} = -\frac{\Delta H_{subl}}{R}\left(\frac{1}{T_{prod}} - \frac{1}{T_{tr}}\right) \tag{4.2}$$

4.1.2 Water Vapour Transport

Three different types of flow are generally encountered in vacuum technology: bulk or continuous flow, molecular flow and Knudsen flow. The Knudsen number (Kn) is the dimensionless parameter that defines the type of flow studied. This parameter is defined by Equation (2.1) as the ratio between the molecular mean free path (λ) and the characteristic length (d_e) of the channel through which the gas is flowing. Equation (4.4) defines the molecular mean free path and it is estimated from the kinetic theory of gases.

$$Kn = \frac{\lambda}{d_e} \tag{4.3}$$

$$\lambda = \frac{3.2\mu}{P}\left(\frac{RT}{2\pi M_w}\right)^{0.5} \tag{4.4}$$

During primary drying four different mass transfer mechanisms are involved: 1) Darcy diffusion, 2) bulk flow, 3) Knudsen flow, and 4) slip flow [159]. Darcy flow occurs due to the existence of a gradient in total pressure. Bulk and Knudsen flow occur due to a partial water vapour pressure gradient. The value of Kn determines if the flow is defined by bulk or Knudsen flow. The mass transport due to slip flow is characterized by non-equilibrium effects (slip velocity and temperature jump) near the walls but continuum within the fluid bulk [160]. This phenomenon is relatively small when compared to the other three mechanisms, and therefore it will be disregarded in this study.

4.1.2.1 Mass transfer under normal molar motion

When the mean free path is much smaller than the characteristic dimension of the channel (Kn < 0.01), the flow is viscous. This will occur mainly in the high-pressure range of the lyophilisation process since the collision among gas molecules occurs more frequently than collisions between gas molecules and the channel walls.

Fick's law determines the mass flux through the dried cake due to gradients in the molar fractions. The mass flux will only depend on bulk diffusion.

$$N_w^D = -\frac{D_{bulk}}{R}\nabla\left(\frac{p_w}{T}\right) \approx -\frac{D_{bulk}}{R}\nabla p_w \tag{4.5}$$

The bulk diffusion coefficient D_{bulk} can be described by Equation (4.6) [159].

$$D_{bulk} = \frac{1.882 \times 10^{-22} T^{3/2}\left[\frac{M_W + M_{Air}}{M_W M_{Air}}\right]^{1/2}}{P\sigma_{W,Air}^2 \Omega_D} \tag{4.6}$$

Ω_D denotes the "collision integral", a dimensionless function of $k_BT/\varepsilon_{W,Air}$, where $\varepsilon_{W,Air}$ is the characteristic energy of interaction between the molecules and k_B is the Boltzmann constant.

The Hagen-Poiseuille law or Darcy's law determines the mass flux caused by viscous flow due to the existence of a pressure gradient.

$$N_w^v = -\frac{r_e^2}{8\mu}\rho_w \nabla P = -\frac{r_e^2}{8\mu}\frac{p_w}{RT}\nabla P = -\frac{c_0}{RT}p_w \nabla P \quad (4.7)$$

When a total pressure gradient exists, the overall mass flux under normal molar motion includes both the contributions from diffusion due to a molar fraction gradient and from viscous flow due to the total pressure gradient.

$$N_w = N_w^D + N_w^v = -\frac{D_{bulk}}{RT}\nabla p_w - \frac{c_0}{RT}p_w \nabla P \quad (4.8)$$

4.1.2.2 Mass transfer under molecular motion

At low pressures the mean free path is larger in comparison to the characteristic dimension d_e (Kn>1), therefore mass transfer is limited by molecular collisions with the channel walls. Flow at large Knudsen numbers is therefore called free-molecule flow, or Knudsen flow. In this regime the gas moves only under the influence of the thermal motion of the molecules and neither laminar nor turbulent flows can be formed. The total flux is controlled by Knudsen diffusion.

$$N_w^K = -\frac{8}{3}\sqrt{\frac{1}{2\pi R M_w T}}\, r_e \nabla p_w = -\frac{D_{Kn}}{RT}\nabla p_w \quad (4.9)$$

D_{Kn} is the Knudsen diffusivity and can be determined by the following equation if the particle sizes are known [161].

$$D_{Kn} = \frac{2}{3} \times r_e \times \left(\frac{8RT}{\pi M_W}\right)^{1/2} \quad (4.10)$$

4.1.2.3 Mass transfer in the transition range

The transition from viscous flow to Knudsen flow occurs at intermediate values of the Knudsen number (0.01 < Kn < 1). Both collisions between the gas molecules and the channel walls and among gas molecules influence the flow characteristics [162]. Therefore, in this range the overall mass transfer coefficient is given by the sum of both molar and molecular mass transfer coefficients [163].The overall diffusivity can be approximated by the Bonsaquet's formula given in Equation (4.11).

$$D = (D_{bulk}^{-1} + D_{Kn}^{-1})^{-1} \quad (4.11)$$

$$D_{bulk} = \frac{1}{3} \cdot \lambda \cdot \bar{v} \tag{4.12}$$

$$D_{Kn} = \frac{1}{3} \cdot l \cdot \bar{v} \tag{4.13}$$

where λ is the mean free path and l is the characteristic length of the porous medium, typically the pore diameter. $\bar{v}$ is the mean thermal velocity of a gas and it is given by Equation (4.14).

$$\bar{v} = \sqrt{\frac{8RT}{\pi M_w}} \tag{4.14}$$

4.2 Experimental Work

Freeze-drying microscopy (FDM) or lyomicroscopy is a common method for characterization of formulations at laboratory scale. The most common use of FDM is the estimation of collapse temperature, however, recently, different applications can be found in literature. Zhai et al. (2003) have developed a method for the description of mass transfer during primary drying through FDM studies [156]. Measured drying rates were modelled by an effective diffusion coefficient ($D_{K,eff}$). Borgognoni et al. (2012) studied the sublimation rate of bovine pericardium by determining the velocity of the moving sublimation front [164]. Raman (2015) investigated the sublimation kinetics of lactose and coffee samples [165].

X-ray microcomputed tomography (µ-CT) is a non-destructive and non-invasive technique that has, in the past years, become a common method for the evaluation of the physical structure of products. Its main applications are microstructural characterization and quantification and visualization of pore structure and size distribution [129], [166], [167]. Furthermore, Pisano et al. (2017) coupled 3D X-ray microcomputed tomography with mathematical modelling in order to estimate the resistance of the dried layer to water vapour mass transfer [168].

This section describes the developed experimental work to study the effect of solid content, freezing rate and annealing on product morphology. Annealing is an optional process step during freezing where the temperature of the substance is raised to a sub-freezing point for a defined period of time and then returns to the freezing temperature. This process intends to decrease the drying time by increasing the size of the ice crystals.

4.2.1 Methodology

4.2.1.1 Sample Preparation

Maltodextrin solution (DE 10-14 from medesign I.C. GmbH) was used as a model system. Maltodextrin solutions (5, 10 and 20% w/w) were prepared by using bi-distilled water. A sample of 10 µl was loaded on a silver block. Four different cooling profiles (slow cooling, fast cooling, Annealing I, Annealing II) were investigated which resulted in 6 different samples. The characteristics of the different samples are shown in Table 4.1.

Table 4.1 – Experimental conditions for sample preparation (concentration, cooling rate and annealing).

	Concentration [%]	Cooling Rate [°C/min]	Annealing
Sample 1	5	0.5	
Sample 2	10	0.5	
Sample 3	10	20	
Sample 4	10	20	Annealing I: - 5 °C for 180 min
Sample 5	10	20	Annealing II: - 10 °C for 90 min
Sample 6	20	0.5	

4.2.1.2 Freeze-Drying Microscope

Experiments were conducted in a freeze-drying microscope in order to study sublimation kinetics of a single particle. The experimental arrangement consists of an Olympus BX51 polarized light microscope (Olympus Microscopy, Essex, UK) with a Linkam FDCS196 freeze-drying cryostage (Linkam Instruments, Tadworth, UK) coupled to a Pixelink PL-A662 camera (Pixelink, Rochester, USA) and it is shown in Figure 4.2. The used vacuum pump was an Edwards rotary vane pump E2M1.5 (Edwards, Burgess Hill, UK). The pressure was measured by a Pirani gauge controlled via a mechanically adjustable fine-regulating needle valve.

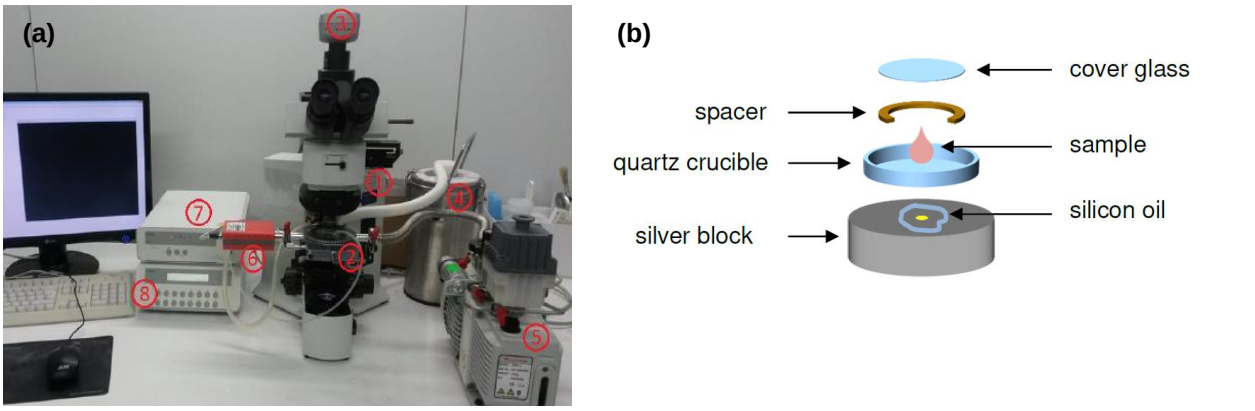

Figure 4.2 – Freeze-drying microscope setup. (a) 1. Olympus BX51 microscope, 2. Linkam FDCS196 variable temperature cryostage, 3. Pixelink PL-A662 camera, 4. Liquid nitrogen container, 5. Vacuum pump, 6. Pirani gauge, 7. Liquid nitrogen pump, 8. Temperature controller. (b) Graphic representation of the sample loader on the freeze-drying microscope.

A cylindrical sample was prepared by placing a 15 mm diameter quartz glass crucible covered with a glass coverslip (13 mm diameter, 0.17 mm thickness) onto a temperature-controlled silver block in the stage. A shim spacer (690 µm) was placed in between the coverslip and the crucible to achieve a uniform thickness. 10 µl of sample were loaded, forming a cylindrical disk with a diameter of 4.3 mm and a height of 690 µm. Silicone oil was used to reach good thermal contact between the silver block and the bottom of the lower coverslip.

The temperature of the silver block was controlled by a combination of liquid nitrogen cooling and electrical heating within the block. The temperature profile was set via the software Linksys 32 (Linkam Instruments, Tadworth, UK). Liquid nitrogen was drawn from the thermos container into the stage by means of a pump integrated in the cooling control unit. Temperature was measured using a Pt100 temperature sensor from Linkam Instruments (accuracy ± 0.1 °C). The nitrogen vapour supply also functioned as a condenser within the drying chamber.

After placing the liquid sample onto the quartz crucible of the cryostage, the stage was sealed and all samples were cooled to -50°C at a defined cooling rate. Two different cooling rates were investigated: 0.5 °C/min and 20 °C/min (Table 4.2). Furthermore, two annealing treatments were investigated: in Annealing I the sample was heated to -5 °C after freezing for 180 min and cooled back to -50 °C, and in Annealing II the sample was heated to -10 °C for 90 min after freezing and cooled back to -50 °C (Table 4.2). The subsequent drying step was carried out with constant drying conditions with a shelf temperature of -18 °C and a pressure of 10 Pa. To evaluate the drying front, a picture was taken every 10 s during primary drying. As soon as primary drying was finished, which was determined by the disappearance of the drying front, the silver block was heated to 30 °C and the secondary drying was carried out overnight until a final water content of approximately 2% was achieved. The secondary drying was carried out to get a stable sample that can be used for further investigations. The samples were then carefully taken out of the cryostage and stored in a desiccator until further evaluation of the dry pore structure by µ-CT.

The drying front was observed by a change in brightness as shown in Figure 4.3. The dry part appears much darker than the frozen part due to stronger light scattering. The evaluation of the drying rate is described in Section 4.2.1.4.

Figure 4.3 – Picture of the drying process performed on a lyomicroscope.. The dark colour corresponds to the dry part of the product and the light colour to the frozen product.

4.2.1.3 X-ray µ-computed tomography measurements & Image analysis

Three-dimensional X-ray µ-CT scans were performed using the XCT1600 system from Nordson Matrix Technologies GmbH (Feldkirchen, Germany). The cylindrical freeze-dried cakes from the FDM were cut with a razor knife to prepare cuboid pieces (2 x 2 x 2 mm). The samples were scanned in at atmospheric conditions and the imaging system was adjusted to operate at a tube voltage of 60 kV and current intensity of 20 µA. X-ray shadow images were acquired with a pixel resolution of 1 µm and 2000 projections with an exposure time of 4487 ms resulting in a total scanning of 160 min. The obtained images were reconstructed into a series of 2-D images using the CERA Xplorer software (Siemens Healthcare GmbH, Erlangen). The resulting 3-D images consisted of more than 2000 slices encoded in 16-bit precision.

For quantitative evaluation of pore size, image processing and analysis were done with the software Modular Algorithms for Volume Images (MAVI) from Fraunhofer ITWM (Fraunhofer Institute for Industrial Mathematics, Kaiserslautern, Germany) and GeoDict (Math2Market GmbH, Kaiserslautern, Germany). Figure 4.4 shows part of the image analysis steps performed with MAVI. First, the original data set was cropped into three cubic sub-volumes of 400x400x400 voxels equivalent to 400x400x400 μm^3 (Figure 4.4 a)). Afterwards, a global threshold was defined to separate pores and solid. For simplicity, the global threshold was adjusted to the water content in the solutions; i.e. 0.8 for the 20% solution, 0.9 for the 10% solution and 0.95 for the 5% solution. After transformation of the greyscale into binary images (Figure 4.4 b)), a Euclidean distance transformation was carried out, which created a distance map by assigning each background voxel a grey value based on the distance to the closest foreground voxel (Figure 4.4 c)). Thereby, local minima were identified. To avoid over-segmentation of pore structure, h-minima transformation was then performed with a global value of h = 10. This value was chosen by comparison of

the results with the two-dimensional ice-crystal structure (results not showed in this thesis). Subsequently, the individual pores were segmented using the watershed segmentation method. All remaining regional minima served as water sources for the flooding. The lines where water from different basins met were identified as the watershed lines. Separated cells were produced from the logical difference between the watershed lines and the initial binary image (Figure 4.4 d)). Finally, the object features tool of MAVI was used to obtain the volume of the individual pores. The equivalent pore diameter values were determined by calculating the diameters of spheres corresponding to the pore volumes. Therefore the equivalent diameter x_v of a sphere with the same volume was determined.

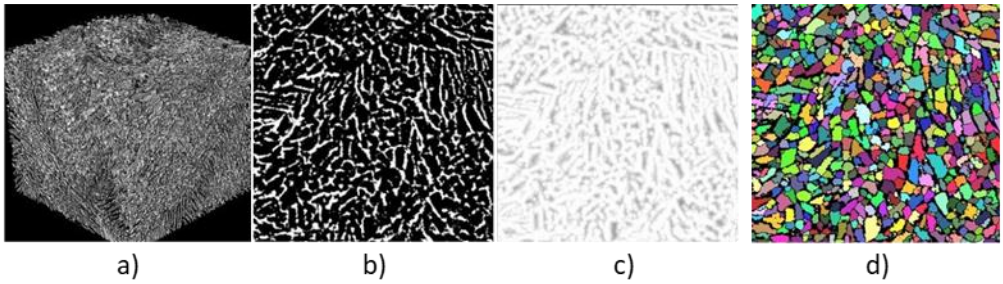

Figure 4.4 – Performed steps for image analysis with MAVI: a) 3D image of cubic sub-volumes of 400x400x400 voxels, b) binarized image, c) distance map after Euclidean distance transform, and d) watershed image.

4.2.1.4 Evaluation of drying rate from lyomicroscopic measurements

After holding the sample at -50°C for 15 min the pressure was decreased to 10 Pa by a rotary vane pump. Then the samples were heated to -18 °C at a rate of 3 °C/min. Due to the discoidal geometry of the sample, the drying proceeded in the radial direction. As the dried part of the sample appears much darker than the frozen part, the radial drying front can be easily visualized (Figure 4.3). The drying front was measured at three positions for each time step with the help of Linksys 32 (Linkam Instruments, Tadworth, UK). Figure 4.5 shows the measuring method. The distance between the edge of the sample (R_0) and the drying front over time r(t) was measured at three positions every minute. From the movement of the drying front Δr the drying rate was calculated according to Equation (4.15). The primary drying time (t) was determined from lyomicroscopic measurements for $r = R_0$.

$$\frac{dm}{dt} = \frac{\rho_{ice} \cdot 2\pi r(t) \cdot h \cdot \theta \cdot \Delta r}{\Delta t} \tag{4.15}$$

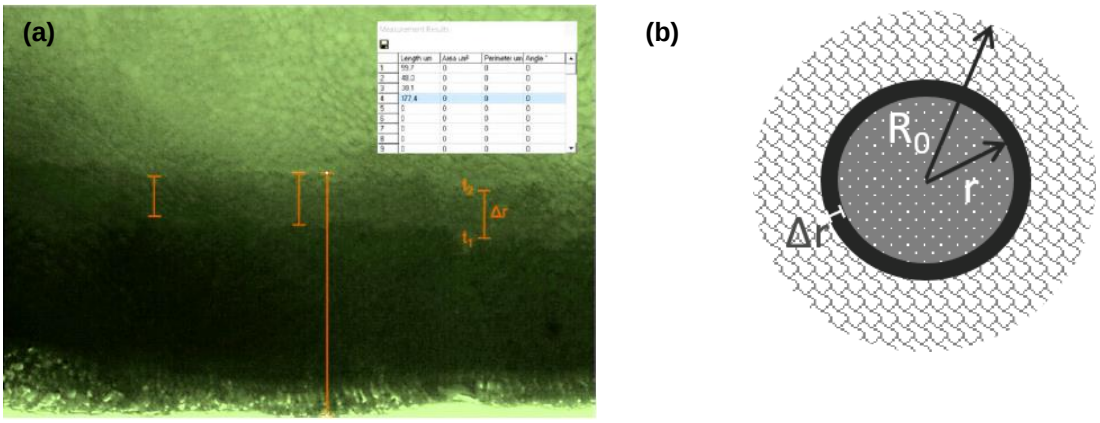

Figure 4.5 – (a) Freeze-dried sample on a lyomicroscope. Measurements of ∆r and R_0-r are represented. (b) Schematic representation of the primary drying process on a lyomicroscope. ∆r is the incremental thickness of the dried cake over a small interval ∆t, r is the radius of the frozen mass and R_0 is the radius of the original sample.

4.2.2 Results and Discussion

4.2.2.1 Morphology of dried cake

The composition of the product and the freezing step will determine the morphology of the product which will have a great effect on the drying behaviour. Therefore, it is of major importance to investigate and establish the relation between product morphology and drying behaviour. Parameters like porosity, average pore size, pore size distribution and tortuosity have a high impact on the effective diffusivity and consequently on the drying time.

Porosity is the volume of void or gas to the total volume (V_{void}/V_{total}), meaning that higher values of porosity correspond to dried products with low density, which facilitates the movement of vapour [169]. Pore size and pore size distribution determine the pattern of internal water transport over the course of the drying process. Therefore, larger pores will ease the mass transport across the porous media [169]. Tortuosity is the ratio between the straight distance connecting two points and the actual path length inside the porous medium, hence lower values of tortuosity are preferable in order to have higher diffusivity.

In the present study the product morphology of maltodextrin samples freeze-dried on a FDM have been analysed by µ-CT scans. Table 4.2 shows the estimated values of average porosity, pore size diameter and tortuosity.

It was found that solid concentration has a large impact on ice crystal size, which is in agreement with the study made by Flores and Goff (1999) which showed decreasing ice crystals with increasing solid concentration for ice cream [170]. The smallest pores were observed for a solid concentration of 20% (Sample 6) and the largest pores for 5% solid concentration (Sample 1).

An annealing treatment at sufficiently high temperatures (Annealing I at -5 °C, Sample 4), lead to much larger ice crystals and a broader ice crystal size distribution (Appendix A). However, no significant difference is observed for the samples that were held at -10 °C for 90 min (Annealing II, Sample 5). Smith et al. (2013) have measured the glass transition temperature of 10% w/w maltodextrin to be -17 °C [171]. Annealing must be performed above the glass temperature in order to enhance the mobility of water molecules which then facilitates diffusion to the ice front and ice crystal growth [172]. The sample where Annealing II was completed (Sample 5) was only 7 degrees above the glass transition temperature which might not be sufficient to detect a difference on the ice crystal size.

Table 4.2 shows that the cooling rate has no significant influence on ice crystal size distribution as both cooling rates lead to the same pore size (Sample 2 and Sample 3). However, a correlation between the freezing rate and the ice crystals size has been extensively reported in literature [21], [167], [169], [173]. Hottot et al. (2004) and Searles et al. (2001) have shown that higher cooling rate lead to a higher degree of super cooling and smaller ice crystals [174], [175]. However, this conclusion could not be confirmed in this study. One of the explanations for the observed results can be that the difference between the two cooling rates (0.5 °C/min and 20 °C/min) is too small to detect a difference in ice crystal size. Hottot et al. (2004) compared freezing by immersion in liquid nitrogen and freezing on a pre-cooled shelf and found large differences in ice crystal size. Immersion in liquid nitrogen leads to very high cooling rates (> 200 °C/min) whereas the cooling rate on precooled shelves is around 1 °C/min [174]. Another reason could be the confined geometry of the sample. As the volume is very small the nucleation is assumed to occur homogeneously for both cooling rates. Finally, the high glass transition temperature Tg' of maltodextrin should also be considered as a cause for the observed results. In solutions with high Tg' the viscosity of the supersaturated solution is too high for crystal growth, leading to a larger number of small ice crystals.

Table 4.2 – Characteristic morphology of maltodextrin samples. Porosity, average pore diameter (d_{pore}, µm) and tortuosity measured through analysis of µ-CT images.

	Porosity [-]	d_{pore} [µm]	Tortuosity [-]
Sample 1	0.71	20	2.01
Sample 2	0.70	14	2.35
Sample 3	0.71	14	2.13
Sample 4	0.87	29	1.42
Sample 5	0.72	14	2.07
Sample 6	0.65	10	2.55

4.2.2.2 Drying Rates and Drying Time

For all samples, the drying rate during primary drying was measured for constant process conditions. Figure 4.6 shows that the drying rate is increasing up to a maximum value and then steadily decreases up to the end of the drying process. The samples that show the highest maximum drying rate also exhibit the shortest primary drying times. The observed drying curves are characteristic for freeze drying. They are characterized by an increase in drying rate for the first 10 minutes followed by a steady decrease until the end of primary drying. The initial increase is due to heating of the system, and the decrease is caused by an increase in mass transfer resistance due to the increasing dry layer thickness.

Comparing the drying rates with the average pore size presented in the previous section (Table 4.2), it is shown that the samples with the smallest pore size (20% solid concentration and 20 °C/min cooling rate) lead to the lowest maximum drying rate and the highest drying time and vice versa. This relationship is shown in Figure 4.6. The shortest drying time was 18.5 min for the sample with Annealing I, the largest drying time was 165.3 min for the sample with 20 % solid concentration. The variation in drying time for a fixed composition and solid concentration of 10% was between 18.5 min for Annealing I and 76.7 min for a cooling rate of 20 °C/min. This means that the drying time can be reduced by a factor of four with an adequate annealing treatment.

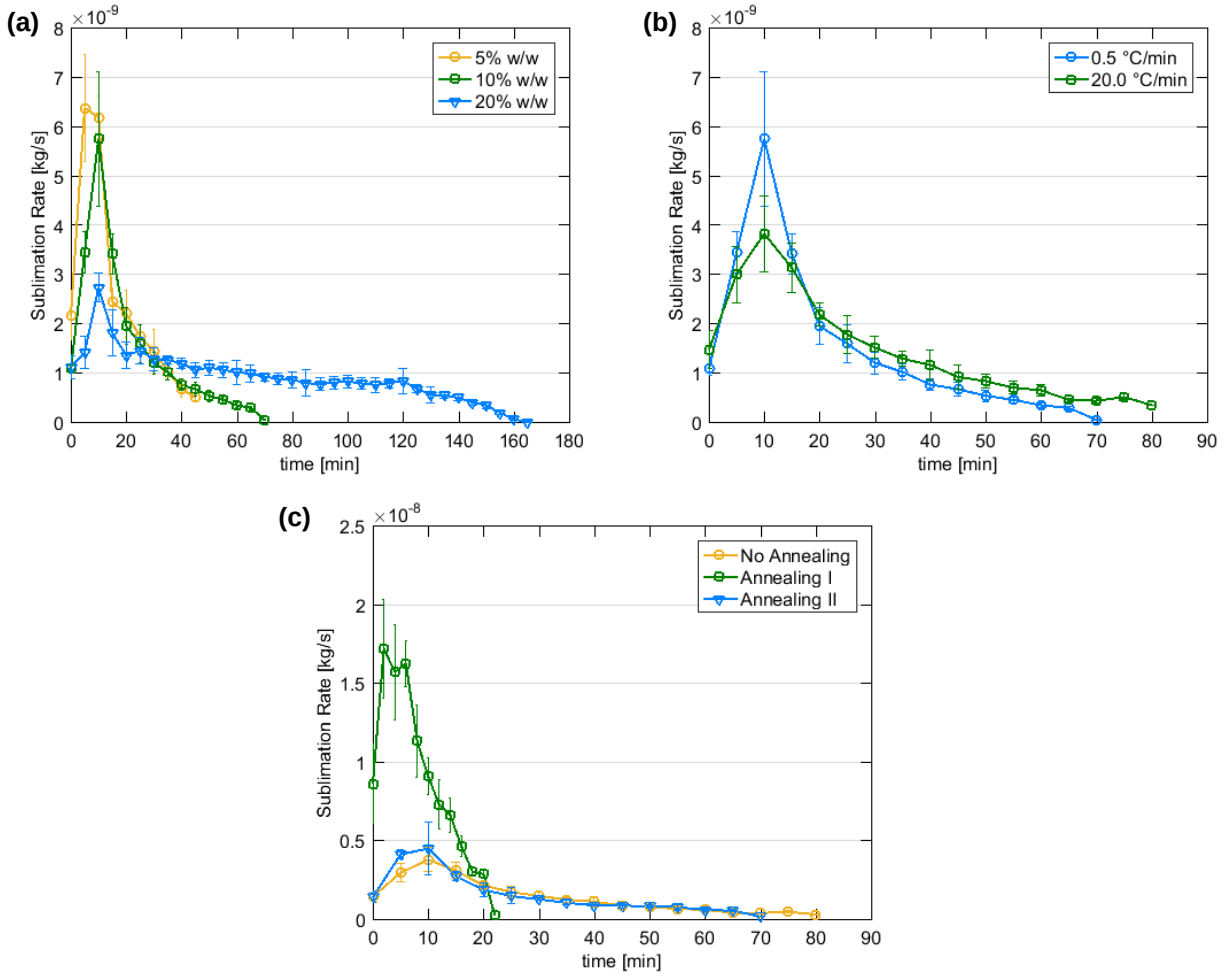

Figure 4.6 – Sublimation rate per drying time for different maltodextrin samples. (a) Samples with different maltodextrin concentrations: 5% w/w (Sample 1), 10% w/w (Sample 2) and 20% w/w (Sample 6). (b) 10% w/w maltodextrin samples frozen with different cooling rates: 0.5 °C/min (Sample 2) and 20.0 °C/min (Sample 3). (c) 10% w/w maltodextrin solution with different annealing conditions: without Annealing (Sample 3), Annealing I (Sample 4) and Annealing II (Sample 5). The error bars indicate the standard deviation obtained from triplicate experiments.

4.2.2.3 Estimation of Effective Diffusivity (D_{eff})

Diffusion mechanisms are present at different stages of drying, and their relevance depends on drying conditions, pore geometry, pore topology and the composition of the sample [169]. Section 4.1 described the different mass transfer phenomena in porous materials.

Freeze-drying processes take place at low working pressures, characterized by few intermolecular collisions. The molecular free path of water vapour is inversely proportional to pressure, resulting in higher values when the working pressure is lower. In the previous section of the thesis average pore diameters of the different samples were calculated (Table 4.2). Small average pore diameters combined with high values of molecular free path result in large Knudsen numbers, meaning that the flow inside a particle is characterized by Knudsen flow.

Gas mass flux in a porous material with large Knudsen numbers is defined by Equation (4.9). The total flux is dependent on Knudsen diffusivity (D_{Kn}) and partial pressure difference. Knudsen diffusion is given by Equation (4.10) which is dependent on the pore diameter. Equation (4.16) gives the effective Knudsen diffusion ($D_{K,eff}$), where the tortuous nature of the channels and the limited cross-sectional area available for flow are also taken in consideration.

$$D_{Kn,eff} = D_{Kn} \cdot \frac{\theta}{\tau} = D_{Kn} \cdot Eff \tag{4.16}$$

The estimated values inTable 4.2 shows that the cooling rate has no significant influence on ice crystal size distribution as both cooling rates lead to the same pore size (Sample 2 and Sample 3). However, a correlation between the freezing rate and the ice crystals size has been extensively reported in literature [21], [167], [169], [173]. Hottot et al. (2004) and Searles et al. (2001) have shown that higher cooling rate lead to a higher degree of super cooling and smaller ice crystals [174], [175]. However, this conclusion could not be confirmed in this study. One of the explanations for the observed results can be that the difference between the two cooling rates (0.5 °C/min and 20 °C/min) is too small to detect a difference in ice crystal size. Hottot et al. (2004) compared freezing by immersion in liquid nitrogen and freezing on a pre-cooled shelf and found large differences in ice crystal size. Immersion in liquid nitrogen leads to very high cooling rates (> 200 °C/min) whereas the cooling rate on precooled shelves is around 1 °C/min [174]. Another reason could be the confined geometry of the sample. As the volume is very small the nucleation is assumed to occur homogeneously for both cooling rates. Finally, the high glass transition temperature Tg' of maltodextrin should also be considered as a cause for the observed results. In solutions with high Tg' the viscosity of the supersaturated solution is too high for crystal growth, leading to a larger number of small ice crystals.

Table 4.2 allow the calculation of effective diffusivity. From Equation (4.16) it is understandable that a material with higher porosity will have a higher effective diffusivity.

Zhai et al. (2003) have developed a diffusion model to describe the diffusion of water vapour through a dried cake by analysis of freeze-drying microscopy data [156]. In this approach the relation between the instantaneous thickness of the dried cake and the drying time is determined. For a thin cylinder, a non-dimensional variable (Ψ) can be defined by integration of the differential equation obtained from a mass balance for an incremental shell of thickness ∆r (Equation (4.17)).

$$\psi = \frac{4}{R_0^2} \frac{M_w \cdot D_{Kn,eff} \cdot p_{sat}}{\theta \cdot \rho_{ice} \cdot R \cdot T} t = 2\Delta^2 \ln(\Delta) - \Delta^2 + 1 \tag{4.17}$$

where $\delta = R_0 - r$ and $\Delta = 1 - \delta / R_0$.

Furthermore, the drying time for primary drying can be calculated through Equation (4.18) which is based on the stationary diffusion equation for cylindrical geometry according to Zhai et al. (2003) [156].

$$t = \frac{R_0^2 \cdot \theta \cdot \rho_{ice} \cdot R \cdot T}{4 \cdot M_w \cdot D_{Kn,eff} \cdot p_{sat}} \tag{4.18}$$

Figure 4.7 shows the relationship between the effective diffusion coefficient and the average pore diameter. The two different methods to calculate $D_{Kn,eff}$ explained previously are represented in Figure 4.7: 1) the method developed by Zhai et al. (2003) [156]; and, 2) the method that uses the morphological characteristics of the product (Table 4.2) and Equation (4.16), which will from now be denominated Dry Matter Characterization Method. The effective moisture diffusivity is greatly influenced by the microstructure and porosity of the material as proven by other authors [169], [176]–[178]. Figure 4.7 follows studies from Baik and Marcotte (2003) showing that an increase in porosity, along with more open pore structure, increases the effective moisture diffusion [179]. Furthermore, a good agreement between the two methods is observed. A higher discrepancy between values obtained with both methods is observed when the average pore diameter increases. After further investigation it was noticed that when the average pore size increases, also the pore size distribution becomes broader [180]. Therefore, when the average pore diameter increases it becomes less accurate to use the average pore diameter as an approximation for calculating the $D_{k,eff}$. This observation is in agreement with the study made by Prachayawarakorn et al. (2008) showing the effect of pore size distribution on transport properties [177]. This study concluded that the effective diffusivity decreases when σ/μ increases, where σ is the standard deviation and μ is the normal size distribution.

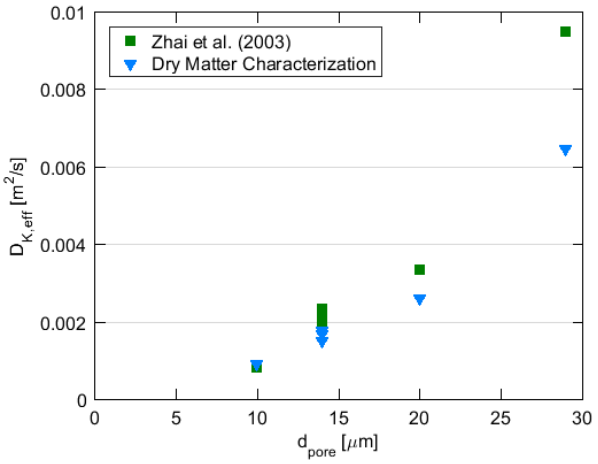

Figure 4.7 – Effective Knudsen diffusion ($D_{Kn,eff}$) vs pore diameter. The squares represent the effective Knudsen diffusion calculated through the method developed by Zhai et al. (2003) [156] **and the inverted triangles represent the effective Knudsen diffusion calculated through Equation (4.16) ($D_{Kn,eff} = D_{Kn}.(\theta/\tau)$) where the morphological parameters are estimated through analysis of μ-CT images.**

4.3 Model

The application of models based on computational fluid dynamics (CFD) to the chemical engineering field has increased significantly in the past years since it leads to improved equipment design. The use of CFD models for the freeze-drying process has been reported in the scientific literature for the characterization of freeze-drying equipment and for the prediction of its performance [67], [105]–[109].

In this section a CFD model is presented to describe the sublimation phenomenon during the drying step of freeze-drying. The model shows the application of CFD for the prediction of drying times of a sample on a freeze-drying microscope. Furthermore, the model was validated with experimental data.

4.3.1 Methodology

Figure 4.8 shows the methodology developed for the setup of the CFD model. Process data like sublimation temperature, saturation pressure, pellet size and ice fraction are model inputs. Furthermore, effective diffusivity is also a model input. Porosity and tortuosity can either be determined through experimental methods or be calculated through correlations developed specifically for each formulation.

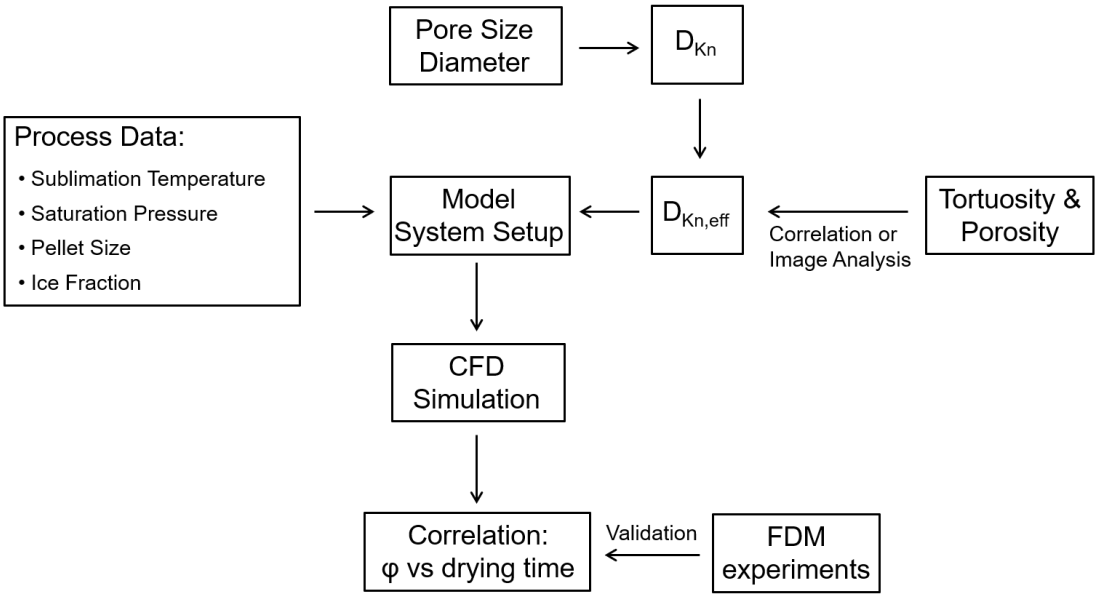

Figure 4.8 – Methodology for the setup of the CFD model. D_{Kn} is the Knudsen diffusion that can be calculated through Equation (4.10). $D_{Kn,eff}$ is the effective Knudsen diffusion which can be calculated through Equation (4.16). φ is a variable that captures the morphology of the sample (porosity, tortuosity and pore size diameter).

Equation (4.19) and Equation (4.20) correlate the pore diameter with effectivity, porosity and tortuosity. The correlations were developed considering the morphology analysis performed on a µ-CT for maltodextrin samples. The developed correlations for effectivity and porosity should be considered as a mathematical parameter rather than an accurate prediction of effectivity and porosity. Furthermore, the

correlations are expected to be only applicable for maltodextrin and in operational conditions similar to the investigated settings in terms of particle size and drying conditions.

$$Eff = 0.7966 - 6.5611/d_{pore} \quad (4.19)$$

$$\theta = 0.5862 \cdot Eff + 0.5119 \quad (4.20)$$

4.3.2 Model Setup

The full volume of the dried cylindrical samples was simulated with the help of a 3-D mesh. Two computational domains were allocated, a fluid domain and a porous domain respectively for the freeze-drying microscope chamber and the sample volume. Figure 4.9 shows the simulated geometry.

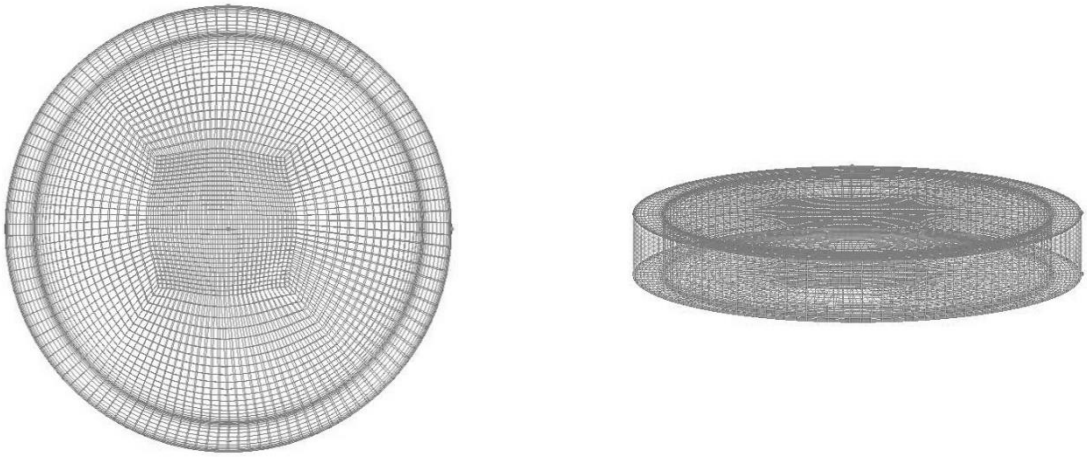

Figure 4.9 – Three-dimensional drawing of the investigated geometry representing a slab on a freeze-drying microscope. The structured hexahedral mesh is shown for both the porous region and the fluid region.

A structured hexahedral mesh for both domains was established using ANSYS ICEM CFD 17.1. The CFD simulations were performed using a full porous model in ANSYS CFX 17.1. This model is a generalization of the Navier-Stokes equations and of Darcy's law, which is commonly used for flows in porous regions.

Porosity was simulated assuming that the volume porosity (γ) at a certain location is given by the ratio between volume V' available to fluid flow in an infinitesimal control cell surrounding the point and the physical volume V of the cell.

$$V' = \gamma \cdot V \quad (4.21)$$

Dynamic simulations were carried out for the determination of drying times. A time-varying porosity is simulated since the porosity term is dependent on the ice fraction present in the sample. The ice fraction was simulated as an additional scalar variable with a very low diffusion (1.10^{-10} $m^2\,s^{-1}$).

The sublimation phenomenon was simulated in a subdomain in the porous domain. Mass source terms were introduced for the water gas and the ice with opposite signs in order to simulate the sublimation phenomenon.

$$\frac{dm_{water\ vapour}}{dt} = \frac{A_{surface}}{V_{surface}} \cdot \sqrt{\frac{M_W}{2 \cdot \pi \cdot R_{gas} \cdot T}} (p_{sat} - p) \tag{4.22}$$

$$\frac{dm_{ice}}{dt} = -\frac{A_{surface}}{V_{surface}} \cdot \sqrt{\frac{M_W}{2 \cdot \pi \cdot R_{gas} \cdot T}} (p_{sat} - p) \tag{4.23}$$

4.3.3 Assumptions

For the development of the model several assumptions were considered:

1) The resistance from the edge of the slide to the chamber is negligible;
2) Isothermal conditions were assumed since the full length of the thin frozen mass is in direct contact with the temperature controlled copper stage, thus it was assumed that the latent heat of sublimation required by the sublimation process was balanced by the rapid heat conduction;
3) The product is assumed to be isotropic and homogenous. Furthermore, it is assumed that the product does not change shape during sublimation;
4) The ice front is assumed to be parallel to the surface of the product and does not suffer any deformation during the sublimation process;
5) Constant pore diameter is assumed throughout the sample.

4.3.4 Results

4.3.4.1 Validation

The model was validated against six independent experimental data sets, which were already discussed in Section 4.2. The model is able to predict drying time, measured sublimation rate and maximum sublimation rate. The model predicts the total drying time to be within 15% of the experimental value for 5 of the 6 evaluated conditions (Figure 4.10). Compared with the other two methods presented previously in this work, the CFD model achieves similar accuracy. The variation in the data of both parity plots can be attributed to uncertainty of the experimental estimation of total drying time, initial fraction ice, average pore diameter and/or tortuosity. It is noticeable that there is an increased lack of accuracy on samples with longer drying times and with higher sublimation rates. Samples with longer drying times are characterized as having smaller pores, decreased values of porosity and higher values of tortuosity. It was found by Foerst et al. (2018) that there is a high discrepancy between the measured pore diameter

values for these samples dependent on the measurement method used (2D or a 3D method) [180]. Although the authors consider that further studies are needed, they anticipate that the shape of pores is dependent on size and that small pores are less spherical, leading to less accuracy on the measurement of the pore size. On the other hand, samples with higher sublimation rate are characterized by having larger pores, increased values of porosity and lower values of tortuosity. The same authors have also shown that for samples that have undergone annealing (leading to decreased drying time) there is a broader distribution of pore size. Therefore, in both cases, it is inaccurate to consider the average pore diameter as constant to the entire sample which leads to a higher discrepancy between the model and the experimental data.

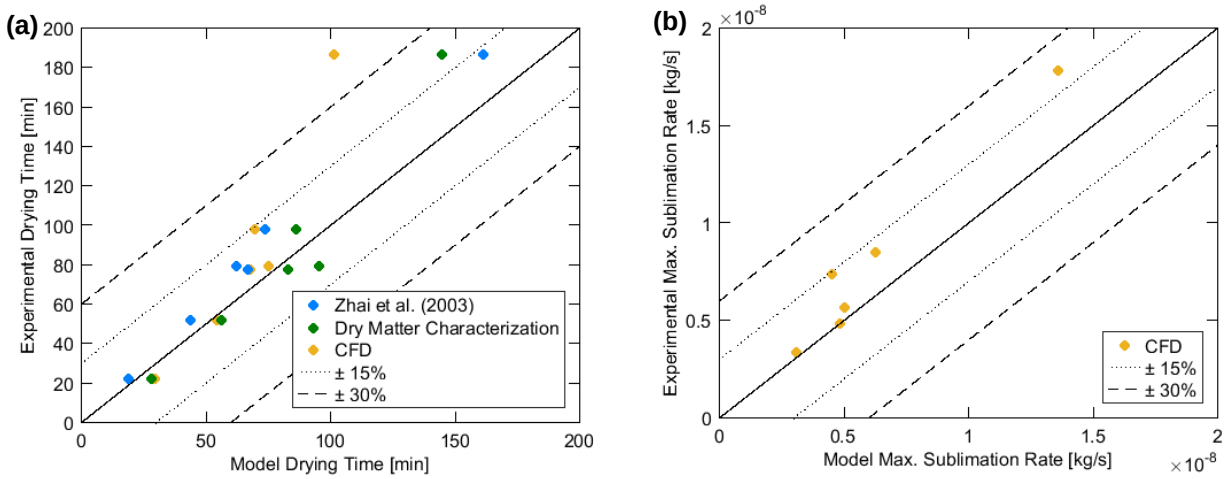

Figure 4.10 – Parity plot of experimentally obtained and calculated/simulated (a) drying time and (b) maximum sublimation rate. The dashed lines indicate the ± 15 % and ± 30 % deviation.

The variation of sublimation rate with time is also predicted by the model. When compared with the experimental data it is observed that the model overestimates the sublimation rate after the maximum sublimation rate has been reached (Figure 4.11). Once more, this might be due to the assumption of constant porosity, pore diameter, pore size distribution and tortuosity along the sample. Through further investigation of the morphology of the sample it was possible to verify that this assumption is not correct. The sample will have smaller pores in the inner part which will increase the resistance to drying over time. Furthermore, the measurements were done in the upper part of the samples, meaning that the average morphology parameters used in the model are based on local measurements.

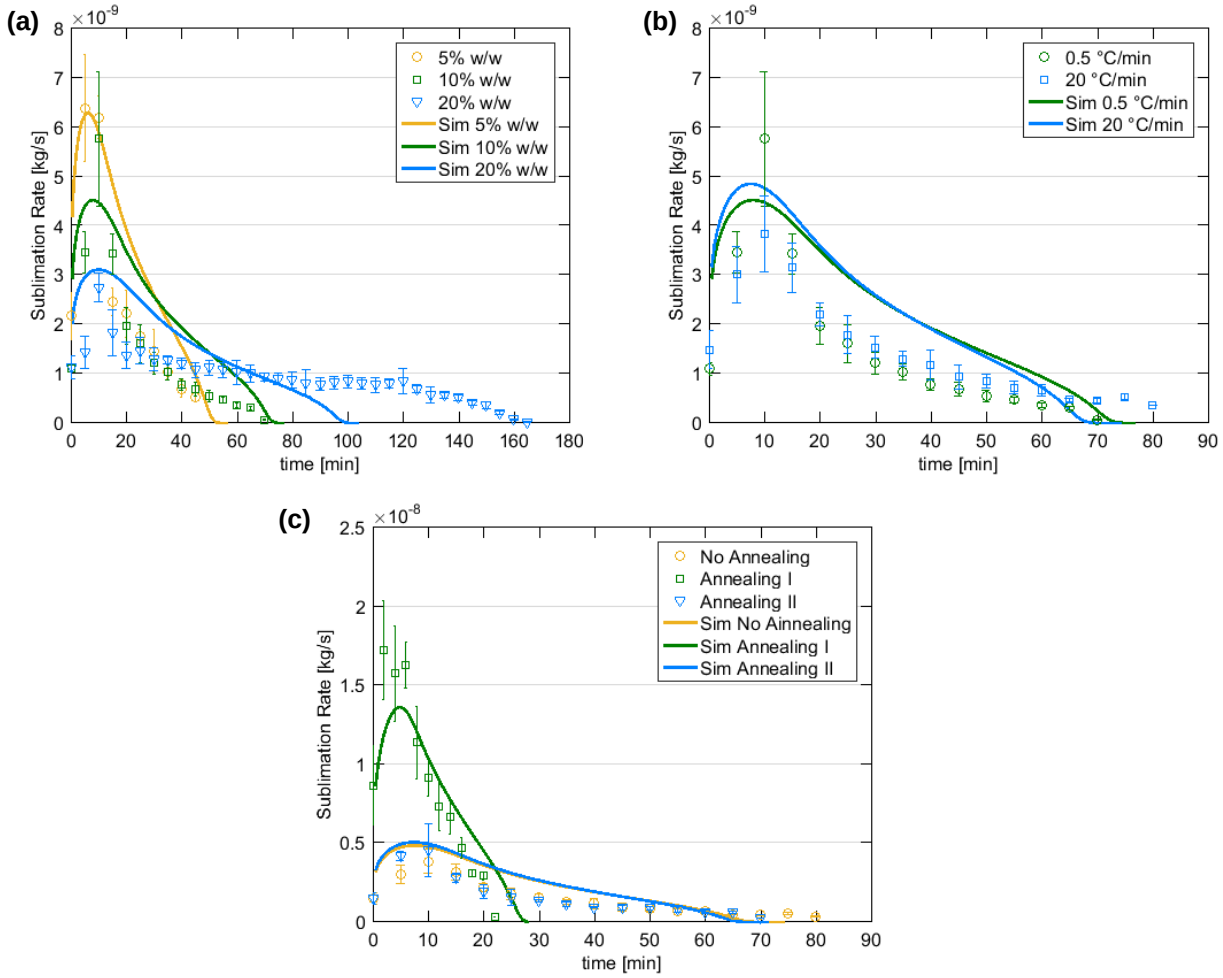

Figure 4.11 - Sublimation rate per drying time for different maltodextrin samples. The points relate to the experimental data and the lines to the data simulated by the CFD model. (a) Samples with different maltodextrin concentrations: 5% w/w (Sample 1), 10% w/w (Sample 2) and 20% w/w (Sample 6). (b) 10% w/w maltodextrin samples frozen with different cooling rates: 0.5 °C/min (Sample 2) and 20.0 °C/min (Sample 3). (c) 10% w/w maltodextrin solution with different annealing conditions: without Annealing (Sample 3), Annealing I (Sample 4) and Annealing II (Sample 5).

4.3.4.2 Drying Time and Sublimation Rate

A correlation exists between the drying time and the sublimation rate of a sample and its morphology. A variable (Φ) was created that captures the morphological characteristics of a sample (tortuosity, porosity and pore diameter) that have an effect on the effective diffusivity and therefore might change the drying behaviour of the sample. The variable Φ represents the product between the effectivity and pore size (Equation (4.24)). Previous studies [177], [180], [181] have correlated drying time with pore diameter. However, in this study it has been observed that the porosity and tortuosity play an important role since the samples were exposed to different freezing treatments, and consequently there is no correlation between tortuosity, porosity and pore diameter.

$$\Phi = d_{pore} \cdot \frac{\theta}{\tau} = d_{pore} \cdot Eff \tag{4.24}$$

Figure 4.12 shows the variation of drying time and maximum sublimation rate over Φ. As expected, longer drying times correspond to lower sublimation rates which also correspond to smaller Φ. The simulated curves follow the methodology described in Figure 4.8 and have used the correlations described in Equation (4.19) and Equation (4.20) since it is intended to depend the least possible on experimental data. The accuracy of the use of these correlations could be discussed since these were based on a small dataset and are product specific. However, when compared with the experimental results represented in Figure 4.12 it is observed that the CFD simulations provide a good prediction, which gives confidence in the developed model.

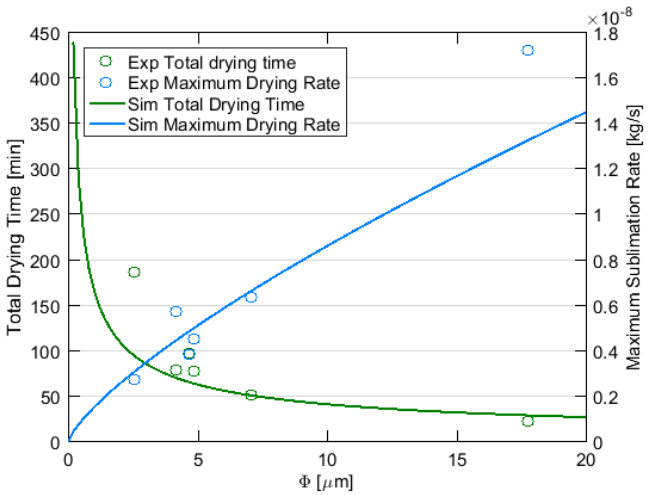

Figure 4.12 – Total drying time and Maximum Sublimation Rate vs Φ ($d_{pore}.(\theta/\tau)$). The symbols represent the experimental results and the lines the simulated results from the CFD model.

4.3.4.3 Dynamic Regime

Since the system is dynamic, the model was set up as a transient regime. Table 4.3 shows the variation of porosity, ice fraction, water vapour and pressure for four different points in time. In the beginning the pellet is frozen and the porosity is approximately 0 and in the end of the drying process (t ≈ 50 min) the ice fraction will be equal to 0.

During the drying process there is an ongoing formation of pores due to the sublimation of frozen water. Therefore, the porosity of the sample increases with time from the outside of the pellet to the inside. Porosity will inversely increase with the decrease of the ice fraction. Frozen water will sublimate and form water vapour at the same rate. However, as presented in Table 4.3, water vapour takes longer to leave the pellet. The process is mainly driven by diffusion, and therefore the rate of transfer of the water vapour from the pellet to the chamber is dependent on the effective diffusivity value. Furthermore, it is possible to

observe that the pressure inside the pellet will also increase with the formation of water vapour. At the end of the process the initial pressure will be re-established.

Table 4.3 – Contour plots of Sample 7 for time equal to 0, 25, 40 and 50 minutes. Predicted porosity, ice fraction, water vapour fraction and pressure for different time points.

	t = 0 min	t = 25 min	t = 40 min	t = 50 min
Porosity	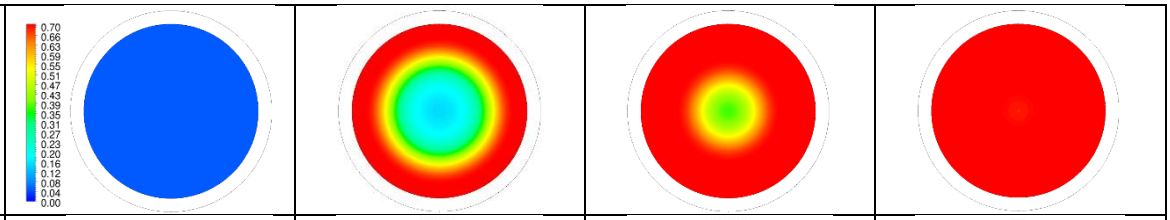			
Ice Fraction	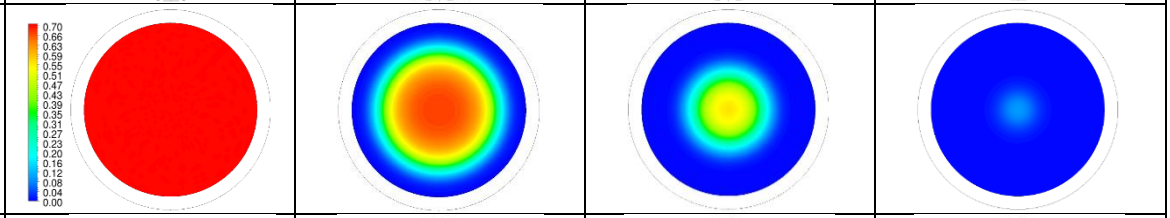			
Water Vapour Fraction	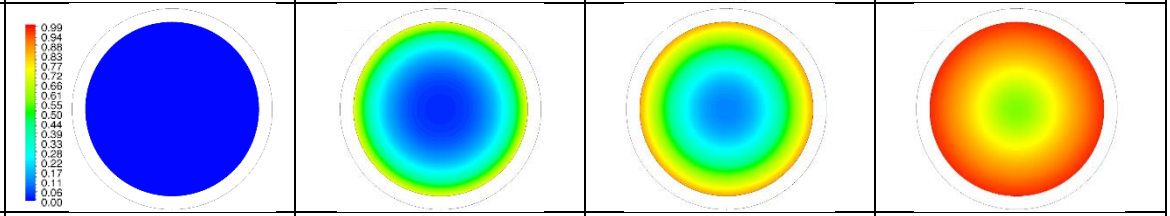			
Pressure	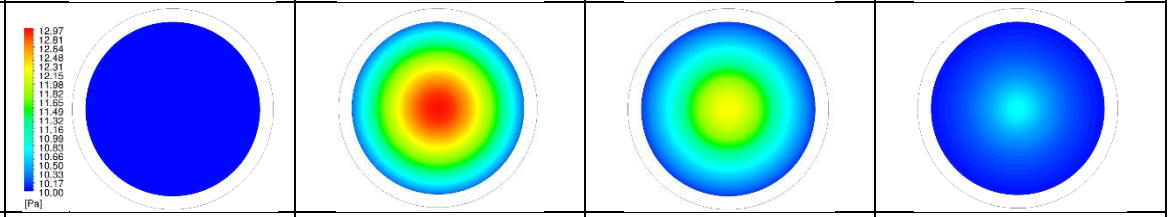			

4.4 Conclusions

The effect of solid concentration, freezing rate and annealing on the dried product morphology was investigated for maltodextrin samples. Furthermore, a CFD model was developed in order to predict the drying time and the rate of sublimation on a freeze-drying microscope.

The importance of the physical state of the dried matrix for the primary drying stage of the freeze-drying process was highlighted and demonstrated in this chapter. It was observed that pore size is strongly dependent on solid concentration and on the existence of an annealing treatment at a temperature above T_g' prior to drying. Furthermore, it has been observed that there is no change in pore size on maltodextrin solutions frozen in a confined geometry and by applying a cooling rate in the range of 0.5 to 20 °C/min. This is contradictory to literature. However, it should be added that the existing studies in the literature have performed fast freezing by immersion in liquid nitrogen, which is one order of magnitude faster than the applied cooling rates in this study.

Porosity, tortuosity and pore diameter were the morphological parameters studied through µ-CT image analysis showing the applicability and the advantages of this method for predicting and better understanding the mass transfer phenomena during primary drying. However, it has been observed that the shape of the pores and their connectivity can probably also contribute to changes of the sublimation rate.

The effective diffusivity was calculated through two different methods. FDM provided a rapid and visual method for the determination of $D_{Kn,eff}$ and the analysis of µ-CT images of dry matter provided a method that can be applied to different kinds of samples freeze-dried in a standard freeze-drying equipment. Larger discrepancies between the two methods were observed for larger pores since the pore size distribution becomes broader for larger pores. $D_{Kn,eff}$ is a critical parameter for the development of a mathematical model describing the drying process of a frozen sample.

The developed CFD model is able to successfully predict the sublimation phenomena during drying on a freeze-drying microscope. The model was compared with the measurements of drying time and sublimation rate for different loadings and process conditions. It was found that while the model was able to accurately predict the drying time and maximum sublimation rate for the majority of the samples, the prediction of these parameters for samples with very low or very high porosities was not very accurate. Model assumptions like constant average pore diameter might lead to these inaccuracies.

With the use of CFD calculations for a simplified setup, like a lyomicroscope, it is possible to obtain a better and improved understanding of the phenomena occurring at the product scale. The approximation to isothermal conditions allowed ignoring heat transfer phenomena which results in a simplified model. Regardless of the already mentioned approximations, and in spite of the fact that the lyophilization process takes place in a Knudsen flow regime, the simulated results are satisfactory. The assembled model is the starting point for the development of a detailed model that couples equipment capability and product characteristics and is able to predict drying rates, product temperature and pressure profiles of a complete freeze-drying process.

Chapter 5

The effect of product morphology, particle size and particle distribution on the drying process

Chapter 4 discussed the importance and influence of product morphology on the drying time behaviour during freeze-drying. It focused largely on factors that affect the porosity ($\theta_{particle}$) of samples being dried, concluding that $\theta_{particle}$ is largely dependent on the solid concentration, the freezing rate and the presence/absence of annealing. However, bulk freeze-drying is characterized by a bimodal pore size distribution, meaning that both the pore size distribution inside the product ($\theta_{particle}$) and the pore size distribution of the bed of particles (θ_{bed}) will have an influence on the drying behaviour. The pore structure formed by the packed frozen particles will provide transport channels for the movement of water vapour on the frozen region of the material being dried. Therefore, the porosity of the bed of particles (θ_{bed}) together with the porosity of each particle ($\theta_{particle}$) when dried will define the space available for movement of the water vapour. The porosity of the bed of particles (θ_{bed}) is given by Equation (3.1) and will be dependent on the particle volume. Furthermore, it will also depend on particle shape, packing and size distribution [182].

$$\theta_{bed} = 1 - \frac{V_{pellets}}{V_{tray}} \tag{5.1}$$

Liapis and Bruttini (2009) and Trelea et al. (2009) developed models to describe the drying process during bulk freeze-drying [85], [117]. The main difference between the two models developed is the studied average size of the particles, which leads to involvement of different flow regimes. Liapis and Bruttini (2009) studied particles with a diameter in the range of 10-20 μm, assuming a sublimation front in the slab parallel to the bottom of the tray, where all pellets situated above the front are dry and below it they are frozen [85]. Trelea et al. (2009) studied particles with an average size of 2 mm leading to a drying front in each particle that will move in the direction of its core. In this section, it is attempted to show how the particle size in a stack of pellets can influence the drying profile over time [117].

Advanced approaches, like Computational Fluid Dynamics (CFD), can assist in understanding the relationship between the morphological characteristics of a porous material and its drying behaviour, and therefore to highlight which is the best configuration for an efficient drying process. This chapter will study the effect of the morphological characteristics of the dried matrix of a single spherical particle and of two case studies where single pellets are organized in larger agglomerations with different packing factors.

The different case studies highlight the importance of mathematical modelling in the investigation of the effect of neighbouring particles and bed porosity (θ_{bed}) on the mass transport phenomena.

5.1 Single particle

The aim of this section is the study of the influence of particle diameter, porosity and pore diameter on the drying behaviour of a single particle. As shown in Chapter 4, the predominant diffusion mechanism when working at low pressure and with average pore diameters of magnitudes between 10-25 µm is Knudsen diffusion, therefore this is the implemented flow regime in the numerical studies.

5.1.1 Model considerations

The CFD simulations were carried out using the commercial software ANSYS CFX 17.1 and the meshing of the different geometries was done using ANSYS ICEM 17.1 (Figure 5.1). An unstructured mesh was employed. The model was set up in the same way as described in Chapter 4. In this section, tortuosity was approximated to 2. Reyes et al. (1991) have demonstrated that the geometric tortuosity of random-loose aggregates is around 1.8 in both the Knudsen and bulk diffusion regime [183]. Furthermore, the observed tortuosity in the previous chapter for different samples was approximately 2. This approximation is, therefore, considered valid.

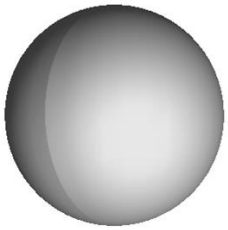

Figure 5.1 - Three-dimensional drawing of the investigated geometry of a single particle. The unstructured hexahedral mesh is shown for the porous region.

5.1.2 Results

5.1.2.1 Effect of particle diameter

Chapter 4 showed the influence of the freezing rate and initial solid concentration on the final product morphology for cylindrical product slabs with constant diameter. This section assumes that product morphology (i.e. porosity, pore diameter, tortuosity) is not dependent on the diameter of the single particle. This assumption is only correct if the undercooling degree and nucleation rate are considered

constant throughout the particle and independent of the particle diameter [184]. O'Brien et al. (2004) have concluded in their studies that slower cooling rates and smaller freezing surfaces generate samples with more homogeneous pore size distributions [185]. Therefore, the approximation represents better the reality for particles frozen at slow cooling rates and with small diameters.

The simulated effect of particle diameter on the drying behaviour of a single spherical particle is shown in Figure 5.2. The particle diameter does not have an influence on the effective diffusion inside the particle since the effective diffusion is only dependent on pore size, porosity and tortuosity, which were kept constant. However, the flux of water that sublimates over time is highly dependent on the sublimation surface area and volume, and therefore dependent on the particle diameter. Figure 5.2 b) shows the dependency between the sublimation rate and the particle diameter. An exponential growth of the sublimation rate is observed when the diameter of the sphere decreases, which by other words means that spheres with smaller diameters will dry faster.

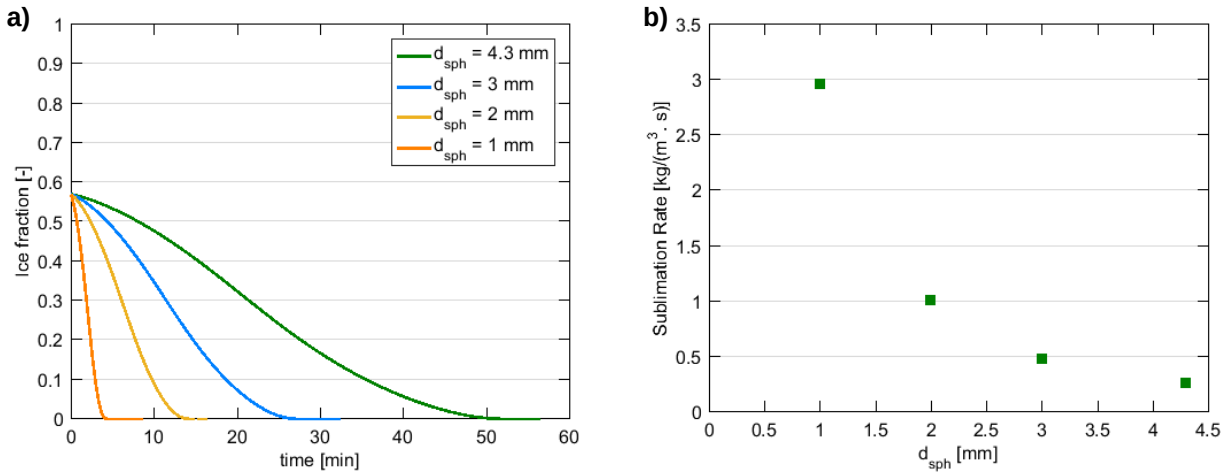

Figure 5.2 – Simulation of the primary drying of single spherical particles with $\theta_{particle}$ = 0.60, $\tau_{particle}$= 2 and d_{pore} = 17 µm as a function of particle diameter (d_{sph}). a) Shows the predicted ice fraction changing over time and b) the predicted sublimation rate.

5.1.2.2 Effect of porosity

The characteristic porosity of the dried product highly depends on the initial fraction of ice, as porosity relates to the volume left by the ice when sublimated. Therefore, porosity of the product changes over time during the drying process. Figure 5.3 shows the simulated effect of particle porosity on the drying behaviour of a single spherical particle. A constant pore and particle diameter were assumed.

From Figure 5.3 a) it is possible to conclude that although samples with lower porosity have a lower amount of ice to be sublimated they take longer to dry. Furthermore, Figure 5.3 b) shows a linear behavior between porosity and drying time. Effective diffusion changes linearly with porosity since a higher percentage of voids leads to an easier diffusion of the water vapour through the sample.

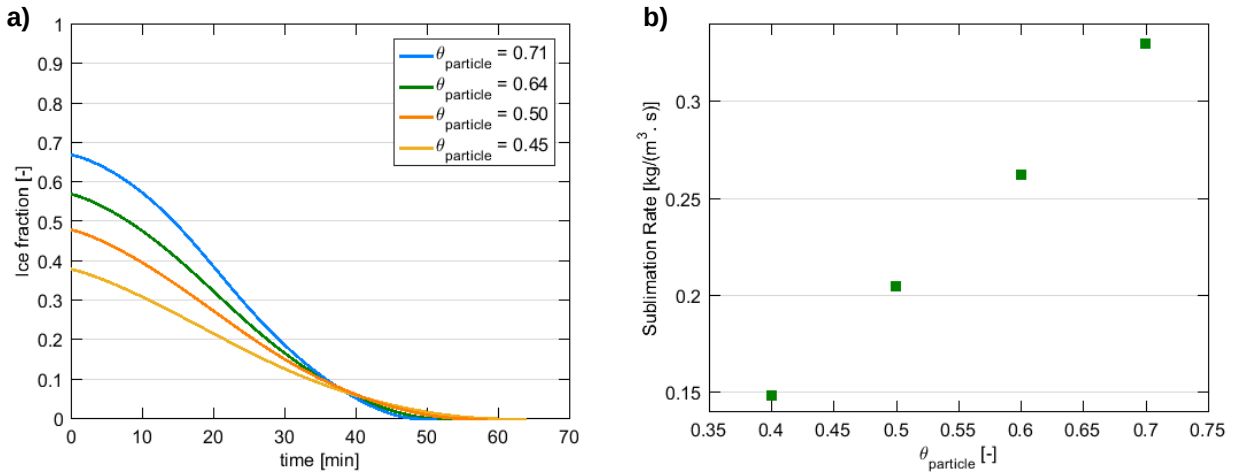

Figure 5.3 – Simulation of the primary drying of single spherical particles with $d_{particle}$ = 4.3 mm, $\tau_{particle}$ = 2 and d_{pore} = 17 µm as a function of particle porosity ($\theta_{particle}$). a) Shows the predicted ice fraction changing over time, and b) the predicted sublimation rate.

5.1.2.3 Effect of pore diameter

Figure 5.4 shows the simulated effect of the pore diameter on the drying behaviour of a single sphere with constant diameter, porosity and tortuosity. As expected, in the Knudsen diffusion regime, larger pores lead to lower drying times. Figure 5.4 b) shows a linear relation between the sublimation rate and the pore diameter, due to the also linear relation between the pore diameter and the effective diffusion (Equation (4.10) and (4.16)). To have a more realistic prediction of the drying profile it would be relevant to also study the importance of the pore connectivity and pore shape (cylindrical pores are assumed in the developed model).

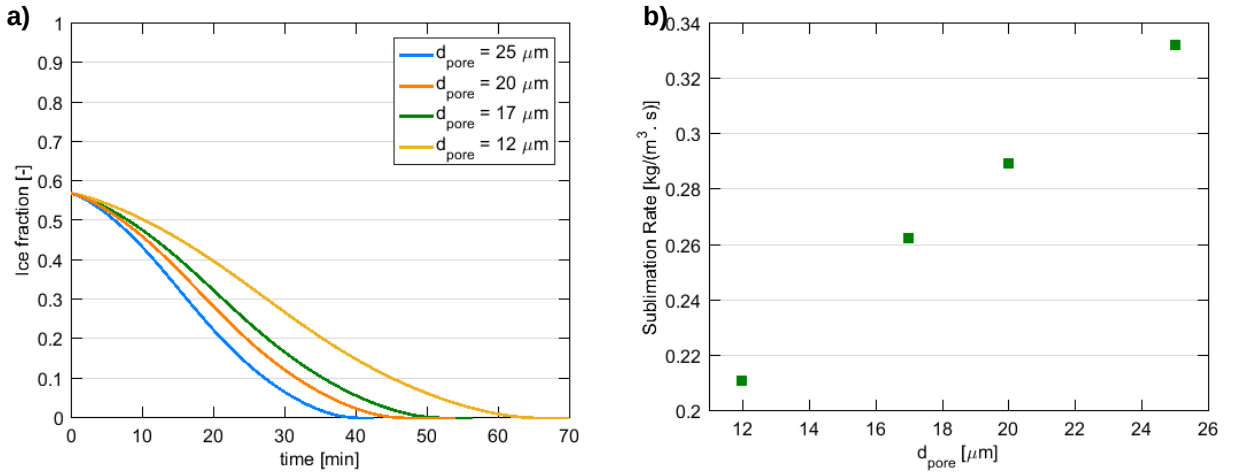

Figure 5.4 – Simulation of the primary drying of single spherical particles with $d_{particle}$ = 4.3 mm,$\tau_{particle}$= 2 and $\theta_{particle}$ = 0.60 as a function of pore diameter (d_{pore}). a) Shows the predicted ice fraction changing over time and b) the predicted sublimation rate.

5.2 Multiple Particles

The previous cases only considered the mass transport inside a single particle. In this section, it is intended to study the effect of neighbouring particles and bed porosity on the drying behaviour. This is illustrated in two different case studies with distinct packing factors of the bed of particles. Once again, the importance of advanced flow dynamic models, such as CFD methods, is highlighted in this section for achieving a better understanding of the drying behaviour during freeze-drying.

As mentioned previously, frozen particulate matter is characterized by a bimodal pore size distribution based on the pore sizes of the inter particle and inner particle void space. Pore size distribution of the particle bed is dependent on the particle volume, shape, packing factor and size distribution [182]. The mean pore diameter formed by the packing of particles can be estimated from the hydraulic diameter (Equation (5.2)) [85], [159].

$$d_{bed,pore} = \left(\frac{1}{3}\right)\left(\frac{\theta_{bed}}{1-\theta_{bed}}\right) d_{sph} \tag{5.2}$$

Dependent on the mean pore diameter formed, the mass transport is generally characterized by a Knudsen flow regime or a transient regime, leading to different diffusion coefficients (Figure 5.5). In the transient regime both bulk and Knudsen diffusion mechanisms contribute, and therefore the overall diffusivity can be approximated by the Bonsaquet's formula given in Equation (4.16)

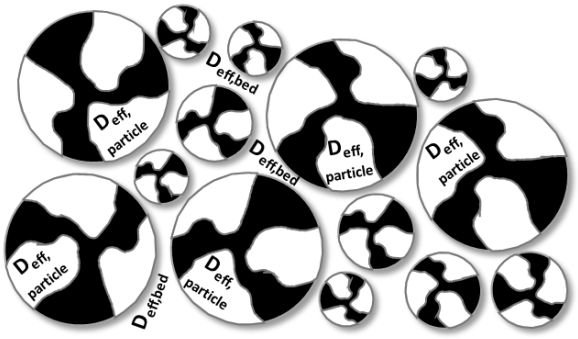

Figure 5.5 – Representation of an agglomerate of multiple particles with different sizes. Black represents frozen water and white the solid material. The effective diffusion will assume different values inside the particles ($D_{eff,particle}$) and between the particles ($D_{eff,bed}$) due to the different characteristic length.

5.2.1 Model considerations

Once again, the CFD simulations were carried out using the commercial software ANSYS CFX 17.1 and the meshing of the different geometries was done using ANSYS ICEM 17.1. An unstructured mesh was employed. Figure 5.6 shows the two different geometries from different perspectives. This study intends to investigate the effect of the neighbouring particles and of bed porosity (θ_{bed}) on the mass transport and on the dynamics of the fluid exiting each particle and the bed of particles.

Different packing factors were achieved by different levels of overlapping of the particles. Figure 5.6 shows that in Case B the pores between the particles are smaller due to an increased overlapping of the particles.

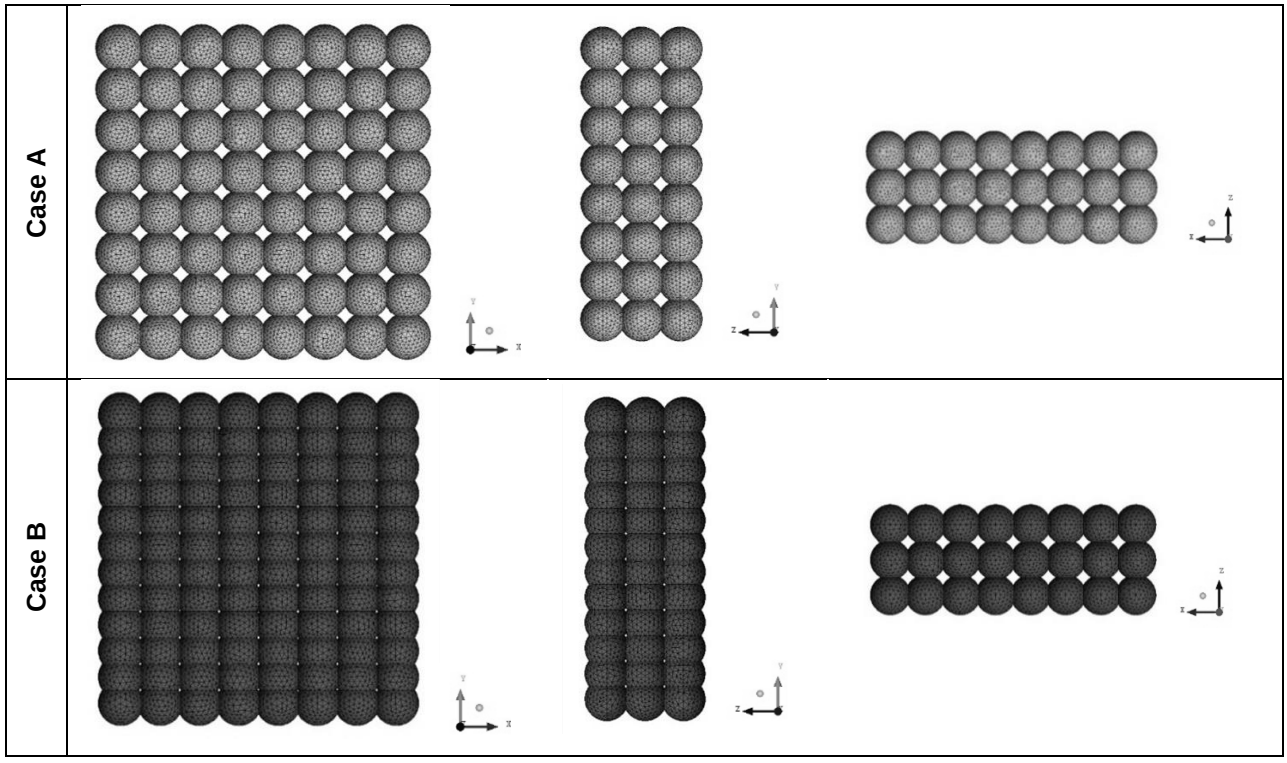

Figure 5.6 - Three-dimensional mesh of the investigated geometries of multiple particles in a stack. The unstructured hexahedral meshes are shown for the porous region. Case A – Particles studied as spheres and with low packing factor. Case B - Particles studied as cylinders and with high packing factor.

The model was set up considering the different diffusion mechanisms in the different porous media. The working pressure was 10 Pa and the sublimation temperature was -42 °C. Therefore, the local diffusion will be given by Equation (5.3).

$$\begin{cases} D_{ice}, \text{ for ice in the particle} \\ D_{eff,particle}, \text{ for water vapour in the particle} \\ D_{eff,bed}, \text{ for water vapour between particles} \end{cases} \quad (5.3)$$

As in the previous cases the ice fraction was simulated as an additional scalar variable with a very low diffusion (D_{ice} = 1.10^{-10} m^2 s^{-1}) in comparison to the $D_{eff,particle}$ or $D_{eff,bed}$ (range). The morphology inside the particle was considered to be equal in all particles, which leads to a constant $D_{eff,particle}$. Table 5.1 shows the characteristics of the particles considered in this study.

Table 5.1 – Morphological characteristics of the particles in the stack ($d_{particle}$, $h_{particle}$, $\theta_{particle}$, d_{pore}, $\tau_{particle}$, $Eff_{particle}$). The particle diameter of the particle is the only parameter that is variable. $D_{eff,particle}$ was calculated considering the measured characteristics of the particles.

$d_{particle}$ [mm]	$\theta_{particle}$ [-]	d_{pore} [µm]	$\tau_{particle}$ [-]	$Eff_{particle}$ [%]	$D_{eff,particle}$ [m^2/s]
4.3; 3.0; 2.0; 1.0	0.60	17.0	2.0	0.3	1.86 x 10^{-3}

D_{bed} will depend on the diameter of the particles, bed porosity and the mean pore diameter formed from the packing of the particles. Table 5.2 shows the morphological characteristics of the bed. The tortuosity was assumed to be $\sqrt{2}$ as described by Liapis and Bruttini (2009) since it provides a reasonable approximation for random porous structures whose pores have good pore connectivity [85].

Table 5.2 – Morphological characteristics of the bed (θ_{bed}, $d_{bed,pore}$, τ_{bed}, Eff_{bed}, $D_{eff,particle}$) dependent on $V_{particles}$ and V_{bed}.

Case	$V_{particles}$ [m^3]	V_{bed} [m^3]	θ_{bed} [-]	$d_{bed,pore}$ [mm]	τ_{bed} [-]	Eff_{bed} [%]
A	7.45 x 10^{-6}	1.53 x 10^{-5}	0.51	1.50	$\sqrt{2}$	0.36
	2.53 x 10^{-6}	5.18 x 10^{-6}	0.51	1.05	$\sqrt{2}$	0.36
	7.49 x 10^{-7}	1.54 x 10^{-6}	0.51	0.70	$\sqrt{2}$	0.36
	9.37 x 10^{-8}	1.92 x 10^{-7}	0.51	0.35	$\sqrt{2}$	0.36
B	8.94 x 10^{-6}	1.12 x 10^{-5}	0.20	0.36	$\sqrt{2}$	0.14
	3.04 x 10^{-6}	3.81 x 10^{-6}	0.20	0.25	$\sqrt{2}$	0.14
	9.00 x 10^{-7}	1.13 x 10^{-6}	0.20	0.17	$\sqrt{2}$	0.14
	1.13 x 10^{-7}	1.41 x 10^{-7}	0.20	0.08	$\sqrt{2}$	0.14

The diffusion mechanism is in the transition regime if 0.01 < Kn < 1 and in the Knudsen regime if Kn > 1. In this study it was considered that the diffusion mechanism was in the transition regime when 0.01 < Kn

< 1.5 since many assumptions were made and in this range the flow is still very close to the transition regime.

Table 5.3 – Effective diffusion in the porous bed. $D_{kn,eff,bed}$ and $D_{bulk,eff,bed}$ were calculated for cases in the transition regime and $D_{eff,bed}$ was calculated by the Bonsaquet's formula. $D_{kn,eff,bed}$ was calculated in cases in the Knudsen regime and $D_{eff,bed}$ is equal to $D_{kn,eff,bed}$.

Case	$d_{particle}$ [mm]	Kn_{bed} [-]	$D_{kn,eff,bed}$ [m^2/s]	$D_{bulk,eff,bed}$ [m^2/s]	$D_{eff,bed}$ [m^2/s]
A	4.3	0.75	6.11×10^{-2}	4.61×10^{-2}	2.63×10^{-2}
	3.0	1.08	4.26×10^{-2}	4.61×10^{-2}	2.22×10^{-2}
	2.0	1.62	2.84×10^{-2}	-	2.84×10^{-2}
	1.0	3.25	1.42×10^{-2}	-	1.42×10^{-2}
B	4.3	3.11	5.88×10^{-3}	-	5.88×10^{-3}
	3.0	4.46	4.10×10^{-3}	-	4.10×10^{-3}
	2.0	6.70	2.73×10^{-3}	-	2.73×10^{-3}
	1.0	13.45	1.35×10^{-3}	-	1.35×10^{-3}

Table 5.3 shows that Case A has a $D_{eff,bed}$ approximately one order of magnitude higher than Case B, which is a consequence of the bed morphology. Equation (4.10) shows that flow diffusion is facilitated in beds with larger pores between particles and with increased values of effectivity (increased values of porosity and decreased values of tortuosity).

The size of the pores in the particle based material ($d_{bed,pore}$) is directly dependent on the size of the particle ($d_{particle}$), Equation (5.2). Therefore, the mass transfer resistance of the bed of particles becomes a function of the particle diameter. It is observable in Table 5.3 that in Case B the value of $D_{eff,bed}$ decreases as the size of $d_{particle}$ decreases. However, in Case A, $D_{eff,bed}$ is very similar for particles with $d_{particle}$ equal to 4.3, 3.0 and 2.0 mm. As already discussed by Liapis and Bruttini (2009), it is important to highlight that very large particle diameters, meaning large values of $d_{bed,pore}$, lead to small values of the Knudsen number which is characterized by flows in the transient or bulk regime [85]. Therefore, as observed in Table 5.3, large particles do not always enhance the mass transfer rate in particle based materials.

5.2.2 Results

5.2.2.1 Effect of particle diameter

Figure 5.7 shows the effect of the particle diameter and volume on the drying time of a single particle and a stack of particles. As observed when drying a single particle, smaller particles dry faster than bigger particles. Figure 5.7 a) shows that for particles with a diameter of 1 mm there is an increase of the drying time of around 2.3x for Case A and around 9.1x for Case B when compared with the drying time of a

single particle. Moreover, it shows that for particles with a diameter of 4.3 mm there is an increase of 1.8x for Case A and around 6.4x for Case B. It is therefore possible to observe an increase of the drying time due to the surrounding particles which gets steeper with the decrease of bed porosity (θ_{bed}) and the decrease of particle diameter. Furthermore, for a single particle, when the particle size decreases from 4.3 to 3 mm, the drying time is reduced by 48%, and when the particle size decreases from 2 to 1 mm the drying time is reduced by 68%. For the multiple particle cases, when the particle size reduces from 4.3 to 3 mm the drying time is reduced by 42% and 41%, respectively for Case A and Case B, and when the particle size decreases from 2 to 1 mm the drying time is reduced by 57% and 64% respectively. It is observed that Case B has a more similar drying behaviour to a single particle drying, which will be further discussed in this section.

Figure 5.7 b) shows that for the same volume of particles an increased value of the bed porosity (θ_{bed}) leads to increased sublimation rates. This is in good agreement with the observations made by Liapis and Bruttini (2009) [85]. The increase of bed porosity (θ_{bed}) leads to lower mass transfer resistance which justifies the increase of the drying rate. Thus, both Figure 5.7 a) and Figure 5.7 b) indicate that as the value of θ_{bed} increases the value of drying time decreases, which is mainly due to the lower amount of available frozen free water and the increase of the available free space for flow movement.

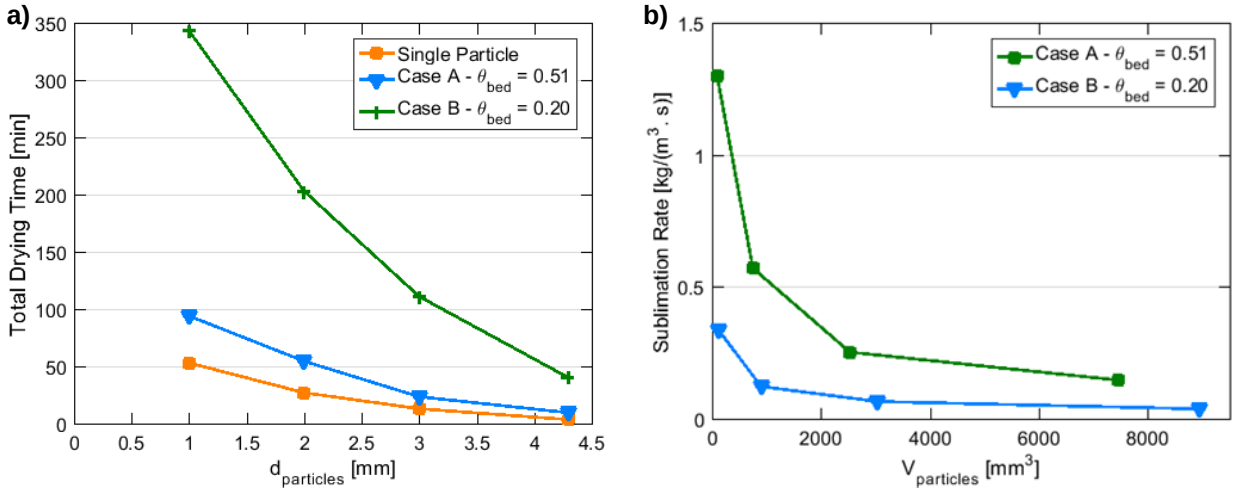

Figure 5.7 – a)Simulation of the total primary drying time as a function of particle diameter ($d_{particle}$) for a single particle, Case A and Case B. The morphological characteristics of the particles are $\theta_{particle}$ = 0.60, $\tau_{particle}$ = 2 and d_{pore} = 17 µm. b) Effect of bed porosity (θ_{bed}) on sublimation rate over total volume of particles ($V_{particles}$) for a stack of particles when $\theta_{particle}$ = 0.60, $\tau_{particle}$ = 2, d_{pore} = 17 µm, θ_{bed} = 0.48 and $\tau_{particle}=\sqrt{2}$.

Figure 5.8 shows the existing ice fraction during the drying process of a stack of particles with a diameter of 4.3 mm. Figure 5.8 a) and c) show a plane cut in the middle of the top layer of particles and Figure 5.8 b) and d) show a plane cut in the middle of the central layer of particles.

It is observable in Figure 5.8 a) and b) that in Case A the sublimation occurs simultaneously in all particles and the sublimation front evolves from the exterior of the pellet to its core, which is in agreement

with the observations made by Trelea et al. (2009) [117]. In Figure 5.8 c) and d) it is possible to observe a unique sublimation front from the outside pellets to the central pellets, similar to the one observed by Liapis and Bruttini (2009) [85]. Since $d_{bed,pore}$ is much smaller, the vapour pressure created by the vapour accumulated in the pores of the bed decreases the sublimation rate. Therefore, in this case the drying behaviour of the stack of pellets can be approximated to the drying of a single pellet as it was also concluded through Figure 5.7.

Furthermore, in the centre of the stack (Figure 5.8 b) and d)) it is observed that the drying is slower since there is a higher resistance to vapour transport, which creates an increase of pressure and consequently a decrease of the sublimation rate.

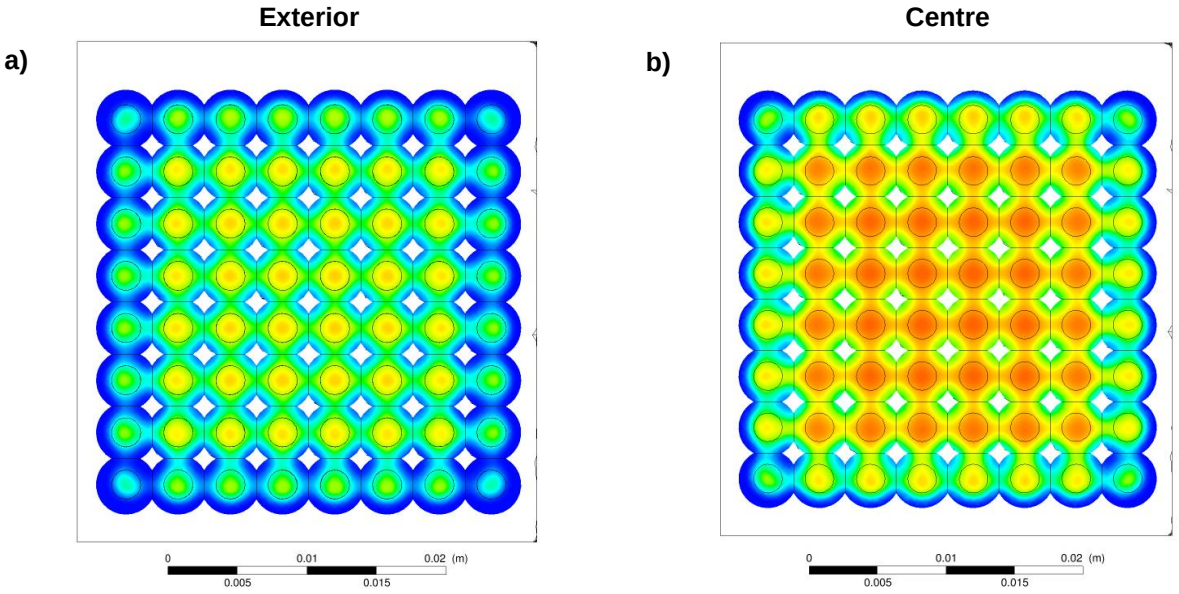

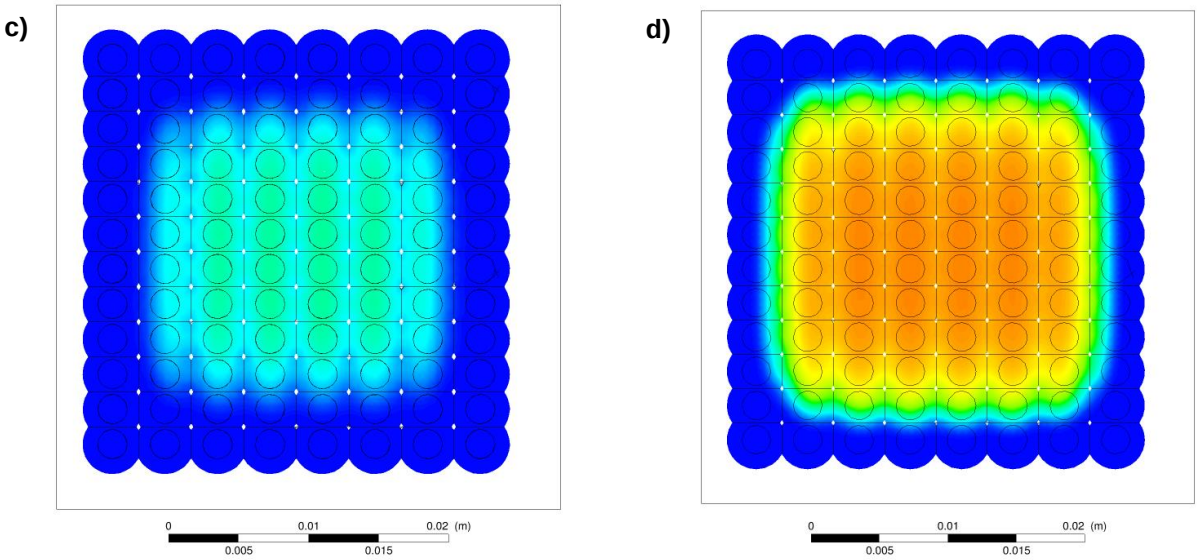

Figure 5.8 – Contour plots representing the fraction of ice present in a stack of particles with a diameter of 4.3 mm after 45 min (a) and b)) and 2.9 h (c) and d)). a) and b) correspond to a stack of particles with θ_{bed} = 0.51 (Case A) and c) and d) correspond to a stack of particles with θ_{bed} = 0.20 (Case B). a) and c) correspond to the exterior layer and b) and d) to the center layer of the stack.

Figure 5.9 shows the partial pressure in Case A and in Case B. The partial pressure was measured along a line placed in the middle of the centre layer of particles that crosses both the particles and the fluid domain between them. In Case A, it is observed that the vapour pressure increases inside the particles and it decreases in the free space between them. This effect is explained by Table 5.2 and Table 5.3 where it is shown that the effective diffusion in the space between the particles ($D_{eff,bed}$) increases about one order of magnitude when compared with the effective diffusion in the particles ($D_{eff,particle}$), meaning that the movement of the flow is facilitated in this location. On the contrary, in Case B, there is no variation in the vapour pressure, which is again explained by Table 5.2 and Table 5.3. This observation leads once more to the conclusion that stacks of particles with low bed porosity (θ_{bed}) tend to have a behaviour similar to one single pellet.

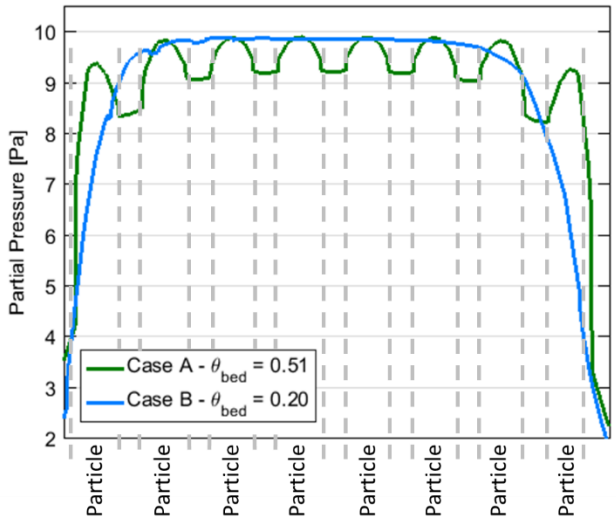

Figure 5.9 – Partial pressure along the stack of particles for Case A and Case B. The measurements were made in the center of the middle layer of the stack of pellets.

5.3 Strategies for identifying the effect of particle size and packing on the drying process

The previous investigated cases highlight variations in the drying behaviour depending on the characteristics of the product. These variations are increasingly pronounced when freeze-drying particle based materials since on these materials both the morphology of the product and of the bed of particles will have an effect on the drying process, introducing complexity to the system.

Experimental methods could be applied to better understand the phenomena associated with the drying of particulate material. However, it is challenging to design experimental strategies that allow the observation of the sublimation front and therefore determine the correct drying behaviour of a bulk of particles. Advanced modelling approaches such as computational fluid dynamics (CFD) are an alternative source of this detailed information and can be used for improved process understanding and troubleshooting.

Since the freeze-drying of particulate materials is nowadays used extensively in the industry, the development of mathematical models that take into consideration both the morphology of the product and of the bed of particles is needed. The optimal design of freeze-drying cycles requires an increased qualitative and quantitative understanding of the effect of mass and heat transport phenomena through the porous material. The qualitative results obtained through the investigated case studies in this section allow a better understanding of the mass transport phenomena occurring in a stack of particles and

ensure further development of models with higher complexity. The possibility to visualize the effect of particle diameter and packing factor is a very useful tool for process development.

5.4 Conclusions

Bulk freeze-drying is characterized by a bimodal pore size distribution, meaning that both the size of the pores inside the product and the size of the pores that characterize the bed of particles will influence the drying behaviour and the diffusion of vapour during sublimation. The mass transfer phenomena during primary drying of single frozen spherical particles and of a stack of spherical particles has been investigated using the computational fluid dynamics model developed in Chapter 4. The model has shown the ability to satisfactorily predict the mass fluid transport inside particles with different configurations (porosity, pore diameter and particle diameter) and in between particles.

The simulated results show that smaller average pore size, lower particle porosity and increased particle diameter lead to decreased drying time and sublimation rates, which is in agreement with the results found in the scientific literature.

The two different configurations of particle stacks display how bed porosity plays a key role in primary drying. Furthermore, the dependency of the drying process on the diameter of the particles is highlighted, since particle size has a direct influence on the mass transfer rates in particle based materials.

Although a validation with experimental data was not possible, suitable and expected drying profiles were achieved leading to the conclusion that CFD is a viable tool for the characterization of the fluid behaviour during primary drying of frozen samples. CFD is able to account for geometrical features and fluid properties both inside the particles and between them. Coupling the developed model with a heat transfer source has extensive potential for increased understanding and optimization of the freeze-drying process.

Chapter 6

CFD Model for a Laboratory/Pilot Scale Freeze-Dryer

Freeze-drying is a process where a product is dried by removal of the present frozen water through sublimation at low pressure and temperature [29]. Lyophilization aims at obtaining a final product with low residual moisture without losing its structure, viability and activity. In order to maximize plant productivity and reduce product cost, the rate of solvent removal should be maximized. Strategies to decrease the drying time of a freeze-drying process go from changes in the process parameters (e.g. increase in temperature) or as discussed in Chapter 4 and Chapter 5 changes in product formulation or in the freezing process. Furthermore, the design of the equipment will also have an effect on the sublimation rate since for example in order to avoid vapor accumulation and subsequent pressure increase in the drying chamber, the rate of vapor production in the drying chamber has to be compatible with the condenser capacity [10]. Moreover, when developing freeze-drying cycles for new products it is not only important to focus on the development of the drying time but also in keeping the activity, viability and structure of the product [186]. Therefore, a combination of equipment and product characterization with monitoring technologies to control the residual amount of ice in the product, its temperature and sublimation rate throughout the process, will lead to more efficient and more controlled freeze-drying cycles [10], [125].

In the traditional approach, the design and optimization of freeze-drying cycles is usually obtained through an extensive amount of experimental work. Alternatively, predictive models can be developed in order to mechanistically understand scale-up issues and to develop robust freeze-drying cycles that facilitate the transfer between equipment. Robust theoretical models which can predict product temperature and drying time have been developed mainly for the pharmaceutical industry [74], [76], [81], [187]. However, these models must be adapted and modified if to be used in other applications, since the accuracy of the model is dependent on the product container. Chapter 6 intends to consider both the product and the equipment characteristics in order to describe the drying behavior of frozen particulate matter dried in a laboratory/pilot scale freeze-dryer. The drying flow rate has been described for particulate materials through mathematical models for different bed porosities, packing factors and particle diameters [85], [117]. However, it is known that the efficiency of the drying process will also be highly affected by the chamber size and configuration and by the condenser capacity, which is not accounted in the previously mentioned studies.

Chapter 4 and Chapter 5 focused mainly on the development of mathematical models for the mass transport of the water vapour from the sublimation front to the drying chamber, considering isothermal

conditions. Chapter 6 intends to describe both the heat and mass transfer during freeze-drying at laboratory/pilot scale by coupling the fluid dynamics in the chamber with the heat and mass transfer phenomena in a tray. In order to analyse the flow behaviour in a pilot scale dryer, a model based on computational fluid dynamics (CFD) will be developed. The CFD model will consider the tray geometry, surface temperatures, fluid properties and pressure boundary conditions at the drying chamber and it will be validated with experimental data collected on a pilot scale freeze-dryer.

6.1 Mechanisms of Heat Transport in Porous Material

Freeze-drying is a complex process that couples heat and multi-phase mass transfer in a vacuum environment. Drying is mainly governed by two transport mechanisms: (i) the energy transport to transform frozen water into water vapour; and (ii) the transport of the water vapour from the sublimation surface through the dried layer of the product and the open spaces between particles, into the drying chamber to the condenser [188]. The mechanisms involved during mass transport in porous material have been described in detail in Section 4.2. Section 6.1 intends to explain the heat transport mechanisms involved during primary drying.

The necessary amount of energy for the sublimation depends on the sublimation temperature, which depends on the partial pressure at the sublimation front. The necessary energy can be transported by different mechanisms: (i) by radiation of heated surfaces, (ii) by conduction from heated plates, gases and neighbouring particles, and (iii) by gas convection [28]. Radiative and contact conduction mechanisms are independent of pressure; however, gas phase conduction and convective mechanisms are pressure dependent. When the mean free path of gaseous molecules is significantly smaller than the characteristic size of gas flows, meaning small Knudsen numbers, non-slip velocity and non-jump temperature are assumed on solid surfaces. However, very often the mean-free path is comparable to the characteristic size. In these cases, if the rarefaction is moderate, the velocity slip and temperature jump boundary conditions can be considered. In cases where the rarefaction is not moderate, the kinetic Boltzmann equation or the Monte Carlo method must be employed. However, these approaches are not easy to implement since no commercial software tool is available based on these methods.

The heating mechanism that contributes most during the process depends on the equipment and product container designs. For cycles in which the product container is in direct contact with the heated shelves, contact conduction serves as a primary source of heat of drying. However, when direct contact is eliminated, radiation is expected to play a larger role in the heat exchange. In laboratory and pilot scale freeze-dryers, the front plexiglass door plays a significant role in contributing to the radiation, which leads to position-dependent drying rates.

6.1.1 Ice Sublimation

As mentioned previously, sublimation is an endothermic process, meaning that heat is absorbed by the system when phase change occurs. The rate of heat transfer during the sublimation process is given by Equation (3.1).

$$\frac{dQ_{product}}{dt} = -\Delta H_{subl} \cdot \frac{dm_{ice}}{dt} = -\alpha\, A_{surface}\, \Delta H_s \sqrt{\frac{M_W}{2\pi RT}} (p_{sat} - p) \tag{6.1}$$

The enthalpy of sublimation (ΔH_{subl}) is the energy necessary to change one mole of a substance from the solid state to the gaseous state at a given pressure and temperature. The specific sublimation enthalpy will vary with temperature. However, this variation is not significant for the range of temperatures applied in the freeze-drying process [189].

6.1.2 Radiation

Radiative heat transfer is independent of pressure and it does not require the presence of an intervening medium. The radiative heat flow between two surfaces depends on the difference between the absolute temperatures of the surfaces to the power four, the emissivity of the surface and the area exposed, and it is governed by the Stefan-Boltzmann relation as shown in Equation (6.2).

$$q_{rad} = \sigma\, \varepsilon\, F_{2-1}(T_2^4 - T_1^4) \tag{6.2}$$

6.1.3 Conduction

Conduction results from the interaction between particles and involves the transfer of energy from the more energetic particles of a substance to the less energetic ones. It can take place in solids, liquids and gases. In the specific case of bulk freeze-drying, conduction occurs in the vapour phase surrounding the particles and between the particles and the tray that contains the product.

The contact conduction contribution is generally independent of pressure. However, the vapour phase conduction can depend on pressure, all depending on the flow regime: (i) continuum flow regime, (ii) transitional or temperature-jump regime, and (iii) free molecular regime.

For flows with Kn < 0.01 the flow is in the continuum regime and it is given by Equation (6.3), which is the Fourier's law of heat conduction.

$$q_{Fourier} = \frac{K}{l}(T_{sh} - T_p) \tag{6.3}$$

For flows with 0.01 < Kn < 0.1 the flow is in the transient regime and the heat flux can be approximated by the first order temperature jump equation (Equation (6.4)).

$$q_{jump} = \frac{T_{sh} - T_p}{\frac{l}{K} + \frac{2}{P}\left(\frac{\gamma - 1}{\gamma + 1}\right)\sqrt{\frac{\pi}{2R}}\left(\sqrt{T_{sh}} + \sqrt{T_p}\right)} \tag{6.4}$$

For flows with Kn > 10 the flow is in free molecular regime and it is given by Equation (6.5).

$$q_{fm} = \frac{T_{sh} - T_p}{\frac{2}{P}\left(\frac{\gamma - 1}{\gamma + 1}\right)\sqrt{\frac{\pi}{2R}}\left(\sqrt{T_{sh}} + \sqrt{T_p}\right)} \tag{6.5}$$

Thus, heat transfer is linearly dependent on pressure in the free molecular regime and it is independent of pressure in the continuum regime.

6.1.4 Convection

The contribution of convective heat to heat transfer is difficult to describe analytically. This is a pressure dependent contribution, and it differs as a function of the temperature difference between the surface and the bulk fluid. Since freeze-drying requires low working pressures, rarefied flow will have an increased effect on the fluid dynamics and it will be mainly dependent on the temperature and pressure of the process. The thermal creep velocity is given by Equation (6.6).

$$u_{creep} = \sigma_T \frac{\mu}{\rho T_W}\frac{\partial T_w}{\partial x} \tag{6.6}$$

6.2 Materials and Methods

6.2.1 Experimental Work

6.2.1.1 Freeze-drying

The batch freeze-drying experiments were carried in a laboratory/pilot scale freeze-dryer (LyoBeta-15, TELSTAR), which was cooled before the start of the drying cycle (Figure 6.1). The different batch freeze-drying operational parameters – i.e. chamber pressure, shelf temperature, drying rate, product and condenser temperature – were studied on a laboratory/pilot scale freeze-dryer.

a)

Laboratory/ Pilot Scale Freeze – Dryer

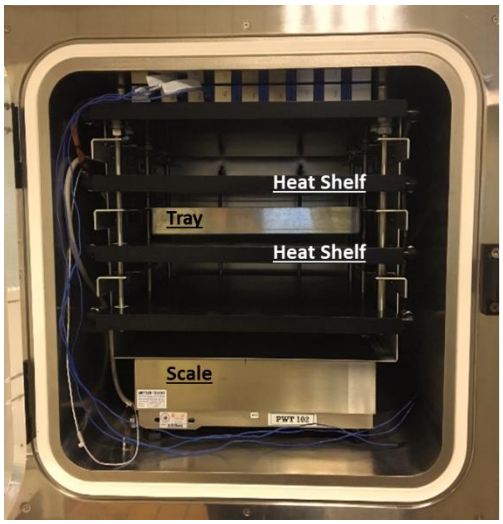

b)

Temperature Probes

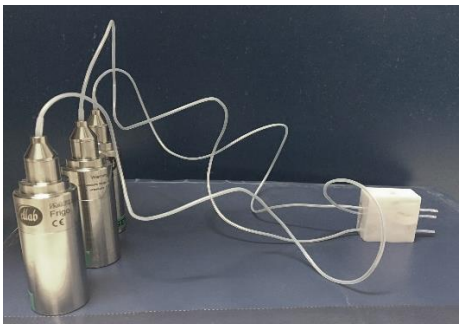

c)

Product Tray

Figure 6.1 – a) Illustration of the drying chamber of the laboratory/pilot freeze-dryer LyoBeta-15, Telstar. b) Temperature probes TrackSense Pro data loggers, Ellab inserted on a plastic block in order to keep the desired height. c) Tray filled with frozen pelletized Maltodextrine solution 10% w/w.

A 10% w/w maltodextrine solution (DE 10-14 from medesign I.C. GmbH) was prepared using bi-distilled water and serves as a model system. The solution was pelletized by quenching on liquid nitrogen. The product obtained after pelletization was loaded onto the metal tray which was cooled down to approximately -55 °C before a freeze-drying cycle. Only one tray was loaded to the freeze-dryer, which corresponds to approximately 700 g of product. Drying was performed at two different chamber pressures 30 Pa and 50 Pa. The shelf temperature was set to 32 °C in both experiments.

The on-line measurements of fluid-inlet the temperature, the temperature at the condenser and the chamber pressure were measured with probe systems incorporated into the freeze-dryer equipment. The freeze-dryer equipment has a scale in-place which can measure the weight loss of the trays.

The temperature of the product was measured at 0.5, 1.0 and 2.0 mm of depth in the product layer with TrackSense Pro data loggers (Ellab) which were inserted in a plastic block in order to keep the desired height (Figure 6.1 b)). The temperature sensors should be positioned such that the tip is as far as possible from the block in order to minimize its effect on heat transfer.

6.2.1.2 Particle Size Distribution

Particle size distribution experiments were done using a simple sieve test. The granulated product was loaded into an analytical sieve shaker (AS 200, Retsch) in order to determine the particle size of the individual product. Sieves of 5.0, 4.0, 3.15, 2.5, 1.8, 1.0 and 0.6 mm were used, and the separation was performed during 10 min with a throwing motion with an amplitude of 2.00 mm every 10 s. The particle size distribution study details are available in the supplementary material.

6.2.2 Model Development

The numerical work is based on a case that resembles the laboratory/pilot scale freeze-dryer and a case that intends to study the effect of the chamber design on the drying process (Figure 6.2).

Table 6.1 presents the geometrical features of the freeze-dryer for Case A and Case B.

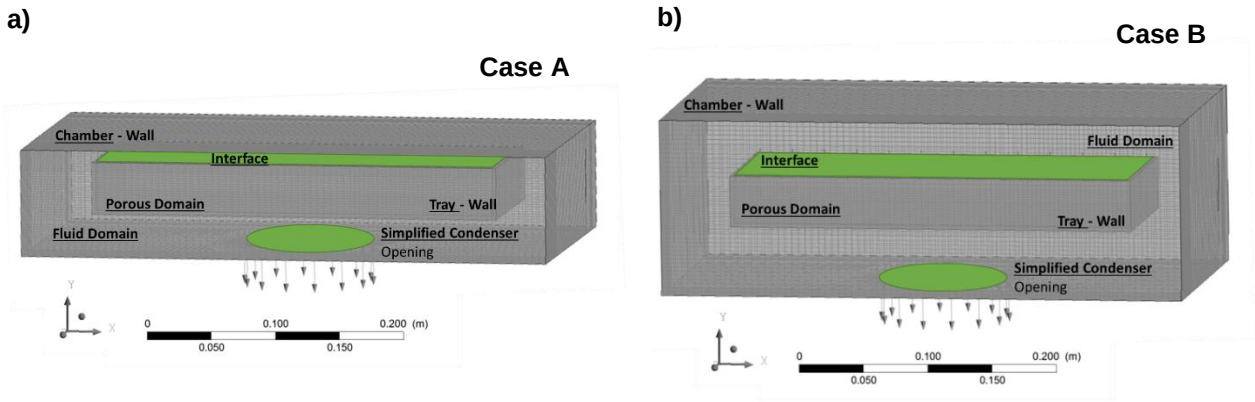

Figure 6.2 – Three-dimensional drawing of the investigated geometry representing the drying chamber. The structured hexahedral mesh is shown for both the tray and the chamber domain. The two cases differ in the distance between the product tray and the top heating shelf a) 0.015 m and b) 0.050 m.

Table 6.1 – Geometrical features of Case A and Case B.

Tray		
Height (m)		0.037
Width (m)		0.120
Length (m)		0.310
Chamber		
Distance between tray and heating shelf (m)	Case A	0.015
	Case B	0.050
Diameter of the condenser (m)		0.100

The CFD simulations and the implementation of the structured mesh were performed using the commercial software ANSYS CFX 17.1 and ANSYS ICEM 17.1, respectively. Transient simulations were

performed, and the domain was divided into a fluid and a porous domain. The flow was set to laminar Stokes flow, where turbulence and inertial effects are not considered.

In the investigated cases in this chapter the working pressure was set to 30 Pa and the temperature of the heating shelf to 32 °C. The sublimation phenomenon was simulated in a subdomain of the porous domain. Mass and energy terms were introduced as described by Equations (6.7), (6.8) and (6.9).

$$\frac{dm_{water\ vapour}}{dt} = \frac{A_{Tray}}{V_{Tray}} \cdot \sqrt{\frac{M_W}{2 \cdot \pi \cdot R_{gas} \cdot T_{prod}}} (p_{sat} - y_W \cdot P) \tag{6.7}$$

$$\frac{dm_{ice}}{dt} = -\frac{A_{Tray}}{V_{Tray}} \cdot \sqrt{\frac{M_W}{2 \cdot \pi \cdot R_{gas} \cdot T_{prod}}} (p_{sat} - y_W \cdot P) \tag{6.8}$$

$$\frac{dQ_{product}}{dt} = -\frac{A_{Tray}}{V_{Tray}} \cdot \Delta H_{subl} \cdot \sqrt{\frac{M_W}{2 \cdot \pi \cdot R_{gas} \cdot T_{prod}}} (p_{sat} - y_W \cdot P) \tag{6.9}$$

Where p_{sat} is the saturation pressure and it is given by Equation (6.10).

$$ln\frac{p_{sat}}{p_{tr}} = -\frac{\Delta H_{subl}}{R}\left(\frac{1}{T_{prod}} - \frac{1}{T_{tr}}\right) \tag{6.10}$$

The model was set up considering different diffusion coefficients depending on the flow regime characteristic of each domain. The local diffusion for each domain is given by Equation (5.3).

$$\begin{cases} \mathrm{D_{ice}}, \text{ for ice in the particle} \\ \mathrm{D_{eff,porous}}, \text{ for water vapour in the porous domain} \\ \mathrm{D_{eff,chamber}}, \text{ for water vapour in the chamber} \end{cases} \tag{6.11}$$

The ice fraction was simulated as an additional scalar variable with a very low diffusion (D_{ice} = 1.10^{-10} m^2 s^{-1}) in comparison to $D_{eff,porous}$ and $D_{eff,chamber}$ (range). As discussed in the previous chapter, the vapour diffusion in the porous domain ($D_{eff,porous}$) is both influenced by the morphological characteristics of the particles present in the tray and the free space between them. In this chapter, the bimodal porous domain will be approximated by a unimodal porous domain, meaning that $D_{eff,porous}$ will be approximated by the weighted average between $D_{eff,particle}$ and $D_{eff,bed}$, given by Equation (6.12).

$$D_{eff,porous} = (1 - \theta_{bed}) \cdot D_{eff,particle} + \theta_{bed} \cdot D_{eff,bed} \tag{6.12}$$

As previously mentioned, two different geometries were investigated, Case A and Case B. Experimental data acquired in laboratory/pilot scale was used for validation and verification studies. The validation

studies were performed in Case A since it resembles the laboratory/pilot scale freeze-dryer. As in the previous chapters maltodextrin was used as a model system (Cases Maltodextrin 30 and Maltodextrin 50). Furthermore, the simulated drying behaviour was compared with the experimental data collected for the freeze-drying of *Streptococcus thermophilus* (ST-B, ST-C, ST-D, ST-H; the experimental methodology related to this data set can be found in Chapter 3).

Table 6.2 summarizes the morphological characteristics of each particle and of the free space between particles in the bed. Table 6.3 presents the calculated diffusion coefficients for each location and the diffusion coefficients implemented in the CFD simulations. Case A and Case B are given as examples in Table 6.2 and Table 6.3, the other cases can be found in the supplementary material.

Table 6.2 - Morphological characteristics of each particle and of the free space between particles in the bed.

Particles							
$d_{particle}$ [mm]		$\theta_{particle}$ [-]		d_{pore} [µm]	$\tau_{particle}$ [-]	$Eff_{particle}$ [%]	
3,96		0.85		14	2	0.4	
Free space between particles							
Case	$Pack_{bed}$ [-]	$V_{particles}$ [m^3]	V_{bed} [m^3]	θ_{bed} [-]	$d_{bed,pore}$ [mm]	τ_{bed} [-]	Eff_{bed} [%]
A / B	0.52	7.28×10^{-3}	1.40×10^{-3}	0.48	1.22	$\sqrt{2}$	0.34

Table 6.3 - Calculated diffusion coefficients for each particle, for the free space between particles and the diffusion coefficients implemented in the CFD simulations.

	Particles	Free space between particles				Unimodal Porous Domain (CFD)	
Case	$D_{eff,particle}$ [m^2/s]	Kn_{bed} [-]	$D_{kn,eff,bed}$ [m^2/s]	$D_{bulk,eff,bed}$ [m^2/s]	$D_{eff,bed}$ [m^2/s]	$D_{eff,porous}$ [m^2/s]	$D_{eff,chamber}$ [m^2/s]
A / B	2.11×10^{-3}	0.29	4.51×10^{-2}	1.33×10^{-2}	1.02×10^{-2}	6.02×10^{-3}	3.91×10^{-2}

6.2.2.1 Boundary Conditions

The walls of the chamber were modelled with a no-slip condition and with an isothermal temperature equal to the one of the heating shelf. The wall of the tray was also modelled with a no-slip condition (this assumption will later be discussed) and an isothermal temperature of 32 °C. The heat transfer from the wall to the solid material was set to be a constant outside temperature corresponding to the heating shelf temperature (32 °C) and the heat transfer coefficient, whose estimation was based on the calculations already presented in Chapter 2 (0.3 W/(m^2.K)). Furthermore, a radiation heat flux, given by Equation (6.13), was set at the interface between the porous and the chamber domain. An opening boundary was set in the bottom of the drying chamber that corresponds to the initial part of the duct that leads to the condenser with a certain pressure and temperature (30 Pa, 32 °C).

$$q_{rad} = \frac{\sigma}{x_{prod}} \left(T_{shelf}^4 - T_{prod}^4\right) \quad (6.13)$$

6.3 Results

6.3.1 Model Validation - Comparison of experimental and simulated drying behavior

The drying behaviour in freeze-drying processes is, besides the process conditions, affected by the design of the apparatus, the product characteristics and the packing factor of the product in the tray.

A simplified geometry of the freeze-drying chamber, Case A, was developed to simulate the drying behaviour of frozen particulate material in a laboratory/pilot scale freeze-dryer. The approximation to a simplified geometry representing the drying chamber is considered valid since in the considered process conditions there are no restrictions to fluid flow originating from limitations in the condenser capacity or choked flow in the duct [10]. This was verified through ice sublimation tests performed in the laboratory/pilot scale freeze-dryer used in this study (Chapter 3) [105].

While the product characteristics were incorporated into the simulation based on experimentally estimated values, it was not possible to measure the packing factor of the particulate material experimentally. Particulate material frozen by quenching in liquid nitrogen is characterized as having irregular shapes and sizes, which will affect the packing structure in the tray [190]. Furthermore, the shaking method used after loading the tray impacts also the degree of packing of the product. Hence, the packing factor is an imprecise parameter, which is laborious and difficult to estimate through experimental methods.

Random packing of granular materials is broadly present in nature and industry; therefore, it is extensively reported in literature. Since experimental measuring methods are laborious and expensive, many research groups focused on numerical simulations instead [190]–[198]. In the present model, the packing factor was estimated through an iterative approach that identified the packing factor that leads to the measured drying time. Each iteration is performed by changing the packing factor in the simulation, and after the convergence of the simulation the predicted drying time is compared with the experimental data. The packing factor is accepted when the difference between the simulated and experimental drying time value is less than 10 %.

It was found for the case study using maltodextrin, that a packing factor of 0.64 is the one that gives a better correlation between the experimental and the simulated drying time. For the production strains a packing factor of 0.4 was found to match the simulation and experimental data reasonably.

The model was validated with the measured drying time from four different freeze-drying cycles of products with identical characteristics to the products used for estimation of the packing factor in terms of particle diameter, shape and porosity. Figure 6.3 presents the parity plot where the correlation between the measured and the simulated values can be evaluated.

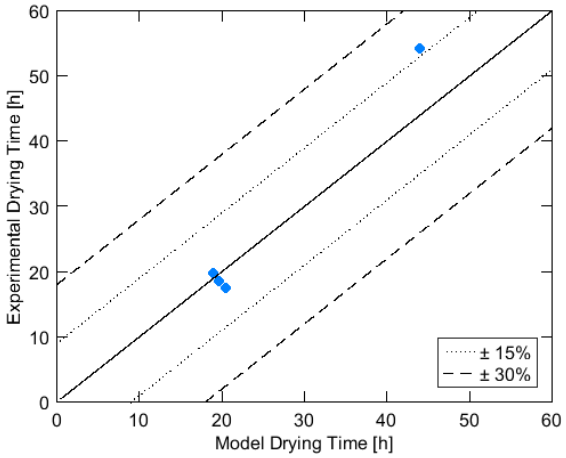

Figure 6.3 - Parity plot of experimentally obtained and simulated drying time. The dashed lines indicate the ± 15 % and ± 30 % deviation.

The simulated drying time is within 15% of the experimental value for three of the four measurements. Therefore, the implemented strategy is assumed to be valid for the prediction of the drying time within reasonable values, even if a large number of assumptions related to product morphology had to be implemented. The variations in the parity plot can be associated with the assumptions made during model development but also with product variations and uncertainties in the experimental determination of the drying time. Furthermore, larger uncertainties were observed in the model when decreasing the pressure of the drying chamber. The choice of the adequate numerical approach to describe heat and mass transfer in freeze-drying is dependent on the significant rarefied flow effects due to the low operating pressures. When the pressure is reduced, the flow behaviour is closer to the molecular regime, meaning that it cannot be described anymore by the Navier-Stokes equation [107].

In order to validate the developed model both drying time and the fraction of ice over time present in the tray are relevant. Therefore, the predicted fraction of ice over time was compared with the measurements from the laboratory/pilot scale freeze-dryer. Figure 6.4 shows the fraction of ice over time for the four different production strains. A good prediction of the fraction of ice present in the tray over time is verified. When looking closely to Figure 6.4 a), an over prediction of the drying time and of the fraction of ice present in the tray at the end of drying is verified for ST-B. As discussed in Chapter 2, this strain results in final dried products with a higher porosity compared with maltodextrin or even with the other production strains. This was not considered during the set up of the simulation, which leads to inaccuracies. However, the developed model gives the possibility to change the considered characteristics of product

morphology, and thus to improve the correlation between the simulated and the experimental values. The previous observations show once more the importance of characterizing the product morphology in order to obtain models that represent the reality better.

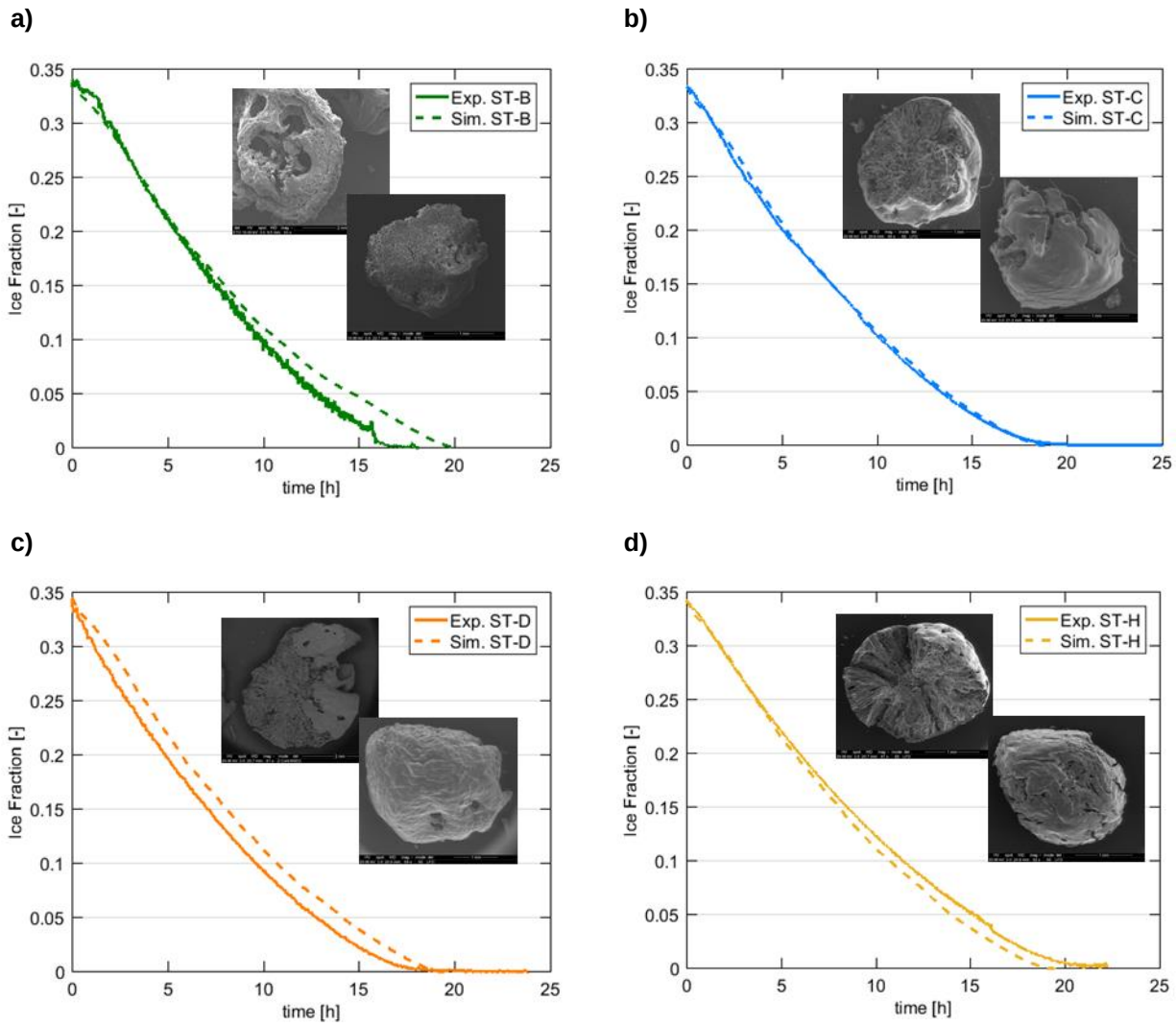

Figure 6.4 – Predicted and measured drying time changing over time during drying of production strains: a) ST-B, b) ST-C, c) ST-D and d) ST-H. The continuous line represents the measured fraction of ice and the dashed line represents the simulated fraction of ice.

When developing a freeze-drying cycle, it is critical to acquire knowledge on product temperature throughout the process. It is essential to identify the appropriate conditions, based on product characteristics, for primary drying. The product temperature should remain below the glass/collapse temperature of the freeze-dried material without being unnecessarily low, resulting in prolonged freeze-drying cycles [125]. Furthermore, the importance of monitoring product temperature during scale-up is recognized in order to assure that the time course of product temperature during process development at a smaller scale and a larger scale are consistent. However, several problems and sources of uncertainty associated with the measurement of product temperature have been reported [125]. One of the sources

of uncertainty is the variation of the drying behavior connected to the presence of temperature probes in contact with the product. Particularly for the freeze-drying of particulate material, problems arise to determine the exact temperature of the product since the probes are only in contact with its surface. Additionally, it is challenging to determine the exact location of the measurement. Figure 6.5 shows the product temperature profile measured during the drying step of Maltodextrin 30. It is observable that the temperature increases at a constant rate until it achieves the sublimation temperature. The sublimation process is an endothermic process meaning that energy is absorbed by the system for the phase change. Therefore, a decrease of the rate at which temperature increases at around -32 °C is noticeable in Figure 6.5, which corresponds to the sublimation temperature at the respective chamber pressure. Furthermore, a steeper increase of the temperature is observed in the probe that is mounted closer to the heating source (bottom of the tray).

Figure 6.5 helps also to evaluate the predicted product temperature by comparison with the performed measurements at laboratory/pilot scale. It is observed that the simulated temperature increases at a much slower rate than the temperature measured by the temperature probes placed in a laboratory/pilot freeze-dryer. A commercial CFD software, ANSYS CFX 17.1, was used in the current work for the simulation of the flow structure during the drying process. CFD calculations are based on continuum Navier-Stokes equations for viscous flows. As mentioned throughout this work, the continuum hypothesis is only valid for flows at small Knudsen numbers. For flows in the transition regime, the non-equilibrium rarefaction will influence the flow near gas-solid interfaces and consequently these effects must be accounted for in the boundary conditions[71]. From the product tray to the condenser, flow goes through several flow regimes. For Maltodextrin 30, the flow in the product tray is in the transition regime (Table 6.3), and therefore a finite slip wall was implemented that considers a temperature jump relation for the heat transfer. However, this implementation was not successful leading to the conclusion that further studies are needed for the correct implementation of heat transfer phenomena during freeze-drying in commercial CFD software.

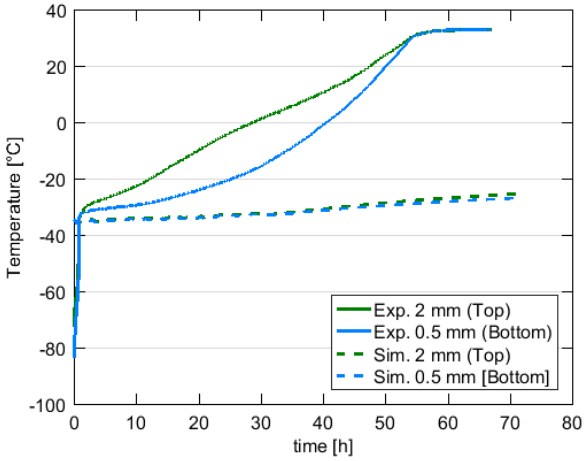

Figure 6.5 – (—) Measured product temperature as a function of time at 0.5 mm and 2 mm from the bottom of the tray. (----) Simulated product temperature as a function of time at 0.5 mm and 2 mm from the bottom of the tray.

6.3.2 Packing Factor Studies

The drying and flow patterns during freeze-drying are both dependent on the characteristics of the product and the characteristics of the equipment. The investigation of the drying pattern allows the development of optimized cycles since it helps to determine possible heterogeneities during drying due to intrinsic heterogeneity of the product or of the drying chamber [199]. However, it is difficult to identify and quantify such effects on the final experimental results. CFD modelling allows the efficient investigation of these effects and the quantitative description of essential parameters that are difficult to obtain through experimental approaches [108], [199]. To analyze the flow structure in a dryer, the developed model considers the dryer geometry, surface temperature, fluid properties, and pressure boundary conditions at the chamber and condenser end [71].

Error! Reference source not found. shows the distribution of ice at different stages of primary drying of two cases with different packing factors, which allows observing the influence of heat transfer on the drying process. In the studied cases heat is transferred through radiation from the top heating shelf and through conduction from the tray where the product is loaded, which was heated through radiation by the bottom heating shelf. Figure 6.6 shows that drying will occur faster in the areas closer to the tray (higher heat transfer) and from the upper part of the tray (less resistance to fluid flow and heating source through radiation). Furthermore, it is possible to observe the effect of different packing factors. When comparing Figure 6.6 b) and d) it is observable that for lower packing factors, since the fluid motion is easier, the drying of the porous material will depend on heat transfer, meaning that areas closer to the heating sources will dry faster. On the contrary when the packing factor is higher, the drying behavior will be similar to the drying of a vial, meaning that the sublimation front will progress from the top to the bottom of the tray.

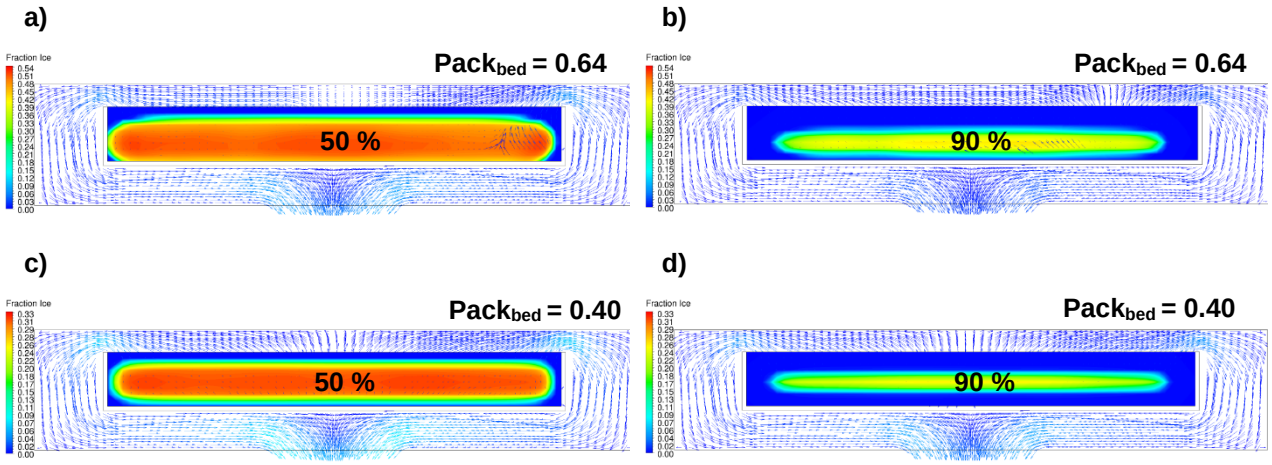

Figure 6.6 – Contour of ice fraction present in the tray and the water gas flow pattern in the chamber at different stages of primary drying and assuming different packing factors: a) 50 % of the ice has sublimated and the packing factor is 0.64, b) 90 % of the ice has sublimated and the packing factor is 0.64, c) 50 % of the ice has sublimated and the packing factor is 0.40, b) 90 % of the ice has sublimated and the packing factor is 0.40.

6.3.3 Chamber Design Studies

The vapor flow in freeze-drying systems is affected by the design of the apparatus as well as by the operating temperature and pressure [106]. The analysis of complex, three-dimensional flow phenomena can be aided by the application of CFD techniques, which have been recognized to be beneficial in the analyses of various designs and process parameters. In this section, it was intended to study the effect of the proximity of the top heating shelf to the product tray. Figure 6.7 a) shows that there is not a significant change in the drying time as a result of an almost 3.5 times increase of the height of the top heating shelf. However, a small decrease of the pressure in the product tray as a consequence of the increase of the height of the shelf temperature is observed in Figure 6.7 b).

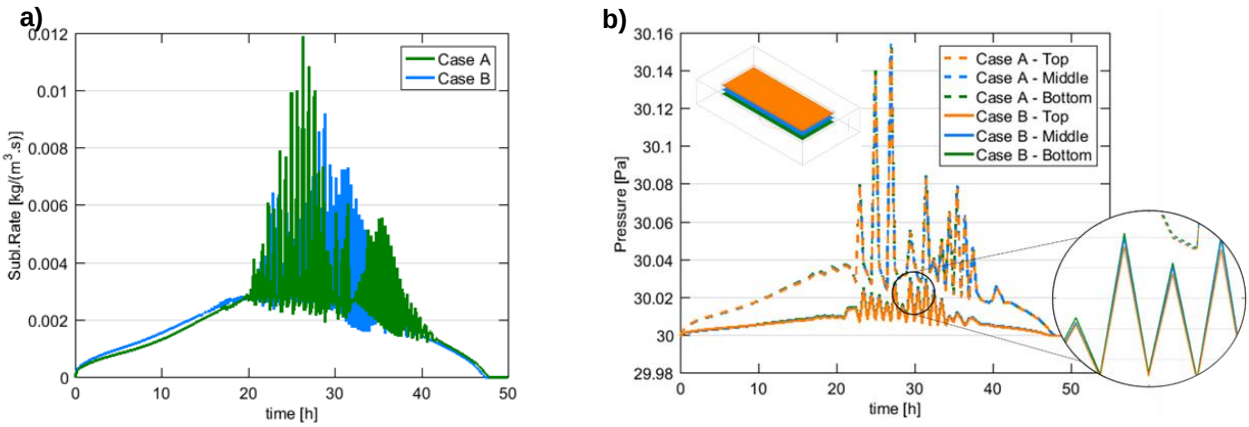

Figure 6.7 – a) Sublimation rate as a function of drying time for Case A and Case B. b) Pressure as a function of drying time in different planes of the tray for Case A and Case B. The top plane is at 3.2 mm, the middle plane at 1.75 mm and the bottom plane at 0.40 mm from the bottom of the tray.

Although, no significant changes were observed in the drying cycle due to the design changes applied in the drying chamber, it is important to mention the possible effect of such changes on the product quality. An increase or decrease of the pressure might lead to a shift of the sublimation temperature which can cause the micro-collapse or even the collapse of the product. It is, therefore, relevant to highlight that different drying rates and/or chamber pressures can produce different freeze-dried products, both in the appearance and viability of the microorganisms present [19].

The potential of the use of computational fluid dynamics (CFD) tools for the investigation of the effect of the equipment design during freeze-drying was illustrated in this section, although in the studied cases there was no significant difference in the drying behaviour due to changes in the equipment design. Computational fluid dynamics (CFD) offers a route to facilitate the design of more coherent freeze-drying cycles with increased knowledge of the process.

6.4 Conclusions

The design of freeze-drying cycles is usually achieved through an extensive amount of experimental work and it consists of the identification of the optimal values of shelf temperature, chamber pressure and process duration. This is an expensive and time consuming approach which does not guarantee that an optimal solution is achieved. Furthermore, the in-line measuring technologies for the important parameters involved in the optimization and control of freeze-drying cycles present several challenges and inaccuracies.

The development of mathematical models is increasingly important for process development in order to satisfy the need for improved process understanding. The available information for the freeze-drying of bulk material in open trays, mainly used in the biotechnology and food industry, is limited. Therefore, this chapter has focused on the development of a model based on computational fluid dynamics (CFD), in order to analyze the flow behavior during primary drying of particulate matter loaded on a tray in a pilot scale dryer. The developed CFD model couples both the dryer hardware and the product characteristics.

The model showed good results in the prediction of drying times, to satisfactorily predict the drying times for different porous materials. Furthermore, the model was able to successfully predict the fraction of ice present in the tray over the time course of the drying process. The simulated results showed the importance of characterizing the product morphology in order to have models that correlate satisfactorily with the experimental measurements.

The model was not successful in the prediction of the product temperature. Gas phase conduction and convective mechanisms are pressure dependent. Since freeze-drying occurs at very low pressures and the flow on the investigated cases was found to be in the transient regime, the model must consider the velocity slip and temperature jump boundary conditions. The implementation of a finite slip wall in the

boundary conditions was not successful. The correct prediction of product temperature is essential for the design of optimal freeze-drying cycles, and therefore, additional studies of the correct implementation of the boundary conditions are needed. A fundamental understanding of heat and mass transfer during drying is essential for the construction of an accurate model.

The presented model can furthermore assist with developing increased process understanding regarding the effect of packing and equipment design. CFD simulations allow further investigation of the possible heterogeneities derived from different packing factors of the particles, which may lead to different drying behaviour. Furthermore, the CFD model allows the study of the effect of the chamber, duct and condenser design on the process and final product characteristics. The investigated cases present differences regarding the distance between the product tray and the heating shelf. However, the developed CFD model allows the study of other geometries as well.

Chapter 7

Conclusions and Future Perspectives

The aim of this thesis was the development of a mathematical model using CFD tools in order to predict and better understand the drying behaviour of lactic acid bacteria during freeze-drying. The main conclusions from each chapter were already presented throughout this thesis. In this section, it is intended to give a broader perspective of the main conclusions and future perspectives.

7.1 Investigation of the Drying Behaviour of Starter Cultures

Starter cultures are nowadays widely used for the production of fermented foods. This project focused on lactic acid bacteria since they are the main microorganisms responsible for fermentation of fermented food products, and therefore one of the most common starter cultures. Freeze-drying of starter cultures allows its easier and less costly handling, transport, storage and application. Furthermore, since freeze-drying operates at low temperature, thermal damage of the products is minimized, and the structural and shape characteristics of the product are preserved. Four production strains from *Streptococcus thermophilus* were used as model organisms.

Product drying behaviour at laboratory/pilot scale and production scale was investigated for the four production strains chosen as model organisms. Differences in their performance were found after an exploratory analysis of production data from the last six years, which motivated further studies with focus on the characterization of the morphology of the product. The investigation led to the conclusion that the composition of the medium after centrifugation and after the addition of cryo- and lyo- protectants influences the final drying matrix (i.e. tortuosity, porosity, pore size distribution, particle diameter) which consequently influences the drying behaviour. Furthermore, the choice of process parameters (pressure and temperature) depends on the composition of the product being freeze-dried since the product temperature should be at all times below the collapse temperature (T_c') in order to keep the structure of the product. Thus, both the composition of the product and the maximum temperature allowed by the product should be considered when designing freeze-drying cycles for new products.

Furthermore, production data of the last six years of freeze-drying of the same strain on different Chr. Hansen sites was also presented in this thesis. No differences were found in the drying behaviour and product quality after the exploratory analysis. However, it was observed that different process parameters (i.e. pressure, temperature and process duration) were applied on the different sites depending on the design of the existent freeze-drying equipment. Which means that cycle optimization had to be performed

in order to transfer the production process of the same product between sites without changing the product quality.

In the traditional approach, the design and optimization of freeze-drying cycles is usually obtained through an extensive amount of experimental work, which has to be repeated every time a new product is implemented or the process is transferred to a larger scale or an equipment with different characteristics. This is an expensive and time consuming approach which does not guarantee the achievement of an optimal solution. Furthermore, the in-line measuring technologies for the important parameters involved in the optimization and control of freeze-drying cycles, present several challenges and inaccuracies. In this thesis a mathematical model was developed in order to overcome these challenges.

7.2 Model Development and Implementation

This thesis has shown the potential of the use of computational fluid dynamics (CFD), as an advanced modelling approach for the prediction of the drying behaviour of particulate material. When compared to the experimental approach outlined above, CFD allows the design of freeze-drying cycles in a more efficient and less expensive way that considers both the characteristics of the product and of the equipment. Therefore, it can be used as a complementary tool in the design and optimization of freeze-drying cycles for new products, for the scale-up of new processes and for process transfer between equipment.

CFD tools support the investigation of the effect of product morphology on the sublimation rate when designing new processes. This thesis focused on the freeze-drying of particulate material, which is characterized by a bimodal pore size distribution, meaning that both the size of the pores inside the product and the size of the pores that characterize the bed of particles influence the drying behaviour and the diffusion of vapour during sublimation. The adopted strategy for model development was based on a scale-up approach – going from the small scale of a single particle where only product characteristics are addressed, to the laboratory/pilot scale where both product and equipment characteristics are taken into account. This approach increased the confidence in modelling predictions and allowed the investigation of the most relevant parameters at each step of the process.

The ability to successfully predict the sublimation phenomena of a porous product at isothermal conditions was demonstrated by comparison with the results collected from a freeze-drying microscope (FDM). The relevance of product characterization (porosity, tortuosity and pore size distribution) in order to achieve an increased understanding of the mass transfer phenomena taking place during primary drying was highlighted by the implementation of the CFD model. Furthermore, the effect of neighbouring particles and bed porosity on the length of a freeze-drying batch was also investigated. The qualitative results obtained in the case studies in this thesis allow a better understanding of the mass transport

phenomena occurring in a stack of particles and ensure further understanding of the optimal particle size that leads to more efficient processes.

The drying behaviour of particle based material is, besides the porous system and the operating conditions, largely affected by the equipment design [71], [109]. The efficiency of the process is affected by the chamber size and configuration, and by the condenser capacity, which is not accounted for in the previously mentioned studies [85], [117]. Therefore, the last section of this thesis focused on the development of a mathematical model where product and equipment characteristics are coupled, and both mass and heat transfer phenomenon can be investigated. CFD simulations showed good results in the investigation of possible heterogeneities in the drying behaviour and drying time derived from different morphological characteristics of the porous product. However, throughout drying, water vapour is produced and transported from the product tray to the condenser through different flow regimes. A commercial CFD software, ANSYS CFX 17.1, was used for the simulation of the flow structure during the drying process. CFD calculations are based on continuum Navier-Stokes equations for viscous flows. As mentioned throughout this work, the continuum hypothesis is only valid for flows at small Knudsen numbers. Since the gas phase conduction and convective mechanisms are pressure dependent and freeze-drying is performed at low pressures, a fundamental understanding of heat and mass transfer during drying is essential for the construction of an accurate model. The prediction of product temperature was not successful leading to the conclusion that further studies are needed for the correct implementation of heat transfer phenomena during freeze-drying in commercial CFD software. Alternatively, kinetic Boltzmann equation or the Monte Carlo method could be employed since these are valid for the different flow regimes. However, no commercial software tool is available based on these methods, and therefore these approaches are not easy to implement since.

In order to leverage the time and computational effort associated with simulations of larger scales processes, the bimodal porous material was simplified to a unimodal porous domain, meaning that the diffusion coefficient and the morphological characteristics of the porous media were approximated by the weighted average. This approximation leads to inaccuracies and lack of understanding of some of the phenomena happening in the process, therefore a multi-scale fully coupled modelling approach could be implemented. However, computational cost increases with the introduction of additional complexity and therefore this compromise should be analysed for each individual case.

In summary, the successful transfer of lyophilization processes from the development laboratory to production and commercial manufacturing sites requires the true understanding of the relations between the formulation composition, the process parameters and the equipment capabilities. The use of mathematical models for the investigation of optimal process conditions opens the possibility to mechanistically understand scale-up issues and to develop robust freeze-drying cycles that facilitate the transfer between different devices. Furthermore, it is important to keep a compromise between product requirements (maximum temperature and pressure) and process parameters (chamber pressure, shelf

temperature and drying time) when developing freeze-drying cycles. Additionally, the survival to freezing and drying will also depend on the strain being freeze-dried and its resistance to dehydration, low pressures and temperature increase. Further studies are needed in order to better understand the mechanisms happening inside the cell during freezing and drying and in order to understand the effect of the final drying matrix on the survival of the bacteria. The combination of CFD and increased knowledge on the protection mechanisms happening in the cell has massive potential in the optimization and development of new freeze-drying processes.

Chapter 8

References

[1] B. Speranza, A. Bevilacqua, M. R. Corbo, and M. Sinigaglia, Eds., *Starter cultures in food production*. Wiley-VCH Verlag GmbH & Co. KGaA, Weinheim, Germany, 2017.

[2] P. Melin, S. Håkansson, and J. Schnürer, “Optimisation and comparison of liquid and dry formulations of the biocontrol yeast Pichia anomala J121,” *Appl. Microbiol. Biotechnol.*, vol. 73, no. 5, pp. 1008–1016, 2007.

[3] S. H. Peighambardoust, “Application of spray drying for preservation of lactic acid starter cultures : a review,” *Trends Food Sci. Technol.*, vol. 22, no. 5, pp. 215–224, 2011.

[4] C. Santivarangkna, U. Kulozik, and P. Foerst, “Alternative Drying Processes for the Industrial Preservation of Lactic Acid Starter Cultures,” *Biotechnol. Prog.*, vol. 23, no. 2, pp. 302–315, 2007.

[5] L. Rey, “Glimpses into the Realm of Freeze-Drying: Classical Issues and New Ventures,” in *Freeze Drying/ Lyophilization of Pharmaceutical and Biological Products*, Third., L. Rey and J. C. May, Eds. informa, 2010, pp. 1–28.

[6] F. Franks, “Freeze-drying of bioproducts: Putting principles into practice,” *Eur. J. Pharm. Biopharm.*, vol. 45, no. 3, pp. 221–229, 1998.

[7] B. Roser, “Trehalose , a new approach to premium dried foods,” *Trends Food Sci. Technol.*, vol. 2, pp. 166–169, 1991.

[8] A. A. Pisano, Roberto; Fissore, Davide; Velardi, Salvatore A.; Barresi, “In-Line Optimization and Control of an Industrial Freeze-Drying Process for Pharmaceuticals,” *J. Pharm. Sci.*, vol. 99, no. 11, pp. 4691–4709, 2010.

[9] H. Sadikoglu and a. I. Liapis, “Mathematical Modelling of the Primary and Secondary Drying Stages of Bulk Solution Freeze-Drying in Trays: Parameter Estimation and Model Discrimination by Comparison of Theoretical Results With Experimental Data,” *Dry. Technol.*, vol. 15, no. March 2015, pp. 791–810, 1997.

[10] D. Fissore, R. Pisano, and A. A. Barresi, “Process analytical technology for monitoring pharmaceuticals freeze-drying – A comprehensive review,” *Dry. Technol.*, pp. 1–27, 2018.

[11] L. De Vuyst, “Lactic acid bacteria as functional starter cultures for the food fermentation industry,” *Trends Food Sci. Technol.*, vol. 15, no. 2, pp. 67–78, 2004.

[12] C. Daly, G. F. Fitzgerald, and R. Davis, “Biotechnology of lactic acid bacteria with special reference to bacteriophage resistance,” *Antonie van Leeuwenhoek, Int. J. Gen. Mol. Microbiol.*, vol. 70, no. 2–4, pp. 99–110, 1996.

[13] P. Capela, T. K. C. Hay, and N. P. Shah, “Effect of cryoprotectants, prebiotics and microencapsulation on survival of probiotic organisms in yoghurt and freeze-dried yoghurt,” *Food Res. Int.*, vol. 39, no. 2, pp. 203–211, 2006.

[14] A. S. Carvalho, J. Silva, P. Ho, P. Teixeira, F. X. Malcata, and P. Gibbs, “Relevant factors for the preparation of freeze-dried lactic acid bacteria,” *Int. Dairy J.*, vol. 14, no. 10, pp. 835–847, 2004.

[15] M. Aschenbrenner, “Freeze-drying of Probiotics,” in *Advances in Probiotic Technology*, P. Foerst and C. Santivarangkna, Eds. CRC Press, 2015, pp. 213–238.

[16] G. Blond and D. Simatos, “Optimized thermal treatments to obtain reproducible DSC thermograms with sucrose+dextran frozen solutions,” *Food Hydrocoll.*, vol. 12, no. 2, pp. 133–139, 1998.

[17] C. Santivarangkna, M. Aschenbrenner, U. Kulozik, and P. Foerst, “Role of Glassy State on Stabilities of Freeze-Dried Probiotics,” *J. Food Sci.*, vol. 76, no. 8, 2011.

[18] T. Nei, “Growth of ice crystals in frozen specimens,” *J. Microsc.*, vol. 99, no. 2, pp. 227–233, 1973.

[19] C. A. Morgan, N. Herman, P. A. White, and G. Vesey, “Preservation of micro-organisms by drying; A review,” *J. Microbiol. Methods*, vol. 66, no. 2, pp. 183–193, 2006.

[20] F. Dumont, P.-A. Marechal, and P. Gervais, “Cell Size and Water Permeability as Determining Factors for Cell Viability after Freezing at Different Cooling Rates,” *Appl. Environ. Microbiol.*, vol. 70, no. 1, pp. 268–272, 2004.

[21] F. Fonseca, M. Marin, and G. J. Morris, “Stabilization of frozen Lactobacillus delbrueckii subsp. bulgaricus in glycerol suspensions: Freezing kinetics and storage temperature effects,” *Appl. Environ. Microbiol.*, vol. 72, no. 10, pp. 6474–6482, 2006.

[22] L. Bâati, C. Fabre-Gea, D. Auriol, and P. J. Blanc, “Study of the cryotolerance of Lactobacillus acidophilus: Effect of culture and freezing conditions on the viability and cellular protein levels,” *Int. J. Food Microbiol.*, vol. 59, no. 3, pp. 241–247, 2000.

[23] I. I. Morozov and V. G. Petin, “The influence of cyclic heating and cooling on Escherichia coli survival,” *Microbiology*, vol. 76, no. 2, pp. 172–176, 2007.

[24] Y. H. Roos, “Frozen State Transitions in Relation to Freeze-Drying,” *J. Therm. Anal.*, vol. 48, pp. 535–544, 1997.

[25] L. Slade *et al.*, “Beyond water activity : Recent advances based on an alternative approach to the assessment of food quality and safety Beyond Water Activity : Recent Advances Based on an Alternative Approach to the Assessment of Food Quality and Safety,” *Crit. Rev. Food Sci. Nutr.*, vol. 30, no. (2-3), pp. 115–360, 1991.

[26] T. A. Jennings, *Lyophilization - Introduction and Basic Principles*. informa healthcare, 1999.

[27] K. S. Pehkonen, Y. H. Roos, S. Miao, R. P. Ross, and C. Stanton, “State transitions and

physicochemical aspects of cryoprotection and stabilization in freeze-drying of Lactobacillus rhamnosus GG (LGG)," *J. Appl. Microbiol.*, vol. 104, no. 6, pp. 1732–1743, 2008.

[28] G.-W. Oetjen, *Freeze Drying*. Wiley-VCH Verlag GmbH & Co. KGaA, Weinheim, Germany, 1999.

[29] G. D. J. Adams, I. Cook, and K. R. Ward, "The Principles of Freeze-Drying," in *Cryopreservation and Freeze-Drying Protocols*, Third Edit., W. F. Wolkers and H. Oldenhof, Eds. 2015, pp. 121–146.

[30] M. Aschenbrenner, P. Foerst, and U. Kulozik, "Freeze-drying of Probiotics," in *Advances in Probiotic Technology*, no. August, F. Petra and C. Santivarangkna, Eds. CRC Press, 2015, pp. 213–241.

[31] M. J. Pikal, "Design of freeze-drying processes for pharmaceuticals: practical advice," *Pharm. Res.*, vol. 21, no. 2, pp. 191–200, 2004.

[32] P. Properties, "Effects of Annealing on Freeze- Dried Lactobacillus acidophilus," *Food Eng. Phys. Prop.*, vol. 68, no. 8, pp. 2504–2511, 2003.

[33] S. Passot *et al.*, "Effect of product temperature during primary drying on the long-term stability of lyophilized proteins," *Pharm. Dev. Technol.*, vol. 12, no. 6, pp. 543–553, 2007.

[34] F. Fonseca, O. Cunin, and M. Marin, "Collapse Temperature of Freeze-Dried Lactobacillus bulgaricus Suspensions and Protective Media," *Biotechnol. Pro*, vol. 20, pp. 229–238, 2004.

[35] F. Franks and T. Auffret, *Freeze-drying of Pharmaceuticals and Biopharmaceuticals*. Cambridge: RSC Publishing, 2007.

[36] P. Sheehan and A. I. Liapis, "Modeling of the primary and secondary drying stages of the freeze drying of pharmaceutical products in vials: Numerical results obtained from the solution of a dynamic and spatially multi-dimensional lyophilization model for different operational policies,"

Biotechnol. Bioeng., vol. 60, no. 6, pp. 712–728, 1998.

[37] G. E. Gardiner *et al.*, “Comparative Survival Rates of Human-Derived Probiotic Lactobacillus paracasei and L . salivarius Strains during Heat Treatment and Spray Drying,” *Appl. Environ. Microbiol.*, vol. 66, no. 6, pp. 2605–2612, 2000.

[38] G. F. de Valdez, G. S. de Giori, A. P. de Ruiz Holgado, and G. Oliver, “Rehydration conditions and viability of freeze-dried lactic acid bacteria,” *Cryobiology*, vol. 22, no. 6, pp. 574–577, 1985.

[39] G. Zayed and Y. H. Roos, “Influence of trehalose and moisture content on survival of Lactobacillus salivarius subjected to freeze-drying and storage,” *Process Biochem.*, vol. 39, no. 9, pp. 1081–1086, 2004.

[40] O. F. Nielsen, M. Bilde, and M. Frosch, “Water Activity,” *Spectrosc. An Int. J.*, vol. 27, no. 5, pp. 565–569, 2012.

[41] M. J. Pikal, S. Shah, M. L. Roy, and R. Putman, “The secondary drying stage of freeze drying: drying kinetics as a function of temperature and chamber pressure,” *Int. J. Pharm.*, vol. 60, no. 3, pp. 203–207, 1990.

[42] G.-W. Oetjen and P. Haseley, “Installation and Equipment Technique: Sections 2.1 and 2.2,” in *Freeze-Drying*, Second Edi., Wiley-VCH Verlag GmbH & Co. KGaA, Weinheim, Germany, 2003.

[43] S. M. Patel and M. J. Pikal, “Freeze-drying in novel container system: Characterization of heat and mass transfer in glass syringes,” *J. Pharm. Sci.*, vol. 99, no. 7, pp. 3188–3204, 2010.

[44] S. M. Patel and M. J. Pikal, “Emerging Freeze-Drying Process Development and Scale-up Issues,” *AAPS PharmSciTech*, vol. 12, no. 1, pp. 372–378, 2011.

[45] G. Broeckx, D. Vandenheuvel, I. J. J. Claes, S. Lebeer, and F. Kiekens, “Drying techniques of probiotic bacteria as an important step towards the development of novel pharmabiotics,” *Int. J.*

Pharm., vol. 505, no. 1–2, pp. 303–318, 2016.

[46] A. S. Carvalho, J. Silva, P. Ho, P. Teixeira, F. X. Malcata, and P. Gibbs, “Effects of Various Sugars Added to Growth and Drying Media upon Thermotolerance and Survival throughout Storage of Freeze-Dried lactobacillus delbrueckii ssp. bulgaricus,” *Biotechnol. Prog.*, vol. 20, no. 1, pp. 248–254, 2004.

[47] J. Palmfeldt, P. Rådström, and B. Hahn-Hägerdal, “Optimisation of initial cell concentration enhances freeze-drying tolerance of Pseudomonas chlororaphis,” *Cryobiology*, vol. 47, no. 1, pp. 21–29, 2003.

[48] Z. Hubálek, “Protectants used in the cryopreservation of microorganisms,” *Cryobiology*, vol. 46, no. 3, pp. 205–229, 2003.

[49] P. B. Conrad, D. P. Miller, P. R. Cielenski, and J. J. De Pablo, “Stabilization and preservation of Lactobacillus acidophilus in saccharide matrices,” *Cryobiology*, vol. 41, no. 1, pp. 17–24, 2000.

[50] David E. Pegg, “Principles of Cryopreservations,” in *Cryopreservationand Freeze-Drying Protocols*, Second., J. G. Day and G. N. Stacey, Eds. Totowa, New Jersey: Humana Press, 2007, pp. 39–57.

[51] C. Santivarangkna, U. Kulozik, and P. Foerst, “Inactivation mechanisms of lactic acid starter cultures preserved by drying processes,” *J. Appl. Microbiol.*, vol. 105, no. 1, pp. 1–13, 2008.

[52] J. H. Crowe, J. F. Carpenter, and L. M. Crowe, “The Role of Vitrification in Anhydrobiosis,” *Annu. Rev. Physiol.*, vol. 60, no. 1, pp. 73–103, 1998.

[53] J. H. Crowe, F. a Hoekstra, and L. M. Crowe, “Anhydrobiosis,” *Annu. Rev. Physiol.*, vol. 54, pp. 579–599, 1992.

[54] L. M. Crowe, “Lessons from nature: The role of sugars in anhydrobiosis,” *Comp. Biochem. Physiol.*

- *A Mol. Integr. Physiol.*, vol. 131, no. 3, pp. 505–513, 2002.

[55] D. T. Welsh and R. A. Herbert, “Osmotically induced intracellular trehalose, but not glycine betaine accumulation promotes desiccation tolerance in Escherichia coli,” *FEMS Microbiol. Lett.*, vol. 174, no. 1, pp. 57–63, 1999.

[56] D. Billi and M. Potts, “Life and death of dried prokaryotes,” *Res. Microbiol.*, vol. 153, no. 1, pp. 7–12, 2002.

[57] R. Pisano, D. Fissore, A. A. Barresi, and M. Rastelli, “Quality by design: scale-up of freeze-drying cycles in pharmaceutical industry.,” *AAPS PharmSciTech*, vol. 14, no. 3, pp. 1137–49, 2013.

[58] K. M. Hangos and I. T. Cameron, *Process modelling and model analysis*. Academic Press, 2001.

[59] H. A. B. te Braake, H. J. L. van Can, and H. B. Verbruggen, “Semi-mechanistic modeling of chemical processes with neural networks,” *Eng. Appl. Artif. Intell.*, vol. 11, no. 4, pp. 507–515, 1998.

[60] M. von Stosch, R. Oliveira, J. Peres, and S. Feyo de Azevedo, “Hybrid semi-parametric modeling in process systems engineering: Past, present and future,” *Comput. Chem. Eng.*, vol. 60, pp. 86–101, 2014.

[61] S. Passot, I. C. Tréléa, M. Marin, M. Galan, G. J. Morris, and F. Fonseca, “Effect of controlled ice nucleation on primary drying stage and protein recovery in vials cooled in a modified freeze-dryer.,” *J. Biomech. Eng.*, vol. 131, no. July 2009, p. 074511, 2009.

[62] H. Sadikoglu, “Optimal Control of the Primary Drying Stage of Freeze Drying of Solutions in Vials Using Variational Calculus,” *Dry. Technol.*, vol. 23, no. July 2014, pp. 33–57, 2005.

[63] P. Chouvenc, S. Vessot, J. Andrieu, and P. Vacus, “Optimization of the Freeze-Drying Cycle: A New Model for Pressure Rise Analysis,” *Dry. Technol.*, vol. 22, no. March 2015, pp. 1577–1601,

2004.

[64] S. A. Velardi and A. A. Barresi, “Development of simplified models for the freeze-drying process and investigation of the optimal operating conditions,” *Chem. Eng. Res. Des.*, vol. 86, no. 1 A, pp. 9–22, 2008.

[65] S. Rambhatla, R. Ramot, C. Bhugra, and M. J. Pikal, “Heat and mass transfer scale-up issues during freeze drying: II. Control and characterization of the degree of supercooling.,” *AAPS PharmSciTech*, vol. 5, no. 4, p. e58, 2004.

[66] K. Nakagawa and T. Ochiai, “A mathematical model of multi-dimensional freeze-drying for food products,” *J. Food Eng.*, vol. 161, pp. 55–67, 2015.

[67] A. a. Barresi, R. Pisano, V. Rasetto, D. Fissore, and D. L. Marchisio, “Model-Based Monitoring and Control of Industrial Freeze-Drying Processes: Effect of Batch Nonuniformity,” *Dry. Technol.*, vol. 28, no. February 2016, pp. 577–590, 2010.

[68] E. Y. Shalaev and G. Zografi, “How does residual water affect the solid-state degradation of drugs in the amorphous state?,” *J. Pharm. Sci.*, vol. 85, no. 11, pp. 1137–1141, 1996.

[69] C. Costantino, HR; Curley, JG; Hsu, “Determining the water sorption monolayer of lyophilized pharmaceutical proteins,” *J. Pharm. Sci.*, vol. 86, no. 12, pp. 1390–1393, 1997.

[70] S. Passot, S. Cenard, I. Douania, I. C. Tréléa, and F. Fonseca, “Critical water activity and amorphous state for optimal preservation of lyophilised lactic acid bacteria,” *Food Chem.*, vol. 132, no. 4, pp. 1699–1705, 2012.

[71] A. Ganguly, A. A. Alexeenko, S. G. Schultz, and S. G. Kim, “Freeze-drying simulation framework coupling product attributes and equipment capability: Toward accelerating process by equipment modifications,” *Eur. J. Pharm. Biopharm.*, vol. 85, no. 2, pp. 223–235, 2013.

[72] S. Basu, U. S. Shivhare, A. S. Mujumdar, S. Basu, U. S. Shivhare, and A. S. Mujumdar, “Models for Sorption Isotherms for Foods : A Review Models for Sorption Isotherms for Foods : A Review,” *Dry. Technol.*, vol. 24, no. 8, pp. 917–930, 2006.

[73] M. Xu, G. Chen, J. Fan, J. Liu, X. Xu, and S. Zhang, “Moisture sorption characteristics of freeze-dried human platelets *,” *J Zhejiang Univ-Sci B (Biomed Biotechnol.*, vol. 12, no. 3, pp. 210–218, 2011.

[74] E. K. Sahni and M. J. Pikal, “Modeling the Secondary Drying Stage of Freeze Drying : Development and Validation of an Excel-Based Model,” *J. Pharm. Sci.*, vol. 106, pp. 779–791, 2017.

[75] S. Adhami, A. Rahimi, and M. S. Hatamipour, “Comparison of quasi-steady-state and unsteady-state formulations in a freeze dryer modeling,” *Heat Mass Transf. und Stoffuebertragung*, vol. 50, no. 9, pp. 1291–1300, 2014.

[76] M. J. Pikal, S. Cardon, C. Bhugra, F. Jameel, and S. Rambhatla, “The Nonsteady State Modeling of Freeze Drying : In-Process Product Temperature and Moisture Content Mapping and Pharmaceutical Product The Nonsteady State Modeling of Freeze Drying : In-Process Product Temperature and Moisture Content Mapping and Pharmace,” *Pharm. Dev. Technol.*, vol. 7450, no. 778575344, 2005.

[77] W. K. Nastaj J, “Numerical model of freeze drying of random solids at two-region conductive–radiative heating,” *Inz. Chem. Proces.*, vol. 25, no. 1, pp. 109–121, 2004.

[78] H. Tu, WP; Chen, ML; Yang, ZR; Chen, “A mathematical model for freeze-drying,” *Chinese J. Chem. Eng.*, vol. 8, no. 2, pp. 118–122, 2000.

[79] R. Peczalski and J. Andrieu, “Freeze-Drying of Pharmaceutical Proteins in Vials: Modeling of Freezing and Sublimation Steps,” *Dry. Technol.*, vol. 24, no. 5, pp. 561–570, 2006.

[80] E. A. Boss, R. M. Filho, and E. C. Vasco De Toledo, “Freeze drying process: Real time model and optimization,” *Chem. Eng. Process. Process Intensif.*, vol. 43, no. 12, pp. 1475–1485, 2004.

[81] A. I. Liapis and R. Bruttini, “A theory for the primary and secondary drying stages of the freeze-drying of pharmaceutical crystalline and amorphous solutes: comparison between experimental data and theory,” *Sep. Technol.*, vol. 4, no. 3, pp. 144–155, 1994.

[82] W. J. Mascarenhas, H. U. Akay, and M. J. Pikal, “A computational model for finite element analysis of the freeze-drying process,” *Comput. Methods Appl. Mech. Eng.*, vol. 148, no. 1–2, pp. 105–124, 1997.

[83] A. Sheehan, P; Liapis, “Modeling of the primary and secondary drying stages of the freeze drying of pharmaceutical products in vials: Numerical results obtained from the solution of a dynamic and spatially multi-dimensional lyophilization model for different operational policies,” *Biotechnol. Bioeng.*, vol. 60, no. 6, pp. 712–728, 1998.

[84] J. H. Nam and C. S. Song, “Numerical simulation of conjugate heat and mass transfer during multi-dimensional freeze drying of slab-shaped food products,” *Int. J. Heat Mass Transf.*, vol. 50, no. 23–24, pp. 4891–4900, 2007.

[85] A. I. Liapis and R. Bruttini, “A mathematical model for the spray freeze drying process: The drying of frozen particles in trays and in vials on trays,” *Int. J. Heat Mass Transf.*, vol. 52, no. 1–2, pp. 100–111, 2009.

[86] I. C. Trelea, F. Fonseca, and S. Passot, “Dynamic Modelling of the Secondary Drying Stage of Freeze-Drying Reveals Distinct Desorption Kinetics for Bound Water,” *Dry. Technol.*, vol. 3937, no. December, p. 150619113428004, 2015.

[87] I. C. Trelea, S. Passot, F. Fonseca, and M. Marin, “An Interactive Tool for the Optimization of Freeze-Drying Cycles Based on Quality Criteria,” *Dry. Technol.*, vol. 25, no. 5, pp. 741–751, 2007.

[88] C. Sung, J. H. Nam, C. Kim, and S. T. Ro, “Temperature distribution in a vial during freeze-drying of skim milk,” *J. Food Eng.*, vol. 67, pp. 467–475, 2005.

[89] R. J. Litchfield and A. I. Liapis, “An adsorption-sublimation model for a freeze-dryer,” *Chem. Eng. Sci.*, vol. 34, pp. 1085–1090, 1979.

[90] M. J. Millman, a. I. Liapis, and J. M. Marchello, “An analysis of the lyophilization process using a sorption-sublimation model and various operational policies,” *AIChE J.*, vol. 31, no. 10, pp. 1594–1604, 1985.

[91] M. J. Millman, A. I. Liapis, and J. M. Marchello, “Guidelines of the desirable operation of batch freeze driers during the removal of free water,” *J. Food Technol.*, vol. 19, pp. 725–738, 1984.

[92] H. Sadikoglu, A. I. Liapis, and O. K. Crosser, “Optimal Control of the Primary and Secondary Drying Stages of Bulk Solution Freeze Drying in Trays,” *Dry. Technol.*, vol. 16, no. 3–5, pp. 399–431, 1998.

[93] F. Jafar and M. Farid, “Analysis of Heat and Mass Transfer in Freeze Drying,” *Dry. Technol.*, vol. 21, no. July 2014, pp. 249–263, 2003.

[94] R. Liapis, A. I.; Bruttini, “Freeze-Drying of Pharmaceutical Crystalline and Amorphous Solutes in Vials: Dynamic Multi-Dimensional Models of the Primary and Secondary Drying Stages and Qualitative Features of the Moving Interface,” *Dry. Technol.*, vol. 13, no. 1, pp. 43–72, 1995.

[95] H. Sadikoglu, “Optimal Control of the Secondary Drying Stage of Freeze Drying of Solutions in Vials Using Variational Calculus Optimal Control of the Secondary Drying Stage,” *Dry. Technol.*, vol. 23, no. 1–2, pp. 33–57, 2005.

[96] A. Gan, KH; Bruttini, R; Crosser, OK; Liapis, “Heating policies during the primary and secondary drying stages of the lyophilization process in vials: Effects of the arrangement of vials in clusters of square and hexagonal arrays on trays,” *Dry. Technol.*, vol. 22, no. 7, pp. 1539–1575, 2004.

[97] A. A. Barresi, D. Fissore, and D. L. Marchisio, “Process Analytical Technology in Industrial Freeze-Drying,” in *Freeze Drying/ Lyophilization of Pharmaceutical and Biological Products*, Informa, 2010, pp. 460–493.

[98] Z. H. Wang and M. H. Shi, “Numerical study on sublimation-condensation phenomena during microwave freeze drying,” *Chem. Eng. Sci.*, vol. 53, no. 18, pp. 3189–3197, 1998.

[99] P. I. Ravikovitch and A. V. Neimark, “Calculations of pore size distributions in nanoporous materials from adsorption and desorption isotherms,” *Stud. Surf. Sci. Catal.*, pp. 597–606, 2000.

[100] A. Grosman and C. Ortega, “Capillary condensation in porous materials. Hysteresis and interaction mechanism without pore blocking/percolation process,” *Langmuir*, vol. 24, no. 8, pp. 3977–3986, 2008.

[101] C. M. Lastoskie and K. E. Gubbins, “Characterization of porous materials using density functional theory and molecular simulation,” *Stud. Surf. Sci. Catal.*, vol. 128, no. Characterisation of Porous Solids V, pp. 41–50, 2000.

[102] M. K. Choudhary, K. C. Karki, and S. V. Patankar, “Mathematical modeling of heat transfer, condensation, and capillary flow in porous insulation on a cold pipe,” *Int. J. Heat Mass Transf.*, vol. 47, no. 26, pp. 5629–5638, 2004.

[103] G. A. Tompsett, L. Krogh, D. W. Griffin, and W. C. Conner, “Hysteresis and scanning behavior of mesoporous molecular sieves,” *Langmuir*, vol. 21, no. 18, pp. 8214–8225, 2005.

[104] M. Hassan Ghajar and S. H. Hashemabadi, “CFD Simulation of Capillary Condensation during Freeze Drying of Porous Material,” *Chem. Eng. Technol.*, vol. 34, no. 7, pp. 1136–1142, 2011.

[105] S. M. Patel, S. Chaudhuri, and M. J. Pikal, “Choked flow and importance of Mach I in freeze-drying process design,” *Chem. Eng. Sci.*, vol. 65, no. 21, pp. 5716–5727, 2010.

[106] A. A. Alexeenko, A. Ganguly, and S. L. Nail, “Computational analysis of fluid dynamics in pharmaceutical freeze-drying,” *J. Pharm. Sci.*, vol. 98, no. 9, pp. 3483–3494, 2009.

[107] A. Ganguly and A. A. Alexeenko, “Modeling and measurements of water-vapor flow and icing at low pressures with application to pharmaceutical freeze-drying,” *Int. J. Heat Mass Transf.*, vol. 55, no. 21–22, pp. 5503–5513, 2012.

[108] M. Petitti, A. A. Barresi, and D. L. Marchisio, “CFD modelling of condensers for freeze-drying processes,” *Sadhana - Acad. Proc. Eng. Sci.*, vol. 38, no. 6, pp. 1219–1239, 2013.

[109] A. A. Rasetto, Valeria; Marchisio, Daniele L.; Fissore, Davide; Barresi, “On the Use of a Dual-Scale Model to Improve Understanding of a Pharmaceutical Freeze-Drying Process,” *J. Pharm. Sci.*, vol. 99, no. 10, pp. 4337–4350, 2010.

[110] L. Ljung, “Black-box models from input-output measurements,” *IMTC 2001. Proc. 18th IEEE Instrum. Meas. Technol. Conf. Rediscovering Meas. Age Informatics (Cat. No.01CH 37188)*, vol. 1, no. 2, pp. 138–146, 2001.

[111] A. F. Gobi and W. Pedrycz, “Fuzzy modelling through logic optimization,” *Int. J. Approx. Reason.*, vol. 45, no. 3, pp. 488–510, 2007.

[112] M. Sugeno and T. Yasukawa, “A Fuzzy-Logic-Based Approach to Qualitative Modeling,” *IEEE Trans. Fuzzy Syst.*, vol. I, no. I, pp. 7–31, 1993.

[113] Y. V. Todorov and T. D. Tsvetkov, “Volterra model predictive control of a lyophilization plant,” *2008 4th Int. IEEE Conf. Intell. Syst. IS 2008*, vol. 2, pp. 2013–2018, 2008.

[114] E. N. Dragoi, S. Curteanu, and D. Fissore, “Freeze-drying modeling and monitoring using a new neuro-evolutive technique,” *Chem. Eng. Sci.*, vol. 72, pp. 195–204, 2012.

[115] P. Van Bockstal *et al.*, “Mechanistic modelling of infrared mediated energy transfer during the

primary drying step of a continuous freeze-drying process," *Eur. J. Pharm. Biopharm.*, vol. 114, pp. 11–21, 2017.

[116] Ö. Cumhur, M. Şeker, and H. Sadıkoğlu, "Freeze drying of turkey breast meat : Mathematical modeling and estimation of transport parameters," *Dry. Technol.*, vol. 34, no. 5, pp. 584–594, 2016.

[117] I. C. Trelea, S. Passot, M. Marin, and F. Fonseca, "Model for heat and mass transfer in freeze-drying of pellets.," *J. Biomech. Eng.*, vol. 131, no. 7, p. 074501, 2009.

[118] T. Chitu, S. Vessot, R. Peczalski, J. Andrieu, B. Woinet, and A. Françon, "Influence of Operating Conditions on the Freeze- Drying of Frozen Particles in a Fixed Bed and Modeling Data Influence of Operating Conditions on the Freeze-Drying of Frozen Particles in a Fixed Bed and Modeling Data," *Dry. Technol.*, vol. 33, no. 15–16, 2015.

[119] L. N. Mockus *et al.*, "Quality by design in formulation and process development for a freeze-dried, small molecule parenteral product: a case study," *Pharm. Dev. Technol.*, vol. 16, no. 6, pp. 549–576, 2011.

[120] "International Conference on Harmonization (ICH). Guidance for industry: Q8 (R2) pharmaceutical development," 2009.

[121] L. X. Yu *et al.*, "Understanding pharmaceutical quality by design.," *AAPS J.*, vol. 16, no. 4, pp. 771–83, 2014.

[122] J. A. Nail, Steven L.; Searles, "Elements of quality by design in development and scale-up of freeze-dried parenterals," *Biopharm Int.*, vol. 21, no. 1, p. 44–+, 2008.

[123] R. Pisano, D. Fissore, and A. a. Barresi, "Quality by Design in the Secondary Drying Step of a Freeze-Drying Process," *Dry. Technol.*, vol. 30, no. 11–12, pp. 1307–1316, 2012.

[124] S. T. F. C. Mortier, P. J. Van Bockstal, J. Corver, I. Nopens, K. V. Gernaey, and T. De Beer, “Uncertainty analysis as essential step in the establishment of the dynamic Design Space of primary drying during freeze-drying,” *Eur. J. Pharm. Biopharm.*, vol. 103, pp. 71–83, 2016.

[125] S. Nail *et al.*, “Recommended Best Practices for Process Monitoring Instrumentation in Pharmaceutical Freeze Drying — 2017,” *AAPS PharmSciTech*, vol. 18, no. 7, pp. 2379–2393, 2017.

[126] M. Yates, R. Moreno, M. Isabel, and C. Tallo, “Porosity of freeze-dried g -Al 2 O 3 powders,” *Ceram. Int.*, vol. 33, pp. 1165–1169, 2007.

[127] V. P. Oikonomopoulou, M. K. Krokida, and V. T. Karathanos, “The influence of freeze drying conditions on microstructural changes of food products,” *Procedia Food Sci.*, vol. 1, pp. 647–654, 2011.

[128] T. Jalanti, “Scanning Electron Microscopy: A Powerful Tool for Imaging Freeze-Dried Material,” in *Freeze Drying/Lyophilization of Pharmaceutical and Biological Products*, 2010, pp. 372–382.

[129] R. Mousavi, T. Miri, P. W. Cox, and P. J. Fryer, “Imaging food freezing using X-ray microtomography,” *Int. J. Food Sci. Technol.*, vol. 42, no. 6, pp. 714–727, 2007.

[130] V. Vicent, P. Verboven, F. T. Ndoye, G. Alvarez, and B. Nicolaï, “A new method developed to characterize the 3D microstructure of frozen apple using X-ray micro-CT,” *J. Food Eng.*, vol. 212, no. May, pp. 154–164, 2017.

[131] R. H. M. Hatley and F. Franks, “Applications of DSC in the development of improved freeze-drying processes for labile biologicals,” *J. Therm. Anal.*, vol. 37, pp. 1905–1914, 1991.

[132] I. Journal and D. Q. M. Craig, “Modulated temperature differential scanning calorimetry : a novel approach to pharmaceutical thermal analysis,” *Int. J. Pharm.*, vol. 135, pp. 13–29, 1996.

[133] I. Journal, “Optimization of Freeze Drying Cycle Protocol Using Real Time Microscopy and Integrated Differential Thermal ...,” *Int. Jpurnal Pharm. Technol.*, vol. 5, no. 7, 2012.

[134] H. Akan *et al.*, “Infrared Thermography for Monitoring of Freeze-Drying Processes Instrumental Developments and Preliminary Results,” *Pharm. Drug Deliv. Pharm. Technol. Infrared*, vol. 103, pp. 2088–2097, 2014.

[135] Cameron P., *Good Pharmaceutical Freeze-Drying Practice*. Interpharm Press Inc., 1997.

[136] X. Tang, S. L. Nail, and M. J. Pikal, “Evaluation of Manometric Temperature Measurement, a Process Analytical Technology Tool for Freeze-Drying: Part I, Product Temperature Measurement,” *AAPS PharmSciTech*, vol. 7, no. 1, pp. 1–9, 2006.

[137] S. L. Milton, N; Pikal, M J; Roy, M L; Nail, “Evaluation of manometric temperature measurement as a method of monitoring product temperature during lyophilization,” *Pda J. Pharm. Sci. Technol.*, vol. 51, no. 1, pp. 7–16, 1997.

[138] S. Schneid and H. Gieseler, “Research Article Evaluation of a New Wireless Temperature Remote Interrogation System (TEMPRIS) to Measure Product Temperature During Freeze Drying,” *AAPS PharmSciTech*, vol. 9, no. 3, 2008.

[139] D. Nowak, P. Piechucka, D. Witrowa-rajchert, and A. Wiktor, “Impact of material structure on the course of freezing and freeze-drying and on the properties of dried substance , as exempli fi ed by celery,” *J. Food Eng.*, vol. 180, pp. 22–28, 2016.

[140] S. M. Patel, T. Doen, and M. J. Pikal, “Determination of End Point of Primary Drying in Freeze-Drying Process Control,” *AA*, vol. 11, no. 1, 2010.

[141] J. Grant Armstrong, “Use Of The Capacitance Manometer Gauge in Vacuum Freeze-Drying,” *Pda J. Pharm. Sci. Technol.*, vol. 34, no. 6, pp. 473–483, 1980.

[142] A. Ganguly, J. Stewart, A. Rhoden, M. Volny, and N. Saad, “Mass spectrometry in freeze-drying: Motivations for using a bespoke PAT for laboratory and production environment,” *Eur. J. Pharm. Biopharm.*, vol. 127, no. February, pp. 298–308, 2018.

[143] I. Vollrath, V. Pauli, W. Friess, A. Freitag, A. Hawe, and G. Winter, “Evaluation of heat flux measurement as a new PAT monitoring tool in freeze drying,” *J. Pharm. Sci.*, no. 96, pp. 1776–93, 2017.

[144] N. S. Rockland LB, “Fundamentals of Water Activity,” *Food Tech*, vol. 34, pp. 42–59, 1980.

[145] J. C. Nlay, E. Grim, M. Roscoe, and J. Westy, “Determination o f residual moisture in freeze ’ dried viral vaccines : Karl Fischer , gravimetric and thermogravimetric methodologies *,” *J. Biol. Stand.*, vol. 10, pp. 249–259, 1982.

[146] A. Kauppinen *et al.*, “Validation of a multipoint near-infrared spectroscopy method for in-line moisture content analysis during freeze-drying,” *J. Pharm. Biomed. Anal.*, vol. 95, pp. 229–237, 2014.

[147] R. Iyer, S. K. Tomar, T. U. Maheswari, and R. Singh, “Streptococcus thermophilus strains : Multifunctional lactic acid bacteria,” *Int. Dairy J.*, vol. 20, no. 3, pp. 133–141, 2010.

[148] L. Eriksson, E. Johansson, N. Kettaneh-Wold, J. Trygg, C. Wikström, and S. Wold, *Multi- and Megavariate Data Analysis*, 2nd ed. Umetrics Academy, 2006.

[149] R. Bro and A. K. Smilde, “Principal component analysis,” *Anal. Methods*, vol. 6, no. 9, pp. 2812–2831, 2014.

[150] Salminen, *Lactic Acid Bacteria*. 2004.

[151] B. M. Corcoran, R. P. Ross, G. F. Fitzgerald, P. Dockery, and C. Stanton, “Enhanced survival of GroESL-overproducing Lactobacillus paracasei NFBC 338 under stressful conditions induced by

drying," *Appl. Environ. Microbiol.*, vol. 72, no. 7, pp. 5104–5107, 2006.

[152] Y. Doleyres, I. Fliss, and C. Lacroix, "Increased stress tolerance of Bifidobacterium longum and Lactococcus lactis produced during continuous mixed-strain immobilized-cell fermentation," *J. Appl. Microbiol.*, vol. 97, no. 3, pp. 527–539, 2004.

[153] X. C. Meng, C. Stanton, G. F. Fitzgerald, C. Daly, and R. P. Ross, "Anhydrobiotics: The challenges of drying probiotic cultures," *Food Chem.*, vol. 106, no. 4 SPEC. ISS., pp. 1406–1416, 2008.

[154] C. P. Champagne, N. Gardner, E. Brochu, and Y. Beaulieu, "The Freeze-Drying of Lactic Acid Bacteria . A Review," *Can. Institue Food Sci. Technol.*, vol. 24, no. 3, pp. 118–128, 1991.

[155] Quast.D and Karel.M, "Dry Layer Permeability and Freeze-Drying Concentrated Rates in Fluid Systems," *J. Food Sci.*, vol. 33, no. 1962, pp. 170–175, 1964.

[156] S. Zhai, R. Taylor, R. Sanches, and N. K. H. Slater, "Measurement of lyophilisation primary drying rates by freeze-drying microscopy," *Chem. Eng. Sci.*, vol. 58, pp. 2313–2323, 2003.

[157] S. Zhai, "Model Based Studies of the Lyophilisation of Biological Materials," University of Cambridge, 2005.

[158] K. J. Kossacki and J. Leliwa-Kopystynski, "Temperature dependence of the sublimation rate of water ice: Influence of impurities," *Icarus*, vol. 233, pp. 101–105, 2014.

[159] R. Byron Bird, W. E. Stewart, and E. N. Lightfoot, *Transport Phenomena*, 2nd Editio. John Wiley & Sons, 2002.

[160] R. N. Moghaddam and M. Jamiolahmady, "Slip flow in porous media," *Fuel*, vol. 173, pp. 298–310, 2016.

[161] A.V. Luikov, “Basic Properties of Capillary-Porous Bodies,” in *Heat and Mass Transfer in Capillary-Porous Bodies*, Pergamon Press, 1966, pp. 189–232.

[162] R. E. Cunningham and R. J. J. Williams, *Diffusion in Gases and Porous Media*. New York, 1980.

[163] C.N. Satterfield, *Mass Transfer in Heterogeneous Catalysis*. M.I.T. Press., 1970.

[164] C. F. Borgognoni, J. da S. Bevilacqua, and R. N. de M. Pitombo, “Freeze-drying microscopy in mathematical modeling of a biomaterial freeze-drying,” *Brazilian J. Pharm. Sci.*, vol. 48, no. 2, pp. 203–210, 2012.

[165] P. Raman, “Freeze drying microscopy as a tool to study sublimation kinetics,” Loughborough University, 2015.

[166] L. Schoeman, P. Williams, A. du Plessis, and M. Manley, “X-ray micro-computed tomography (µCT) for non-destructive characterisation of food microstructure,” 2016.

[167] R. Mousavi, T. Miri, P. W. Cox, and P. J. Fryer, “A Novel Technique for Ice Crystal Visualization in Frozen Solids Using X-Ray Micro-Computed Tomography,” *Food Eng. Phys. Prop.*, vol. 70, no. 7, pp. 223–229, 2005.

[168] R. Pisano, A. A. Barresi, L. C. Capozzi, G. Novajra, I. Oddone, and C. Vitale-Brovarone, “Characterization of the mass transfer of lyophilized products based on X-ray micro-computed tomography images,” *Dry. Technol.*, vol. 35, no. 8, pp. 933–938, 2017.

[169] M. U. H. Joardder, A. Karim, C. Kumar, and R. J. Brown, *Porosity: Establishing the Relationship between Drying Parameters and Dried Food Quality*. 2015.

[170] A. A. Flores and H. D. Goff, “Ice Crystal Size Distributions in Dynamically Frozen Model Solutions and Ice Cream as Affected by Stabilizers,” *J. Dairy Sci.*, vol. 82, no. 7, pp. 1399–1407, 1999.

[171] G. Smith, M. S. Arshad, E. Polygalov, and I. Ermolina, “An application for impedance spectroscopy in the characterisation of the glass transition during the lyophilization cycle: The example of a 10% w/v maltodextrin solution,” *Eur. J. Pharm. Biopharm.*, vol. 85, no. 3 PART B, pp. 1130–1140, 2013.

[172] G. Smith, M. S. Arshad, E. Polygalov, and I. Ermolina, “Through-vial impedance spectroscopy of the mechanisms of annealing in the freeze-drying of maltodextrin: The impact of annealing hold time and temperature on the primary drying rate,” *J. Pharm. Sci.*, vol. 103, no. 6, pp. 1799–1810, 2014.

[173] N. Harnkarnsujarit, K. Kawai, and T. Suzuki, “Impacts of freezing and molecular size on structure, mechanical properties and recrystallization of freeze-thawed polysaccharide gels,” *LWT - Food Sci. Technol.*, vol. 68, pp. 190–201, 2016.

[174] A. Hottot, S. Vessot, and J. Andrieu, “A direct characterization method of the ice morphology. Relationship between mean crystals size and primary drying times of freeze-drying processes,” *Dry. Technol.*, vol. 22, no. 8, pp. 2009–2021, 2004.

[175] J. A. Searles, J. F. Carpenter, and W. R. Theodore, “The ice nucleation temperature determines the primary drying rate of lyophilisation for samples frozen on a temperature controlled shelf,” *J. Pharm. Sci.*, vol. 90, no. 7, pp. 860–871, 2001.

[176] F. A. N. Fernandes, M. I. Gallão, and S. Rodrigues, “Effect of osmotic dehydration and ultrasound pre-treatment on cell structure: Melon dehydration,” *LWT - Food Sci. Technol.*, vol. 41, no. 4, pp. 604–610, 2008.

[177] S. Prachayawarakorn, P. Prakotmak, and S. Soponronnarit, “Effects of pore size distribution and pore-architecture assembly on drying characteristics of pore networks,” *Int. J. Heat Mass Transf.*, vol. 51, no. 1–2, pp. 344–352, 2008.

[178] P. Prakotmak, S. Soponronnarit, and S. Prachayawarakorn, “Modelling of moisture diffusion in pores of banana foam mat using a 2-D stochastic pore network: Determination of moisture diffusion coefficient during adsorption process,” *J. Food Eng.*, vol. 96, no. 1, pp. 119–126, 2010.

[179] O. D. Baik and M. Marcotte, “Modeling the moisture diffusivity in a baking cake,” *J. Food Eng.*, vol. 56, no. 1, pp. 27–36, 2003.

[180] P. Foerst, M. Vorhauer, N. Schuchmann, and E. Tsotsas, “Experimental investigation on pore size distribution and drying kinetics during lyophilization of sugar solutions,” in *21st International Drying Symposium*, 2018.

[181] T. Metzger and E. Tsotsas, “Influence of pore size distribution on drying kinetics: A simple capillary model,” *Dry. Technol.*, vol. 23, no. 9–11, pp. 1797–1809, 2005.

[182] G. E. Mueller, “Radial porosity in packed beds of spheres,” *Powder Technol.*, vol. 203, no. 3, pp. 626–633, 2010.

[183] S. C. Reyes and E. Iglesia, “Effective diffusivities in catalyst pellets: new model porous structures and transport simulation techniques,” *J. Catal.*, vol. 129, no. 2, pp. 457–472, 1991.

[184] A. Hottot, S. Vessot, and J. Andrieu, “Freeze drying of pharmaceuticals in vials: Influence of freezing protocol and sample configuration on ice morphology and freeze-dried cake texture,” *Chem. Eng. Process. Process Intensif.*, vol. 46, no. 7, pp. 666–674, 2007.

[185] F. J. O’Brien, B. A. Harley, I. V. Yannas, and L. Gibson, “Influence of freezing rate on pore structure in freeze-dried collagen-GAG scaffolds,” *Biomaterials*, vol. 25, no. 6, pp. 1077–1086, 2004.

[186] L. C. Capozzi, G. Boccardo, A. A. Barresi, and R. Pisano, “Computer-Aided Property Estimation of Microparticles in Packed-Beds for Freeze-Drying Applications,” in *The 20th International Drying Symposium*, 2016.

[187] V. Koganti, S. Luthra, and M. J. Pikal, “The Freeze-Drying Process: The Use of Mathematical Modeling in Process Design, Understanding, and Scale-Up,” *Chem. Eng. Pharm. Ind.*, 2011.

[188] G.-W. Oetjen and P. Haseley, *Freeze-Drying*. Wiley-VCH Verlag GmbH & Co. KGaA, Weinheim, Germany, 2004.

[189] R. Feistel and W. Wagner, “Sublimation pressure and sublimation enthalpy of H2O ice Ih between 0 and 273.16 K,” *Geochim. Cosmochim. Acta*, vol. 71, no. 1, pp. 36–45, 2007.

[190] S. Zhao, N. Zhang, X. Zhou, and L. Zhang, “Particle shape effects on fabric of granular random packing,” *Powder Technol.*, vol. 310, pp. 175–186, 2017.

[191] C. R. A. Abreu, F. W. Tavares, and M. Castier, “Influence of particle shape on the packing and on the segregation of spherocylinders via Monte Carlo simulations,” *Powder Technol.*, vol. 134, no. 1–2, pp. 167–180, 2003.

[192] B. D. Lubachevsky and F. H. Stillinger, “Geometric properties of random disk packings,” *J. Stat. Phys.*, vol. 60, no. 5–6, pp. 561–583, 1990.

[193] L. K. Roth and H. M. Jaeger, “Optimizing packing fraction in granular media composed of overlapping spheres,” *Soft Matter*, vol. 12, no. 4, pp. 1107–1115, 2016.

[194] A. Jaoshvili, A. Esakia, M. Porrati, and P. M. Chaikin, “Experiments on the Random Packing of Tetrahedral Dice,” *Phys. Rev. Lett.*, vol. 104, no. 18, pp. 1–4, 2010.

[195] J. D. Bernal, “A geometrical approach to the structure of liquids,” *Nature*, no. 4655, pp. 55–56, 1959.

[196] A. Donev *et al.*, “Improving the Density of Jammed Disordered Packings Using Ellipsoids,” *Science (80-.).*, vol. 303, no. 5660, pp. 990–993, 2004.

[197] J. Baker and A. Kudrolli, “Maximum and minimum stable random packings of Platonic solids,” *Phys. Rev. E - Stat. Nonlinear, Soft Matter Phys.*, vol. 82, no. 6, 2010.

[198] H. P. Zhu, Z. Y. Zhou, R. Y. Yang, and A. B. Yu, “Discrete particle simulation of particulate systems: A review of major applications and findings,” *Chem. Eng. Sci.*, vol. 63, no. 23, pp. 5728–5770, 2008.

[199] A. A. Barresi *et al.*, “Model-Based Monitoring and Control of Industrial Freeze-Drying Processes : Effect of Batch Nonuniformity Model-Based Monitoring and Control of Industrial Freeze-Drying Processes : Effect of Batch Nonuniformity,” *Dry. Te*, vol. 28, no. 5, pp. 577–590, 2010.

Appendix A

Supplementary material to Chapter 4.

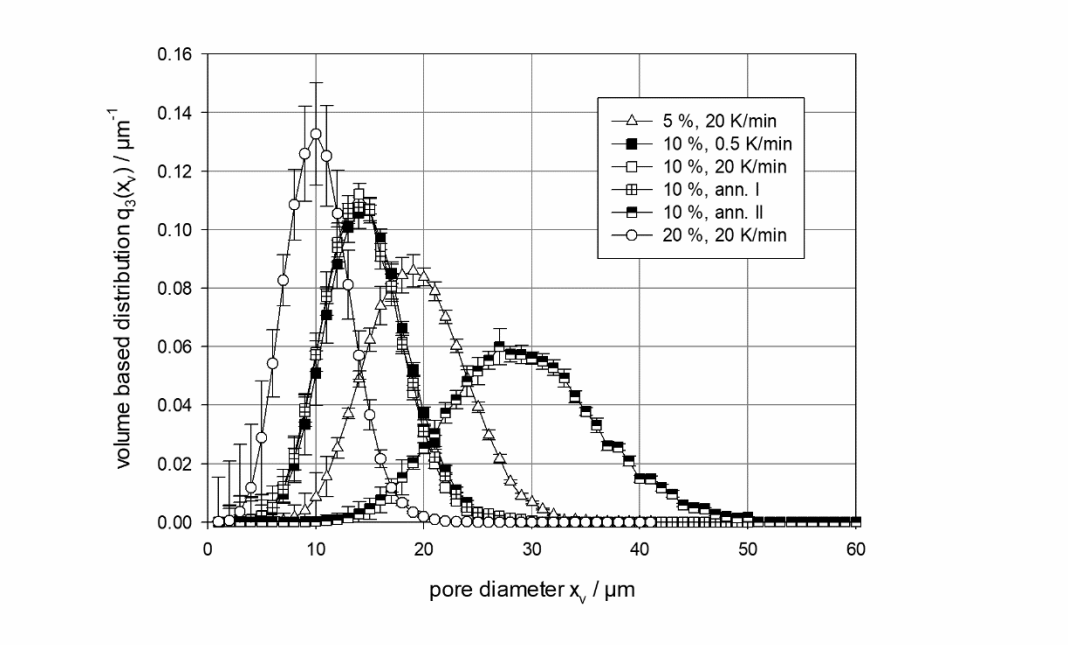

Figure 8.1.1 – 3D pore size distribution analyzed by µ-computed tomography.

Appendix B

Supplementary material to Chapter 6.

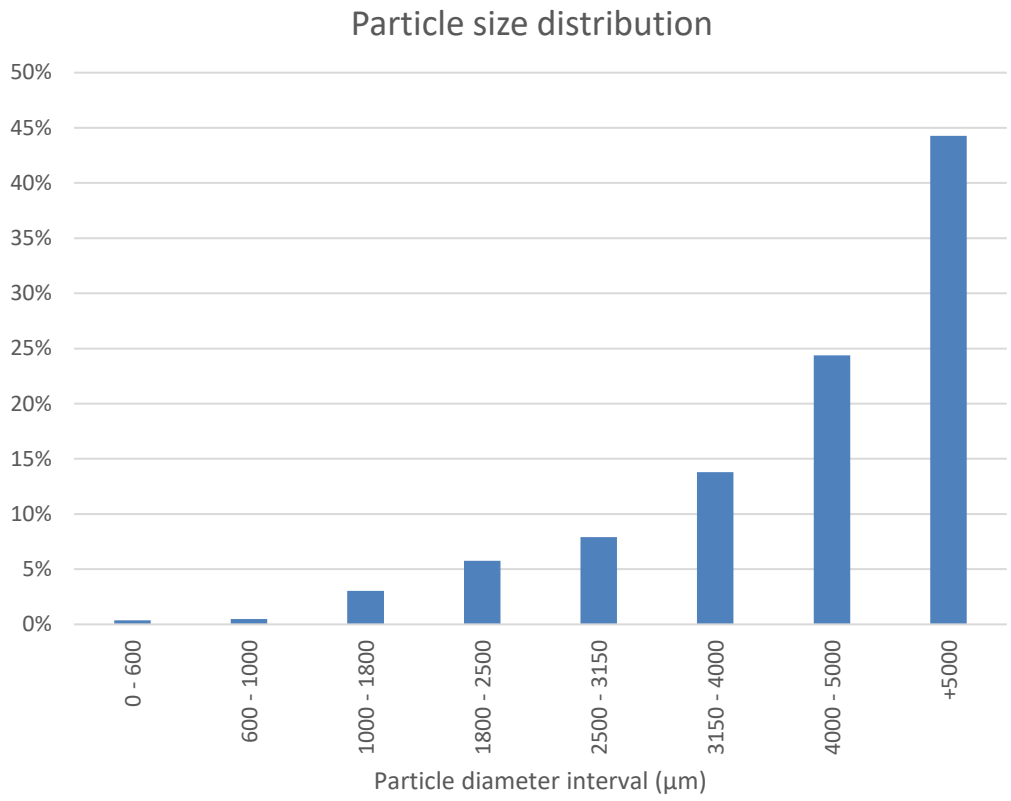

Figure B.1 – Maltodextrin 10 % w/w particle size distribution.

Table B.1 - Morphological characteristics of each particle and of the free space between particles in the bed.

Particles							
$d_{particle}$ [mm]		$\theta_{particle}$ [-]		d_{pore} [µm]	$\tau_{particle}$ [-]	$Eff_{particle}$ [%]	
3,96		0.85		14	2	0.4	
Free space between particles							
Case	$Pack_{bed}$ [-]	$V_{particles}$ [m^3]	V_{bed} [m^3]	θ_{bed} [-]	$d_{bed,pore}$ [mm]	τ_{bed} [-]	Eff_{bed} [%]
Maltodextrin 30	0.64	8.96×10^{-4}	1.40×10^{-3}	0.36	0.74	$\sqrt{2}$	0.25
Maltodextrin 50	0.64	8.96×10^{-4}	1.40×10^{-3}	0.36	0.74	$\sqrt{2}$	0.25
ST-B	0.40	5.60×10^{-4}	1.40×10^{-3}	0.60	1.98	$\sqrt{2}$	0.42
ST-C	0.40	5.60×10^{-4}	1.40×10^{-3}	0.60	1.98	$\sqrt{2}$	0.42
ST-D	0.40	5.60×10^{-4}	1.40×10^{-3}	0.60	1.98	$\sqrt{2}$	0.42
ST-H	0.40	5.60×10^{-4}	1.40×10^{-3}	0.60	1.98	$\sqrt{2}$	0.42

Table B.2 - Calculated diffusion coefficients for each particle, for the free space between particles and the diffusion coefficients implemented in the CFD simulations.

	Particles	Free space between particles				Unimodal Porous Domain (CFD)	
Case	$D_{eff,particle}$ [m^2/s]	Kn_{bed} [-]	$D_{kn,eff,bed}$ [m^2/s]	$D_{bulk,eff,bed}$ [m^2/s]	$D_{eff,bed}$ [m^2/s]	$D_{eff,porous}$ [m^2/s]	$D_{eff,chamber}$ [m^2/s]
Maltodextrin 30	2.13×10^{-3}	0.49	2.08×10^{-2}	1.02×10^{-2}	6.84×10^{-3}	3.83×10^{-3}	4.00×10^{-2}
Maltodextrin 50	2.13×10^{-3}	0.29	2.08×10^{-2}	6.12×10^{-3}	4.73×10^{-3}	3.06×10^{-3}	2.40×10^{-2}
ST-B	2.14×10^{-3}	0.11	9.24×10^{-2}	1.02×10^{-2}	9.18×10^{-3}	6.36×10^{-3}	2.40×10^{-2}
ST-C	2.09×10^{-3}	0.11	9.24×10^{-2}	1.02×10^{-2}	9.18×10^{-3}	6.35×10^{-3}	2.40×10^{-2}
ST-D	2.16×10^{-3}	0.11	9.24×10^{-2}	1.02×10^{-2}	9.18×10^{-3}	6.37×10^{-3}	2.40×10^{-2}
ST-H	2.15×10^{-3}	0.11	9.24×10^{-2}	1.02×10^{-2}	9.18×10^{-3}	6.37×10^{-3}	2.40×10^{-2}